Inertial and Frequency Response of an Offshore Wind Turbine: Effect on Extreme and Fatigue Loads

L.J. Douma

TUDelft

Inertial and Frequency Response of an Offshore Wind Turbine: Effect on Extreme and Fatigue Loads

by

L.J. Douma

to obtain the degree of Master of Science in Sustainable Energy Technology

at Delft University of Technology,

to be defended publicly on August 30th, 2023.

Wind Energy Group, Faculty of Aerospace Engineering, Delft University of Technology

An electronic version of this thesis is available at `http://repository.tudelft.nl/`.

TUDelft

Acknowledgements

First and foremost, I want to express my gratitude to Michiel Zaayer for his invaluable support throughout the course of this project. His expert advise, guidance and constructive feedback have been instrumental in sharpening the focus of my research and elevating the level of my work. It would not have been possible to complete this thesis without him.

Furthermore, I extend my appreciation to Dominic von Terzi and Milos Cvetkovic for reviewing my work as part of my thesis committee.

Last but not least, I am thankful to my friends, family and girlfriend for their encouragement and support during this journey.

<div align="right">

L.J. Douma
Utrecht, August 2023

</div>

Abstract

The replacement of conventional generation units with variable renewable energy sources could have a negative impact on the balance of supply and demand of electricity. Moreover, since the variable renewable energy sources are inverter based and therefore decoupled from the grid, the overall grid inertia will decrease. To solve this problem, the traditional mechanical frequency response can be replaced by synthetic inertial response and fast frequency response (FFR) alternatives from wind turbines. However, there is uncertainty about the order of magnitude of these ancillary services and how these ancillary services will affect the ultimate and fatigue loads on the wind turbine. The aim of the study is to gain an understanding of the extent to which an offshore wind turbine can provide synthetic inertia and fast frequency response and how this affects the fatigue and ultimate loads on the wind turbine.

Simulations were performed in FASTTool to study the response of the IEA 15MW offshore wind turbine using the baseline controller, synthetic inertia controller and FFR controller. The moments at the blade roots and tower base were used to perform a fatigue and ultimate load analysis. Three different grid frequency data sets were used for the grid frequency inputs of the synthetic inertia controller and FFR controller. In addition, the response of the wind turbine was studied at two different response sizes for both the synthetic inertia controller and the FFR controller.

This study showed a significant increase in fatigue damage equivalent load and maximum stresses due to an increase in the response size of the synthetic inertia and FFR controller. The results therefore showed that the extent to which an offshore wind turbine can provide synthetic inertia and FFR depends mainly on the magnitude of the controller response and not on the size of the wind turbine.

Contents

List of Figures

List of Tables

Nomenclature

Abbreviations

Abbreviation	Definition
DLC	Design load case
EOG	Extreme operating gust
ETM	Extreme turbulence model
FDEL	Fatigue damage equivalent load
FRR	Fast frequency response
IEA	International Energy Agency
IEC	International Electrotechnical Commission
NTM	Normal turbulence model
(v)RES	(Variable) Renewable energy source
RoCoF	Rate of change of frequency
TSO	Transmission system operator

Symbols

Symbol	Definition	Unit
C_P	Power coefficient	[-]
C_Q	Torque coefficient	[-]
D	Rotor diameter	[m]
d_{max}	Maximum deflection distance tip before hitting the tower	[m]
d_j	Partial damage	[-]
E	Young's Modulus	[Pa]
E_k	Kinetic energy	[J]
f_{grid}	Measured grid frequency	[Hz]
f_{nom}	Nominal grid frequency of 50 Hz	[Hz]
F_D	Load at the knee-point of the Wöhler curve	[Pa]
F_j	Applied load	[Pa]
GM	Gain margin	[dB]
H	Inertia constant	[s]
I_{ref}	Expected turbulence intensity at hub height at a 10 min average wind speed of 15 m/s	[-]
I	Inertia	$[kg/m^2]$
K	Stiffness of a material	$[Nm^2]$
$K_{De-loaded}$	De-loaded mode gain of the torque controller	$[Nm/(rad/s)^2]$
K_{in}	Inertial gain of the synthetic inertia controller	[-]
K_0	Proportional constant synthetic inertia controller	[-]
K_{opt}	Optimal mode gain torque controller	$[Nm/(rad/s)^2]$
K_p	Proportional gain pitch controller	[-]

Symbol	Definition	Unit
K_i	Integral gain pitch controller	[-]
M	Mass	[kg]
$M_{flap-wise}$	Moment on the blade root of the wind turbine in the flap-wise direction	[Nm]
$M_{edge-wise}$	Moment on the blade root of the wind turbine in the edge-wise direction	[Nm]
$M_{fore-aft}$	Moment on the tower base of the wind turbine in the fore-aft direction	[Nm]
$M_{side-side}$	Moment on the tower base of the wind turbine in the side-side direction	[Nm]
N_D	Number of points until the knee-point of the Wöhler curve	[-]
N_j	Allowed number of cycles at load j	[-]
P	Power	[W]
$P_{de-loaded}$	De-loaded power of the wind turbine	[MW]
P_{Rated}	Rated power of the wind turbine	[MW]
PM	Phase margin	[deg]
ΔP_L	Load change in the grid	[W]
ΔP_m	Mechanical power change in the grid	[W]
r_{gen}	Radius generator	[m]
$r_{gearbox}$	Ratio of the gearbox	[-]
R	Radius of the wind turbine	[m]
R_{prop}	Droop constant	[%]
R_0	Proportional droop constant	[%]
ΔT	Change in torque demand	[Nm]
V_{av}	Annual average wind speed at hub height	[m/s]
V_{e1}	Expected extreme wind sped with a recurrence interval of 1 year	[m/s]
V_{gust}	largest gust magnitude at hub height with expected recurrence period of 50 years	[m/s]
V_{hub}	Wind speed at hub height	[m/s]
y_{tip}	Tip deflection	[m]
$\alpha_{De-loaded}$	De-loading factor	[-]
β_{meas}	Measured pitch angle	[deg]
$\Delta\beta$	Change in pitch angle	[deg]
σ_1	Turbulence standard deviation	[m/s]
$\sigma_{flap-wise}$	Stresses in the flap-wise direction on the blades	[Pa]
$\sigma_{edge-wise}$	Stresses in the edge-wise direction on the blades	[Pa]
$\sigma_{fore-aft}$	Stresses on the tower in the fore-aft direction	[Pa]
$\sigma_{side-side}$	Stresses on the tower in the side-side direction	[Pa]
σ_{max}	Maximum stress	[Pa]
$\sigma_{ultimate}$	Ultimate stress	[Pa]
Λ_1	Turbulence scale parameter	[m]
γ_f	Load partial safety factor	[-]
γ_m	Material partial safety factor	[-]
γ_n	Consequence of failure partial safety factor	[-]
ω_{gen}	Measured generator speed	[RPM]

Symbol	Definition	Unit
ω_{max}	Maximum generator speed	[RPM]
ω_{min}	Minimum generator speed	[RPM]
ω_{rated}	Rated generator speed	[RPM]
ω_{new}	New cross-over frequency	[rad/s]
ω_{ref}	Reference cross-over frequency	[rad/s]
ω_c	Cross-over frequency pitch controller	[rad/s]
τ_{gen}	Generator torque	[Nm]
$\tau_{De-loaded}$	De-loaded generator torque	[Nm]
λ	Tip speed ratio of the wind turbine	[-]
$\lambda_{overspeed}$	New tip speed ratio due to overspeeding	[-]
η_{gen}	Efficiency of the generator	[%]
$\eta_{gearbox}$	Efficiency of the gearbox	[%]
ρ	Density	kg/m^3

<div style="text-align: right; font-size: 3em;">1</div>

Introduction

1.1. Background Information

Over the past years, conventional generation units have been replaced by renewable energy sources (RES). In 2021, 13.4 percent of the energy used in the Netherlands came from RES; which was an increase of almost 2 percent when compared to 2020 [1]. With an increase of 36 percent for wind energy and 29 percent for photovoltaic energy, these are the fastest increasing RES used in the Netherlands [1]. However, the intermittent nature of these variable RES (vRES) could have a negative effect on the balance of supply and demand of electricity. Imbalances between generation and consumption cause frequency variations in a power system, which can cause black outs [2]. In order to maintain a stable system, frequency stability needs to be met at all times. Using PV and wind together could smoothen the energy output, as they are seen as complementary to each other; adding an energy storage system for either long or short term energy storage could make this effect even larger.

Since these vRES are inverter-based resources, they are decoupled from the grid and therefore do not add natural inertia to the grid. Since the vRES replace conventional generation units, which have inertia from rotating generators, the overall inertia in the grid decreases. Inertia is important for grid stability; during an energy imbalance, energy can be extracted from or stored in the grid's inertia [3]. To solve this problem the sources of frequency response can be changed, replacing traditional mechanical frequency response with inertial response and fast frequency response (FFR) alternatives from RES. Whereas the inertial response of a RES mimics the conventional inertial response of large traditional generators, FFRs refer to resources that are able to increase their energy supply much faster than traditional mechanical frequency responses [3]. Additionally, using FFR alternatives also decreases the amount of inertia that is needed in the grid.

When frequency deviations occur, there are different time scales on which frequency control should be performed. Generally, the frequency response is threefold: it consists of primary frequency control, secondary frequency control and tertiary frequency control [4]. Primary frequency control is used to stabilize frequency fluctuations in the first 0-30 seconds [5]. Secondary frequency control is used to restore the frequency to the reference level, usually up to 5-10 minutes after the frequency drift [5]. Finally, tertiary frequency control is used to restore primary and secondary frequency control, manage congestion in the transmission network and restore the frequency level if the secondary frequency control is unable to do so [4]. The timescales for tertiary frequency control vary widely, but always take place after secondary frequency control.

To provide frequency support in unbalanced situations, vRES can integrate several solutions to balance the system. Wind turbines are the only vRES that naturally have inertia; this inertia can be

<div style="text-align: center;">1</div>

used to mimic the inertial response of conventional generators to supply or withdraw power during frequency changes [5]. This is done by injecting the kinetic energy stored in the wind turbine blades into the grid [6]. In literature, this inertial response has many names and is referred to as emulated, virtual, hidden, artificial, simulated and synthetic inertia; from now on, it will be referred to as synthetic inertia. Synthetic inertia is defined in [7] as the controlled contribution of electrical torque from a unit that is proportional to the rate of change of frequency (RoCoF) at the terminals of the unit. There is extensive literature on the topic of synthetic inertia. [8] and [9] discuss the theory for using synthetic inertia through a torque controller. Several controllers have been developed to emulate synthetic inertia, such as GE WindINERTIA^{TM} [10], ENERCON IE [11] and KEC I and KEC II [12]. Whereas in [13] the authors give an improved version of the ENERCON IE controller in which the recovery time is prolonged to limit the active power drop. Trigger mechanisms to activate a synthetic inertia controller have first been discussed in [14].

Inertial control thus corresponds to the controlled response of a wind turbine to mimic the rotational energy exchange of conventional machines. Any other form of fast controlled response can be classified as FFR [7]. Whereas synthetic inertia responds proportionally to the RoCoF, FFR is the controlled contribution of power that responds to a deviation in frequency. This response can be proportional to the frequency deviation or based on a particular scheme [7]. A proportional response can be supplied using a DROOP control [15]. A DROOP controller produces an active power change for which the steady-state properties is defined as the per unit change in power divided by the per unit change in frequency [16]. The active power change associated with the DROOP controller is thus proportional to the frequency deviation. A scheduled response can be given in which the reserve power can be used according to a predefined response [15]. The predefined response is based on a threshold level of the grid frequency. If the grid frequency drops below this threshold, the controller increases the new power set-point from the de-loaded power set-point to the maximum power operating point. An example of a scheduled control that uses the kinetic energy of the wind turbine, is the fast power reserve emulation approach [17]–[19]. This controller reserves additional kinetic energy by changing the rotational speed of the wind turbine. For both a proportional and a scheduled FFR control the de-loaded operation of the wind turbine is needed. When the wind turbine is de-loaded, the wind turbine produces power at a sub-optimal power point. This can be achieved by pitching the blades of the wind turbine, or by changing the rotor speed with a change in the generator torque [16].

The penetration of RES in the grid must continue to increase in order to drive the energy transition forward. In order to ensure a stable grid with limited frequency deviations, it is necessary to replace the conventional inertia and frequency responses that are disappearing. In order to do so, information is needed on how to operate wind turbines in such a manner that they are able to supply inertia and frequency response to the grid, while still considering the consequences of these responses on the wind turbines themselves.

1.2. Problem Analysis
As was discussed in section 1.1, to maintain a stable grid operation without relying on traditional power generation units, alternative sources for inertia and frequency control will need to be found; this will require significant changes to the current grid operations. Supplying part of the necessary amount of inertia to limit the RoCoF can be done by utilising the natural inertia of a wind turbine as synthetic inertia. Using wind turbines as a synthetic inertia source is of great interest, as it does not require de-loading. On the other hand, to effectively supply FFR as a primary frequency control mechanism, the de-loaded operation of PV panels or wind turbines will be necessary. If de-loading is not applied, there will be no room to supply extra power as the vRES is already operating at its maximum power operating point.

Some obstacles may be encountered in supplying synthetic inertia and FFR with wind turbines.

Firstly, during the supply of synthetic inertia the rotational speed of the wind turbine decreases. A large decrease should be prevented as this can induce a second (sometimes even larger) frequency dip. While keeping in mind that a large dip in rotor speed should be hindered, it is of interest to see how much synthetic inertia a wind turbine can supply to the grid. As the synthetic inertia supplied by the wind turbine does not need to be directly proportional to the RoCoF and hence could be larger compared to conventional inertia from directly coupled machines. The amount of synthetic inertia which is supplied to the grid can be expressed as a percentage of the output power, or as a constant value of power. In order for wind turbine owners to make good decisions about the amount of synthetic inertia and/or FFR that their wind turbine(s) can supply, more knowledge is required about the order of magnitude of these ancillary services that a wind turbine could supply.

Besides affecting the performance of the wind turbine, these ancillary services could also have an impact on the loads imposed on the wind turbine. By providing synthetic inertia and FFR, a wind turbine has to absorb not only wind-induced loads, but also loads corresponding to frequency deviations in the grid. These frequency deviations could have a negative effect on the loading of the wind turbine.

To ensure safe operation of the wind turbine, a load assessment is executed. In the load assessment of a wind turbine both the maximum loads, or the ultimate design loads, and the fatigue loads need to be taken into account to ensure that those loads will not become too high over the entire lifetime of the wind turbine. The minimum design requirements for an offshore wind turbine are mandated by the International Electrotechnical Commission (IEC) document 61400-3 [20]. Synthetic inertia and FFR are not specifically taken into account in the design load cases (DLC's), but need to be assessed in similar situations.

While much research has been done on the wind-induced loads, there is only little on the loads corresponding to the frequency deviations. In [21], the loads associated with creating a power reserve are studied using DLC's from the IEC document 61400-1 for onshore wind turbines. Adding to this, in [22] a start is made to assess the loads corresponding to synthetic inertia emulation from a 600 kW wind turbine. Next, it has been shown that a notch filter in combination with synthetic inertia can limit the loads on the shaft [23]. Finally, [24] studies some loads induced by synthetic inertia on a wind turbine of the 3.x MW class using grid frequency measurements from the Indian grid. However, from the existing research it stays unclear how the loads on the wind turbine would change if the size of the wind turbine would be increased, thus being able to have larger responses, or if the synthetic inertia ratio would be increased. Next, FFR can only be supplied if the wind turbine is de-loaded. Nonetheless, in supplying FFR not only the loads regarding the de-loading, as assessed in [21], are of importance, but also possible loads when reacting to grid frequency changes. Additionally, it is not set in stone how much FFR can safely be supplied by one wind turbine. Uncertainty also arises around the question whether it would be better to use as little wind turbines as possible or to spread the loads over a large amount of turbines. These situations should all be investigated while keeping in mind the requirements of the IEC.

It is not clear if and how future grid inertia and frequency needs and requirements might change. However, knowledge on the amount of inertia and frequency response a wind turbine can deliver, as well as knowledge on the effect of these responses on the wind turbine need to be gained. This is valuable information for the control and design of future wind plants and possibly even entire electricity grids.

1.3. Research Goal

In line with the introduction and the problem analysis, the final goal can be formulated as follows:

Gain an understanding of the extent to which an offshore wind turbine can provide synthetic inertia and fast frequency response and how this affects the loads on the turbine.

1.4. Research Questions

To reach the goal of this research, two main research questions will be answered.

1. How do the different control strategies affect the performance, flexibility and freedom of the wind turbine in terms of inertial response and FFR?

2. What is the effect of supplying synthetic inertia and FFR to loads on the wind turbine?

1.5. Scope

The scope of this research will focus on wind turbines in a large electricity system. The main reason for this is that the robustness of the grid, and therefore its frequency variations, is very much dependent on the size of the grid. The frequency measurement itself is left out of the scope of this research, it is therefore assumed that the necessary grid frequency data is available. The wind turbine used in this study is an offshore wind turbine with a size representative of current developments in offshore wind turbines. The turbine used is the International Energy Agency (IEA) 15MW reference turbine [25]. Even though an offshore wind turbine is used, hydrodynamic loads will be left out of the scope of this research. The perspective used in the project will be that of the wind turbine developer. The focus will therefore be on what are the opportunities and drawbacks for the wind turbine in providing synthetic inertia and FFR, and not on what the impact will be on the grid.

1.6. Thesis Outline

The rest of this thesis is structured as follows. Chapter 2 provides an in-depth exploration of the methodology used in this research. The chapter starts with an overview of the research design, followed by an examination of the modelling of the baseline controller, synthetic inertia and FFR controller in FAST-Tool. Furthermore, the approach for the fatigue and ultimate load analysis is described.

Next, chapter 3 introduces the wind turbine system. Starting with a general overview, after which the electricity grid the wind turbine is placed in and the specific wind turbine studied in this research are introduced.

Chapter 4 provides an in-depth description of the baseline controller, synthetic inertia controller and FFR controller used to study the wind turbine in the case study. This includes a description of the de-loading strategy used to enable the wind turbine to supply FFR. This chapter is finalised with the validation of the controllers.

Following this, the case study itself is discussed in chapter 5. This chapter starts with the development of the three different cases. Subsequently, the results of the baseline, synthetic inertia and FFR case will be discussed separately. Finally, the results from the individual cases are compared to each other.

Chapter 6 discusses the results of the case study from three different perspectives. The perspectives used are that of the wind turbine owner, the perspective from the system the wind turbine is located, and finally from a market perspective.

Finally, chapter 7 provides a conclusion for the thesis, followed by some recommendations for future research.

2

Methodology

This chapter sets out the general methodology for answering the research questions introduced in chapter 1. Firstly, the research design for this thesis is outlined, including the different scenarios which will be investigated in the case study. After this, the controller modelling for the wind turbine is discussed. Next, the data collection and analysis for wind and frequency data is explained. Finally, the load analysis for both the ultimate and fatigue load analysis is discussed.

2.1. Research Design

The aim of this research is to gain an understanding of how a wind turbine can provide synthetic inertia and FFR and how this affects the loads on the wind turbine. The research method chosen for this study is a comparative case study using quantitative data, as it involves simulations and data analysis to compare different cases. The main difference between a comparative case study and a single case study is that a number of related cases are compared instead of just one [26]. The comparative case study is used because it makes it possible to point out opportunities and weaknesses of using a wind turbine as a source of inertia or to use it in a frequency market. In addition, by comparing different cases, similarities and differences in the provision of synthetic inertia and FFR can be identified. The individual cases are first assessed as if they existed as a series of individual case studies. The results from the individual cases will then be used as input for a comparative study.
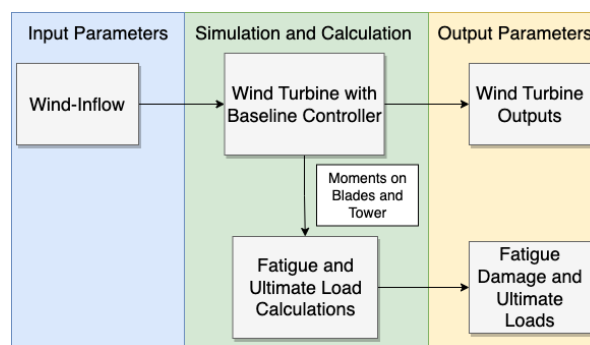
Figure 2.1: Block diagram of the baseline scenario.

As only a few cases can be analysed, the cases are chosen strategically instead of randomly [26]. The choice of cases here is therefore based on the research goal and research questions. Firstly, the normal operation of a wind turbine will be studied which acts as the baseline sample. A block diagram showing an overview of the baseline scenario can be found in figure 2.1. In the baseline scenario, only

the wind profile is used as an input for the model. During the simulations the wind turbine parameters are outputted. The moments on the blade roots and the tower base are used as inputs for the load calculations, which outputs the fatigue damage and ultimate loads.
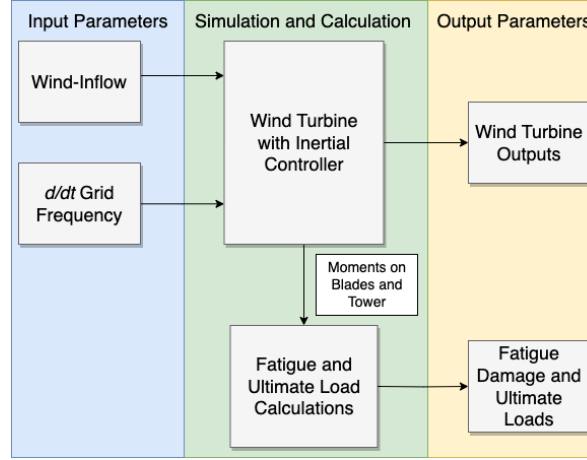
Figure 2.2: Block diagram of the synthetic inertia scenario.

Next, the wind turbine will be studied while supplying synthetic inertia which is derived from the natural inertia of the rotating parts of the wind turbine. Hence, no de-loading of the turbine is needed in this type of operation. A block diagram showing an overview of the synthetic inertia scenario can be found in figure 2.2. As the inertial controller reacts proportional to the RoCoF, the derivative of the grid frequency is used as an input to this scenario, as well as the wind-inflow similar to the baseline scenario. The past processing of the simulations is similar to the baseline scenario.
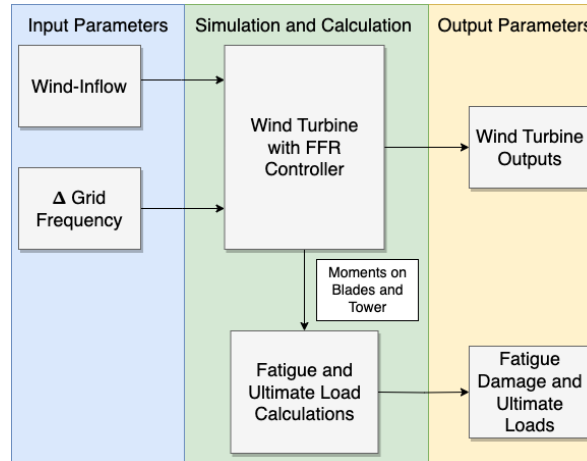
Figure 2.3: Block diagram of the FFR scenario.

The third case which will be studied is the de-loaded operation of the wind turbine in order to supply FFR using a DROOP controller. A block diagram showing an overview of the FFR scenario can be found in figure 2.3 below. Using the FFR controller will allow the wind turbine to operate in the primary frequency market. Differently from the synthetic inertia scenario, the FFR scenario reacts to the deviation of the grid frequency from the nominal grid frequency of 50 Hz. This deviation is therefore used as an input to the model instead of the RoCoF.

A possible fourth scenario could be to combine the supply of synthetic inertia and FFR. This could

allow one wind turbine to both supply inertia to the grid, as well as primary frequency control. However, as the focus of this research is on the effects of the separate controllers, this scenario will not be studied.

To analyse the performance of the wind turbine, a simulation model will be used in Matlab Simulink. This simulation model is an altered version of the Matlab Simulink tool named FASTTool [27]. This tool is used at TU Delft to analyse the operation of a wind turbine. FASTTool incorporates the wind turbine simulation software FAST (Fatigue, Aerodynamics, Structures and Turbulence), which is a comprehensive aeroelastic simulator which can be used to predict both the extreme and fatigue loads of two- and three-bladed horizontal-axis wind turbines [28]. Using this altered version of FASTTool will allow for the gathering of data on the scale of synthetic inertia and FFR which can be supplied, as well as data on the loads on the wind turbine and how these change under different conditions.

All data needed in order to compare the three cases will be collected from the simulations. Relevant data which will be extracted is all information used to assess the operation of the wind turbine. This includes the wind speed, the rotor speed, the generator power, the generator torque, the pitch angle of the blades and finally the moments on the blades and tower of the wind turbine.

The collected data for each case will be analysed, where after these analyses can be compared to each other. Using this data, the stresses on and deflections of the wind turbine for different ultimate state analyses will be calculated. With these stresses both the extreme load cases and fatigue load cases will be analysed. Where fatigue damage occurs under the varying loads on the WT over its lifetime and ultimate load cases refer to the highest loads on the WT in its lifetime.

As simplifications will need to be made in the simulation model, it is of great importance to assess the validity and reliability of the data and the results. This can firstly be done by assessing the model itself. As the FAST software used in the simulation model is a state-of-the-art tool for simulating the coupled dynamic response of wind turbines, this will ensure a good wind turbine output if the correct input settings are given by the Matlab Simulink model connected to it. These are checked by comparing the outputs of the model to theoretically derived power en torque curves, as well as the synthetic inertia and FFR responses of the model to those available in literature.

2.2. Wind Turbine Controller Modelling

As was explained in section 2.1, the controllers for the baseline wind turbine, the synthetic inertia controller and finally the FFR controller will be developed in FASTTool. The FAST block used in this tool can predict the loads in different design cases, thus enabling the assessment of the loads in both the normal situation as well as when the wind turbine delivers ancillary services.

It should be noted that it is not possible to model hydrodynamic loads within FASTTool. As the main focus of this research is to assess the performance of the wind turbine while delivering synthetic inertia and FFR, and to study the effect of supplying synthetic inertia and FFR to loads on the wind turbine, hydrodynamic loads are not implemented in the model and are therefore left out of the scope of the model.
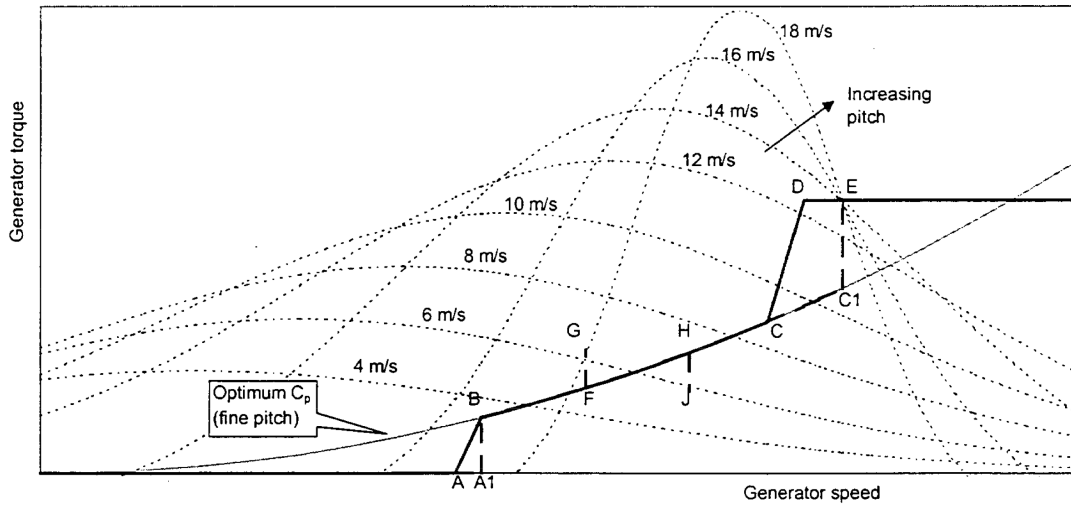
Figure 2.4: Torque-speed curve for a variable speed wind turbine. Region B-C refers to below rated power. Point E marks the rated power for the wind turbine [29].

To study the baseline wind turbine, FASTTool firstly needs inputs for the wind turbine blades, airfoils, tower, nacelle and drive-train. Next, the torque and pitch control of the wind turbine need to be defined. The torque controller implemented in FASTTool is active below rated power, and follows the optimal power curve on the torque-speed curve. This optimal power curve can be seen in figure 2.4, and is located between points B and C. In this region the torque controller varies the generator torque to follow the optimum generator speed. Above rated power, which is after point E in figure 2.4, the torque is set constant and the pitch angle is used to reach the desired maximum generator speed. As can be seen in figure 2.4, to achieve the constant rotor speed and generator torque after point E, the wind turbine blades are pitched to reach less optimal operation points. The pitch controller uses a gain scheduled PI controller. The gain scheduling of the pitch controller is not included in [25] and [30], but can be fine tuned within FASTTool using the Bode plots.

In order to include synthetic inertia in the FASTTool model, a new controller is added to the existing Simulink model. The aim of the synthetic inertia controller is to output an increase or decrease in torque set point, as a reaction to the grid frequency input. The reaction of this controller is not to the absolute grid frequency, but to the RoCoF. The working of the rest of the controller will be treated in section 4.2, and is firstly seen as a black box. Eventually, the goal of adding this synthetic inertia controller is to simulate the wind turbine delivering this ancillary service. The controller set points are then fed into the FAST Simulink block, which is used to study the loads associated with synthetic inertia.

Lastly, the FFR controller will be developed. To supply FFR, two main parts need to be included in the simulation model. Firstly, the de-loading of the wind turbine is needed. The energy used in FFR should be retained using a power reserve, this power will be outputted once the FFR is triggered. De-loading of the wind turbine can be done using a lower torque set point, and by changing the pitch angle. The torque set point can be changed in FASTTool by adjusting the optimal mode gain, and the pitch angle can be directly altered by adjusting the fine pitch angle. To find the most suitable de-loading strategy, a de-loading strategy using only a lower torque set point and a de-loading strategy using a lower torque set point and a different pitch angle will be compared. One of these de-loading strategies will then be chosen to be used in the case studies. Secondly, the FFR itself should be modelled. As the operating point of the wind turbine should be shifted back (partly) to the maximum power point, the response should react on both the de-loaded optimal mode gain and fine pitch angle. Similar to the synthetic inertia controller, the controller itself is firstly seen as a black box and will be elaborated upon in section 4.3. Similar to the synthetic inertia controller, the FFR controller outputs are fed into the

FAST Simulink block together with the existing controllers to study the loads associated with FFR.

2.3. Data Collection

The simulation model used for the case studies will need several data inputs. For all cases wind data is needed, grid frequency data is needed for all cases in which synthetic inertia or FFR is supplied. The wind data can be directly generated in FASTTool based on a desired wind profile. As FASTTool is not designed to study frequency responses, grid frequency data can of course not be generated directly in the simulation tool. Therefore the grid frequency data should be studied separately and thereafter be included in the model.

This section will firstly discuss the wind profiles used. Next, the grid frequency data collection and analysis will be discussed.

2.3.1. Wind Data

Firstly, the generated wind profiles will be discussed. The wind-inflow data used in FASTTool is the same as those described in the DLC's. The wind conditions used in the simulations are the Normal Turbulence Model (NTM), the Extreme Turbulence Model (ETM) and the Extreme Operating Gust (EOG). All formulas in this section are retrieved from the IEC document 61400-1 [31].

Normal Turbulence Model

The normal turbulence model is used to describe the normal wind conditions subjected on the wind turbine. The value for the turbulence standard deviation, σ_1, is given by:

$$\sigma_1 = I_{ref}(0.75V_{hub} + b) \tag{2.1}$$

in which I_{ref} is the expected turbulence intensity at hub height at a 10 min average wind speed of 15 m/s, V_{hub} is the wind speed at hub height and b = 5.6 m/s.

Extreme Turbulence Model

The extreme turbulence model (ETM) is used to describe, as the name states, extreme wind conditions subjected to the wind turbine. The standard deviation for the turbulence used for the ETM, σ_1, is given by:

$$\sigma_1 = c \cdot I_{ref}(0.072(\frac{V_{av}}{c} + 3)(\frac{V_{hub}}{c} - 4) + 10) \tag{2.2}$$

in which c = 2 m/s, I_{ref} again is the expected turbulence intensity at hub height at a 10 min average wind speed of 15 m/s, V_{av} is the annual average wind speed at hub height and V_{hub} is the wind speed at hub height.

Extreme Operating Gust

The hub height gust magnitude (V_{gust}) for the extreme operating gust (EOG) is defined in the document as:

$$V_{gust} = min\left\{1.35(V_{e1} - V_{hub}); 3.3\left(\frac{\sigma_1}{1 + 0.1(\frac{D}{\Lambda_1})}\right)\right\} \tag{2.3}$$

in which σ_1 is given by equation 2.1, V_{e1} is the expected extreme wind speed with a recurrence interval of 1 year, V_{hub} is wind speed at hub height, Λ_1 is the turbulence scale parameter and D is the rotor diameter.

2.3.2. Grid Frequency Data

Next, grid frequency data is needed to simulate synthetic inertia and FFR. The first important characteristic of the grid frequency data-set is its timescale; this should be small enough to capture the rapid

changes that occur in grid frequency fluctuations. Secondly, the grid frequency fluctuations should be representative for a large connected grid. A large grid is more robust and is less likely to have very big drops in grid frequency when a generator breaks down.

To gain insight in normal and extreme grid frequency behavior, the grid frequency should be analysed before using it in the simulation model. Firstly, the individual monthly data sets are combined to get to the complete data set for a full year. As this data set contains some measurement errors, these should be taken out before the normal and extreme behavior is extracted. These errors are deleted by using a 3-point moving average. If the absolute value of the difference between the 3-point moving average and the original value exceeds a threshold the data point is deleted from the data set.

Next, the extreme behavior is obtained from the data set in the form of a smaller data set consisting of 660 seconds of data. This is similar to the simulation time prescribed by the IEC. For the extreme behavior a distinction is made between the maximum slope of the change in grid frequency, the extreme RoCoF, and the extreme absolute difference in grid frequency. The extreme RoCoF is calculated for the entire data as:

$$RoCoF = \frac{df}{dt} \tag{2.4}$$

where f is the grid frequency and t is the time. The part of the data set containing the maximum absolute RoCoF is extracted to be used in the simulation model. Similarly, this is also done for the maximum frequency deviation from 50 Hz. This point of the data set is found by subtracting 50 Hz from all data points to find the maximum deviation. This part of the data set is used as the maximum difference grid frequency behavior.

Finally, the normal grid frequency behavior needs to be extracted. This is done by deleting the 1% highest RoCoF and the 0.01% highest absolute difference values. The RoCoF and frequency difference are calculated similar as before. By deleting these values, the data set that is left displays the normal frequency behavior without extremes. To get to the final data set that can be used in the model, a random sample of 660 seconds is extracted from the total data set.

2.4. Load Analysis

2.4.1. Overview Load Analysis

As was introduced in section 2.1, fatigue and ultimate load cases are simulated to assess the loads on the wind turbine. From the FASTTool model, several loads could be taken. Both for the blades and the tower, the model outputs loads corresponding to different locations in the structure. The output parameters taken from the FASTTool model are the tower base fore-aft and side-to-side moment, as well as the blade root edgewise and flap-wise moment. For the ultimate load analysis the moments of all three blades are taken into account, whereas for the fatigue load analysis only the loads on one blade are used. It is then assumed that the loads on the three blades are similar regarding the fatigue loads.

In the ultimate and fatigue load analysis, not the moments, but the stresses imposed on the wind turbine are used. The moments therefore need to be translated into stresses. To ensure a conservative enough load analysis, the estimated loads are multiplied with a partial safety factor. As the geometry of the wind turbine stays the same for all cases and only the controls differ, the safety factors will have a similar effect for all cases. As the numerical results from the load analysis should be considered with care, the safety factors might not have great importance. However, the load analysis might show which loads are design driving. For this reason, the safety factors are taken into account.

In translating the moments to stresses, the moment of inertia is needed. It is assumed that the material assessed is homogeneous. This is a misrepresentation of the actual situation, as especially in

the blade root stress concentrations will occur. However, this simplification is made in order to simplify the comparison between the different cases. Because of this, the stresses should be assessed with great care.

Once the moments are translated into stresses, these stresses can be used in the ultimate and fatigue load analysis. For the ultimate load analysis, the maximum stresses imposed on the wind turbine during the load cases is determined. Differently, for the fatigue load analysis it is checked how the variable load cycles impact the fatigue damage on the wind turbine. This is done using Miner's rule. The maximum amount of load cycles until failure is determined using the Wöhler curve. By using the Wöhler curve, the mean of the stress cycles is not taken into account. This is not a major issue for the tower. Nonetheless, it should be taken into account that the results for the blade root might not be thrust worthy regarding the absolute damage calculations. However, as the main goal of the fatigue calculations is to compare different fatigue damages, and not to determine if the wind turbine fails or not, this is justified. Besides the damage using Miner's rule, the fatigue damage equivalent load is calculated (FDEL). The FDEL allows for the comparison of different load distributions based on one number. Even though the FDEL also does not include mean loads, and is therefore debatable to use for fatigue design of the wind turbine, it is very use full in order to compare different load distributions. For this reason, the FDEL will be used as the main parameter to compare the fatigue damage of the different cases.

2.4.2. Safety Factors

The partial safety factors used are the load factor (γ_f), the material factor (γ_m) and the consequence-of-failure factor (γ_n) [32]. A summary of the safety factors can be found in table 2.1. In the rest of this section these safety factors will be elaborated upon.

Firstly, the partial safety factors for the loads depend on the type of design situation. Most of the DLC's regarding ultimate load analysis and tip deflection are studied in normal design situations. For these normal design situations the load factor is equal to 1.35 [20]. This document also states that the load factor for fatigue load analysis should be equal to 1 when appropriate fatigue damage calculations are made, which is the case in this research.

Next, the material factor shall be determined also based on the IEC document. For parts of the wind turbine such as its blades and the tower, the material factor should be no less than 1.2 when global buckling is an issue and no less than 1.3 when there are dangers of rupture because tensile or compression strength is exceeded [20]. If this is not the case, a more general rule states that the material factor should be no less than 1.1. Based on this information, the material factor for the ultimate strength analysis is set to be 1.3, for the fatigue analysis to be 1.2 and 1.1 for the tip deflection.

Finally, the blades and tower of the wind turbine are seen as a component of class 2, which means that they are seen as a "non fail-safe" structural components. For which the IEC document states: "whose failure may lead to the failure of a major part of a wind turbine" [20]. Because of this the consequence-of-failure factor is equal to 1 for the ultimate strength analysis, 1.15 for the fatigue analysis and 1 for the tip deflection.

Safety Factor	Ultimate Strength Analysis	Fatigue Analysis	Tip Deflection
γ_f	1.35	1.0	1.35
γ_m	1.3	1.2	1.1
γ_n	1.0	1.15	1.0
γ_{total}	1.755	1.38	1.485

Table 2.1: Safety factors used in the ultimate load analysis and fatigue load analysis.

2.4.3. Ultimate Load Analysis

To determine the ultimate loads, the design load cases need to be analysed. FASTTool outputs the moments subject on the wind turbine. These moments can firstly be analysed in an ultimate load analysis. In this analysis it is checked what the stresses on the wind turbine are, and if these stresses exceed the limit state.

The first step in doing the ultimate load analysis, is to translate the moments into stresses. This needs to be done both for the flap-wise and the edge-wise moments for the blade root, and for the fore-aft and side-side moments for the tower base. The stresses in flap-wise ($\sigma_{flap-wise}$), edge-wise ($\sigma_{edge-wise}$), fore-aft ($\sigma_{fore-aft}$) and side-side direction ($\sigma_{side-side}$) are calculated as:

$$\sigma_{flap-wise} = M_{flap-wise} \cdot \frac{y}{I} \tag{2.5}$$

$$\sigma_{edge-wise} = M_{edge-wise} \cdot \frac{x}{I} \tag{2.6}$$

$$\sigma_{fore-aft} = M_{fore-aft} \cdot \frac{y}{I} \tag{2.7}$$

$$\sigma_{side-side} = M_{side-side} \cdot \frac{x}{I} \tag{2.8}$$

in which M is the moment calculated by FASTTool, y and x equal half the outer diameter of the cylinder (assuming the tower or blade root is analysed) and I is the area moment of inertia. The inertia can be calculated based on the stiffness (K) of the material and the Young's Modulus of the material (E) as:

$$I = \frac{K}{E} \tag{2.9}$$

These stresses should then be compared to the ultimate stress of the material of which the blade or tower is made, while taking into account the safety factors determined in section 2.4.2. This can be done by the following relation:

$$\gamma_f \cdot \sigma_{max} \leq \frac{1}{\gamma_n \cdot \gamma_m} \cdot \sigma_{ultimate} \tag{2.10}$$

in which σ_{max} is the maximum stress subject on all three blade roots or on the tower base during the simulation and $\sigma_{ultimate}$ is the ultimate stress of the material.

It should be noted that only the maximum stress is used for each load case. As the stresses are mostly dominated by aerodynamic loads, the wind data set generated is of great influence on the maximum stresses. It is therefore necessary to run several simulations for the ultimate load analysis. As specified in the IEC document [31], for load cases with specified deterministic wind field events, the highest maximum of all the maxima computed is taken. For load cases with a turbulent inflow, the mean of all the maximum stresses is taken. Additionally, the document states that for DLC's 2.1, 2.2 and 5.1 the mean value of the largest half of the maximum loads needs to be used.

Besides the ultimate loads, also the tip deflection should be checked. As the tip deflection is connected to the loads, this is also of importance for the cases. The tip deflection is one of the outputs of the FASTTool model, and can thus directly be analysed. The tip deflection should be compared to the maximum allowable tip deflection while taking into account the safety factor using the following equation:

$$\gamma_{total,tip} \cdot y_{tip} \leq d_{max} \tag{2.11}$$

in which y_{tip} is the tip deflection during the simulation and d_{max} is the maximum deflection distance the tip can have before hitting the tower.

2.4.4. Fatigue Load Analysis

Besides the ultimate load analysis, the loads on the wind turbine should also be compared for fatigue damage. Fatigue damage occurs through the varying forces that are acting on the wind turbine during its lifetime. Therefore, the operational life of a wind turbine is influenced by the number of cycles it can take until failure.

Similarly to the ultimate load analysis in section 2.4.3, the fatigue on the wind turbine is calculated using the moments outputted by the simulation model. To do so, the same formulas (2.5, 2.6, 2.7 and 2.8) can be used. Differently from the ultimate load analysis, all stresses calculated are used; thus, not only the maximum stresses.

As the stresses on the wind turbine don't have a constant amplitude but a stochastic variation, the stress cycles need to be extracted from the seemingly random data. These cycles are determined using the rainflow counting method. The rainflow counting method is a commonly known method to do this. The rainflow counting algorithm from the Mathworks FileExchange is used in this research [33].

From these load cycles, the fatigue damage can be calculated. However, before doing so the allowed number of cycles at a certain stress amplitude should be determined. The allowed number of load cycles (N_j) can be calculated using the following equation:

$$N_j = (\frac{\Delta F_D}{\Delta F_j})^m \cdot N_D \tag{2.12}$$

in which ΔF_D is the load of the knee-point of the Wöhler Curve, ΔF_j is the applied load and N_D is the number of points until the knee-point of the Wöhler Curve. This knee-point is the point at which the loads have become to low and start a crack in the material.

Once both the number of cycles at a certain stress amplitude and the allowed number of cycles at that same stress amplitude have been calculated, these can be used to calculate the partial damage. The partial damage is calculated using Miner's rule. Miner's rule is based on partial damage and cumulative fatigue. The partial damage, d_j, can be calculated as:

$$d_j = \frac{n_j}{N_j} \tag{2.13}$$

in which n_j is the number of stress cycles at the j-th amplitude and N_j as in equation 2.13.

The cumulative fatigue damage is then the sum of all partial damages. The cumulative damage can be calculated for the 10-minute simulations, where after these damages can be converted to the total lifetime damage. The total damage calculated should be smaller than 1. If this value reaches 1 the material fails. The total damage, D, can calculated using the following equation:

$$D = \sum_j d_j = \sum_j \frac{n_j}{N_j} \leq 1 \tag{2.14}$$

When taking into account the safety factors for fatigue analysis from section 2.4.2, the criterion for the fatigue damage is described as:

$$D = \sum_j \frac{n_j}{N(\gamma_f \gamma_m \gamma_n \cdot S_j)} \leq 1 \tag{2.15}$$

in which S is the load range. The partial safety factors are thus applied to the load range [31].

The cumulative damage can also be captured in one representative number; namely, in the FDEL. The FDEL can be used to compare different fatigue loads with each other. The FDEL is calculated

using the following equation:

$$FDEL = (\frac{1}{N_{EQ}} \sum_j n_j \Delta S_j^m)^{\frac{1}{m}} \tag{2.16}$$

in which N_{EQ} is the reference number of equivalent cycles, m is the slope of the SN-curve and ΔS_j the load range at j. N_{EQ} is not a set variable, and can be changed according to the likes of the research.

If the FDEL is calculated using the load cycles corresponding to a 10-minute simulation for each wind speed in the operational range of the wind turbine with steps of 1 m/s, this FDEL for each wind speed can be used to calculate the FDEL over the entire lifetime of the wind turbine. From now on, this will be referred to as the lifetime FDEL. The lifetime FDEL makes it possible to compare all cases based on only one number. The lifetime assumed in this study is 20 years.

To calculate the lifetime FDEL, firstly, the number of occurrences for each wind speed in the operational range of the wind turbine with a wind step of 1 m/s in a 20 year lifetime is found. This is done by multiplying the probability of occurence for each wind speed, which can be found using the Weibull distribution, with the total number of 10 minute windows over 20 years. This gives the total number of 10-minute time frames for all wind speeds in the operational range of the wind turbine over a 20 year lifespan. The next step is to multiply the load cycles from the simulations with the number of 10-minute frames corresponding to the mean wind speed of the simulation the load cycle was found in. This gives the total number of load cycles at each stress range for the entire lifetime of the wind turbine. Finally, after determining the reference number of equivalent cycles, the lifetime FDEL can be calculated using equation 2.16.

3

System Description

This chapter provides an overview of the wind turbine system. Firstly, an overview of the overall system will be given. After this, the electrical grid the wind turbine is positioned in is motivated and the specifics for the grid frequency data set are given. Finally, the wind turbine itself will be chosen and its key design properties and controller specifics will be given. The controller overview includes the addition of a synthetic inertia and FFR controller.

3.1. Overall System

As was already mentioned shortly in the scope in section 1.5, the system in which this research is positioned is a large robust electrical grid. In this grid, the wind turbine supplies electricity either normally in the day ahead market, or the output power is increased or decreased to enable the supply of synthetic inertia and FFR. These ancillary services are introduced to help ensure a stable grid operation.

The wind turbine will be located offshore, as a large increase in offshore wind is expected [34]. Focusing on offshore wind turbines will therefore contribute to the relevance of the research. As the main grid criteria is that the wind turbine is connected to a large electricity grid, and measurements of the European grid are seen as most suitable, the wind turbine will be located in the North Sea close to the Netherlands. Apart from which grid the wind turbine is connected to, this has an influence on the wind and wave distribution.

3.2. The Electrical Grid

The electrical grid in which the system for this research is placed has a vast impact on the scenarios which will be simulated, as the synthetic inertia and FFR both respond to the grid frequency. The change in frequency is directly linked to the synchronous machines connected to the grid and the inertia these machines add to the system. When there is a sudden disturbance in the electrical grid, the frequency of the grid will change. The initial response of the system is mainly determined by the total inertia present in the grid [7].

The relationship between the power mismatch and the frequency deviation is defined by the swing equation as in the following equation:

$$\Delta P_m(t) - \Delta P_L(t) = 2H\frac{d\Delta f(t)}{dt} + D\Delta f(t) \tag{3.1}$$

where ΔP_m is the mechanical power change, ΔP_L is the load change, H is the inertia constant, Δf is the frequency deviation and D is the load damping coefficient. From this equation it can be seen that

the mismatch in power directly affects the grid frequency. Additionally, it shows that the inertia is able to limit the RoCoF and the damping affects the overall frequency difference.

Figure 3.1 shows the change in grid frequency after a contingency took place. A contingency resulting in a frequency change this big is mostly related to the breakdown of one of the generators. However, in a future grid with a different grid configuration these big frequency changes can take place also because of unexpected weather conditions in which the vRES in the energy system suddenly cannot supply power. From the frequency signal two main properties can be seen; these are the RoCoF and the frequency difference deviating from 50Hz. The RoCoF is the slope of the frequency at any point in time.

The figure demonstrates how high and low inertia in the system affects the RoCoF and the frequency difference of the system. A system with high inertia has a less steep RoCoF and lower frequency difference compared to a system with low inertia.
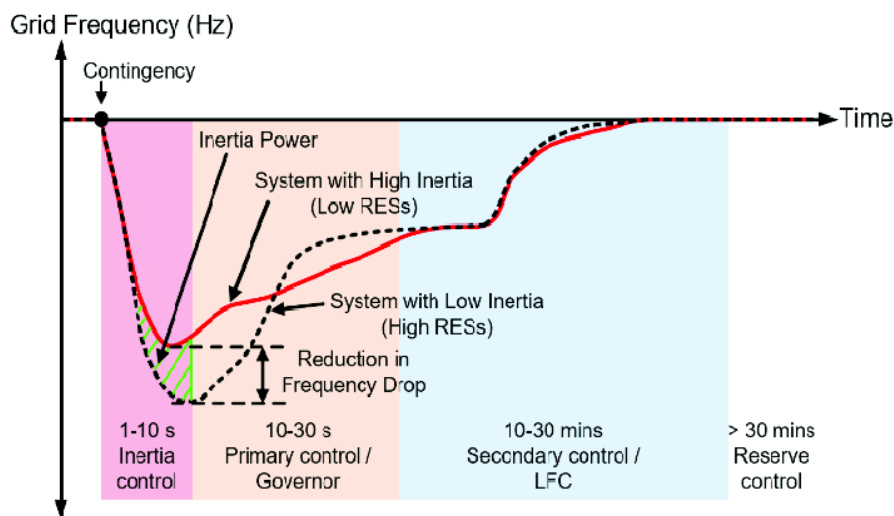
Figure 3.1: Grid frequency change for a system with high and low amount of inertia [35].

The grid data which will be used for the simulations is part of recordings made in 2021 for the entire year during research activities at the Wind Energy Technology Institute (WETI) at the Flensburg University of Applied Sciences [36]. Thus, the recordings are also taken in Flensburg, Germany, which is part of the Continental European Grid. The recordings have a resolution of 0.164 seconds (6.1 Hz) with a precision of 3 decimal places. This data-set therefore meets the two main requirements which were determined for the grid. It has a small timescale and is taken in a part of a large grid.

The frequency measurements available are from Germany. However, the assumption is made that the grid frequency measurements taken in Germany are representative for the entire grid. This is acceptable as it is most important that the grid behavior is similar to that of the chosen location. As the grid of Continental Europe is synchronous, the measured frequency at any point in the grid will be very similar to that measured in Germany. For this reason, the wind turbine studied can be placed at any location connected to this grid.

3.3. IEA 15-Megawatt Offshore Wind Turbine
3.3.1. Wind Turbine Choice and Key Design Properties
In order to generate relevant results, it is of importance to investigate a realistic wind turbine. Following the trends in offshore wind turbines, in 2020 the International Energy Agency (IEA) developed a reference turbine of 15 MW [25]. This reference turbine has proven to be of realistic capacity as Siemens

Gamesa developed a 14MW direct drive wind turbine which is operational, whereas Vestas has an operational prototype of a 15MW geared wind turbine [37], [38]. Adding to this, as this is an open source reference turbine, it has been used in several studies. Due to this, the turbine has been well documented. As the IEA15MW reference turbine is thus a relevant representation of cutting edge turbines and on the other hand is well documented, it is very suitable to be used in this research. The inputs for FASTTool are based on the description of the IEA for its 15-MW offshore wind turbine [25] and on the associated GitHub page [30]. An overview of the key design properties can be found in table 3.1.

Power rating	15	[MW]
Turbine class	IEC class 1B	[-]
Specific rating	332	[W/m^2]
Number of blades	3	[-]
Control	Variable speed Collective pitch	[-]
Design tip-speed ratio	9	[-]
Minimum rotor speed	5	[RPM]
Maximum rotor speed	7.55	[RPM]
Rotor diameter	240	[m]
Nacelle		
Hub length	7.94	[m]
Hub height	150	[m]
Hub mass	190	[t]
Hub overhang	11.35	[m]
Hub shaft Tilt angle	6	[deg]
Hub diameter	7.94	[m]
Nacelle weight total minus hub	630.888	[t]
Nacelle Length minus hub	3.945	[m]
Nacelle diameter minus hub	3.352	[m]
Drivetrain		
Gearbox ratio	1	[-]
Gearbox efficiency	100	[%]
Generator efficiency	96.55	[%]
Generator inertia	5681878	[$kg \cdot m^2$]
Controller		
Cut-in wind speed	3	[m/s]
Cut-out wind speed	25	[m/s]
Rated torque	21197000	[Nm]

Table 3.1: Key design properties of the IEA 15-MW Reference Turbine [25].

A key design property which is not included in [25], is the generator inertia. This is especially important when synthetic inertia will be modelled. As the inertia is not present in the documentation made by IEA, it should be estimated separately. The inertia of the generator can be estimated using the following equation:

$$I = \frac{1}{2}Mr_{gen}^2 \tag{3.2}$$

where M is the total mass and r is the outermost radius of the generator. The total mass of the generator is 372 [t] and the total radius can be calculated by adding the air-gap radius, the slot height and the stator yoke height. These values are available in the IEA documentation [25]. This results in a total radius of 5.527 [m] and an inertia of 5,681,878 [kg m^2].

3.3.2. IEA 15MW Wind Turbine Control

Control Overview

Before going into the individual control elements of the wind turbine, an overview of the entire control will be given. This can be found in figure 3.2.
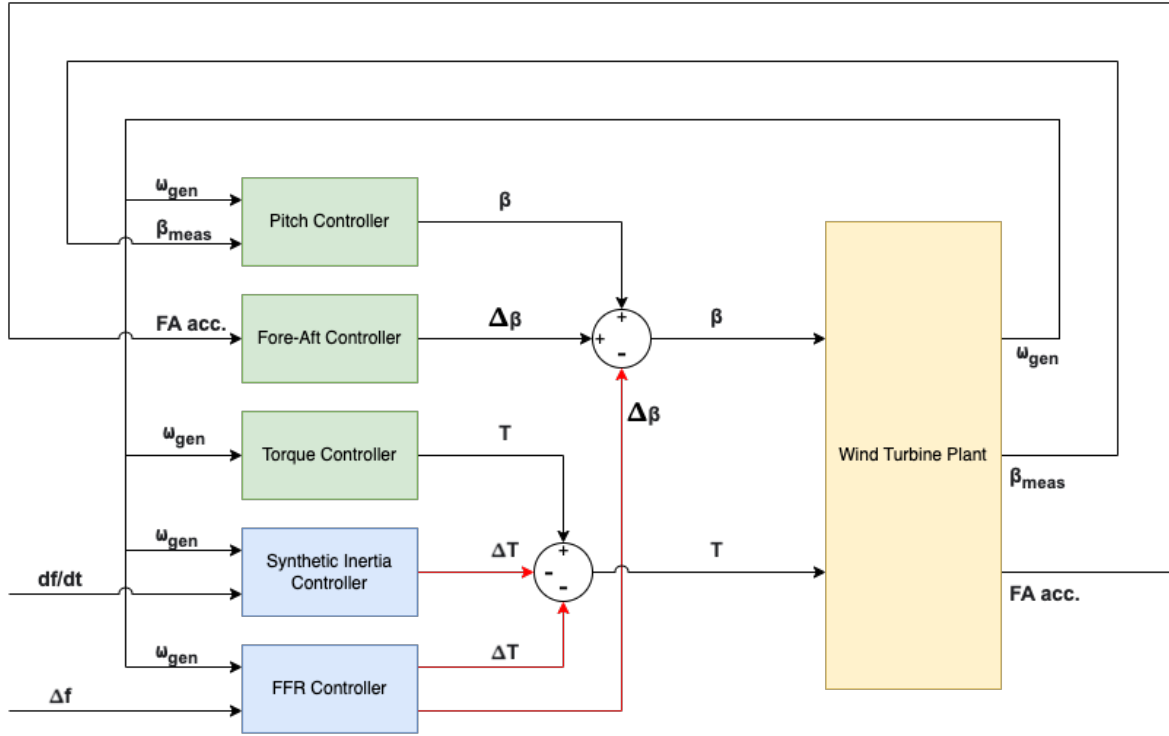
Figure 3.2: Overview of all controllers based on the controller implementation in FASTTool.

The figure firstly shows the baseline control of the wind turbine including the pitch controller, fore-aft controller and the torque controller. These are shown as green boxes in the figure. Furthermore, the additional synthetic inertia controller and FFR controller are shown in blue.

The inputs for the pitch controller are the measured generator speed, ω_{gen}, and the measured pitch angle, β_{meas}. The pitch controller outputs the blades pitch angle. Next, the fore-aft controller is used to damp the movements of the tower in the fore-aft direction. The fore-aft controller takes as an input the fore-aft acceleration, FA acc., and outputs a change in the pitch angle, $\Delta\beta$. The torque controller is the last controller of the baseline control. The torque controller gets the generator speed as an input, and outputs the torque demand.

The last two controllers are the synthetic inertia controller and FFR controller. The output of these two controller in figure 3.2 is red, as these are not used at the same time in this research nor are they used in the baseline control. The red lines can therefore be seen as optional. The inputs for the synthetic intertia controller are the generator speed and the RoCoF of the grid frequency, here denoted as df/dt. The synthetic inertia controller then outputs a change in torque demand, ΔT. The FFR controller gets the measured generator speed and the deviation in grid frequency, Δf, as inputs. The output of the FFR controller depends on the de-loading mechanism used. It always outputs a change in torque demand. Additionally, it outputs a change in the pitch angle if the wind turbine is de-loaded with a fine pitch angle above 0 degrees.

Baseline Control

In order to supply synthetic inertia and FFR, the control of the wind turbine needs to be modified. To understand the modifications required, the normal control of the IEA 15MW wind turbine is first discussed. The documentation of the IEA 15MW wind turbine describes 3 main control areas. The control areas can be referred to as the low wind speed area, the medium wind speed area and the high wind speed area. Both the low and medium wind speed ranges are at partial load of the wind turbine, the high wind speed range is when the wind turbine has reached rated power. The partial load range of the wind turbine is divided in the low and medium wind speed area to optimise the power generation at low wind speeds. At low wind speeds, i.e. between 3 and 6.98 m/s, the wind turbine operates at its minimum rotor speed (5 rpm). The rotor speed is kept constant by a PI controller on the generator torque and a scheduled pitch. Next, above 6.98 m/s but below the rated wind speed (medium wind speed range), the wind turbine operates at its optimum tip speed ratio to maximise the power coefficient. Finally, above the rated wind speed (high wind speed range), the rotor speed is controlled by a PI controller on the pitch angle while keeping the torque constant.

Even though it is very logical that the 15MW wind turbine is designed to generate as much power as possible while ensuring the integrity of the structure, the division of the partial load range into a low and medium wind speed area adds additional complexity to the modelling which is not necessary for the purpose of this research. In this system the partial load range is therefore not divided into two separate control areas, and is fully controlled by the torque controller. The torque controller follows the optimal power curve on the torque-speed curve using the generator speed as an input. In doing so, the turbine is able to stay close to the optimal power coefficient over a wide variety of wind speeds.

Above rated wind speed, the rotor speed is controlled by a PI controller with scheduled gains, just as described in the document for the 15 MW reference turbine. An overview for the pitch controller can be found in the block diagram in figure 3.3. The pitch controller uses a feedback loop, in which the measured generator speed, ω, is subtracted from the reference generator speed, ω_{ref}, to get to the error, ω_{error}, which is then fed into the PI controller alongside the measured blade pitch angle, β_{meas}. In the feedback loop a low-pass filter and a notch filter are used to filter out unwanted measurements. The PI-controller then outputs a pitch angle setting, which is inputted into the turbine plant.
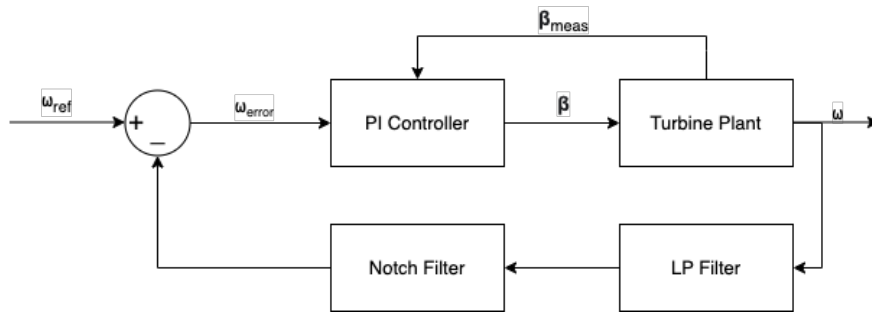
Figure 3.3: Pitch controller block diagram using a PI controller. The feedback loop of the controller incorporates both a notch filter and a low-pass filter. Based on [39].

Lastly, a fore-aft damping controller is used to damp the fore-aft movements of the tower. Damping the fore-aft movements of the tower can have a positive effect on the lifetime of the tower of the wind turbine.

Synthetic Inertia Control

In order to supply synthetic inertia with a wind turbine, an extra controller should be added to the overall control. This controller will be called the inertial controller. The inertial controller needs the RoCoF of

the electrical grid as an input. It then outputs an addition or subtraction from the torque set point of the general torque controller. The exact working of the inertial controller is elaborated upon in section 4.2.

The inertia controller is active both below and above rated power. This is possible, as the power change is extracted from or put into the inertia of the wind turbine rotor. By doing so, the otherwise decoupled inertia of the wind turbine is synthetically added to the grid frequency. Supplying synthetic inertia could thus help increase the system inertia of a electric grid with a high penetration of RES. The increased system inertia results in higher grid stability and better frequency regulation.

Fast Frequency Response Control

Unlike the inertial controller, the controls for FFR do not respond to the derivative of the grid frequency, but to the difference between the measured grid frequency and the nominal value. The controller corresponding to the supply of FFR will be called the FFR controller from now on. Similarly to the inertial controller, the FFR controller is also a controller which needs to be added separately to the wind turbine.

An important difference between the supply of synthetic inertia and FFR, is that for supplying FFR the de-loaded operation of the wind turbine is required. This is because synthetic inertia is supplied directly from the inertia present in the rotors and FFR requires a longer energy supply which is not proportionally linked to the rotational speed of the rotors. De-loading of the wind turbine is not determined by the FFR controller itself, but is changed in the design properties of the torque and pitch controller. The exact working of the FFR controller is elaborated upon in section 4.3.

Similar to the inertial controller, the FFR can be active both below and above rated wind speed. However, as the FFR controller does not react proportionally to the RoCoF, but reacts to the difference in grid frequency, more freedom exists in the design of the FFR controller. This allows the FFR controller to supply energy as a primary frequency response.

4

Controller Design

This chapter will describe the design of the controllers needed in the case study to investigate the normal operation of the wind turbine, as well as the controllers needed to supply synthetic inertia and FFR. This will firstly be done by describing the general input parameters of the baseline controller, as well as the torque and pitch controller used in the baseline controller. After this the synthetic inertia controller and the FFR controller design will be given. As supply of FFR needs the wind turbine to be de-loaded, two de-loading strategies will be explained. Finally, a model validation will be given.

4.1. Baseline Controller
4.1.1. General Input Parameters
As previously mentioned in chapter 3, the IEA15MW reference turbine is used in FASTTool as the baseline controller. The FASTTool model used is the main version developed and used at the TU Delft. The FASTTool inputs needed for the airfoil, blade, tower, nacelle and drive train design are derived from the IEA documentation on the 15MW reference turbine [25], or from the connected GitHub database [30]. In the GitHub database several projects are listed which give their input parameters for the IEA15MW reference turbine. After inputting these parameters, a rotor performance as in figure 4.1 is found. In this figure the power coefficient for different tip speed ratios is portrait at different pitch angles. The curves are developed using FASTTool.
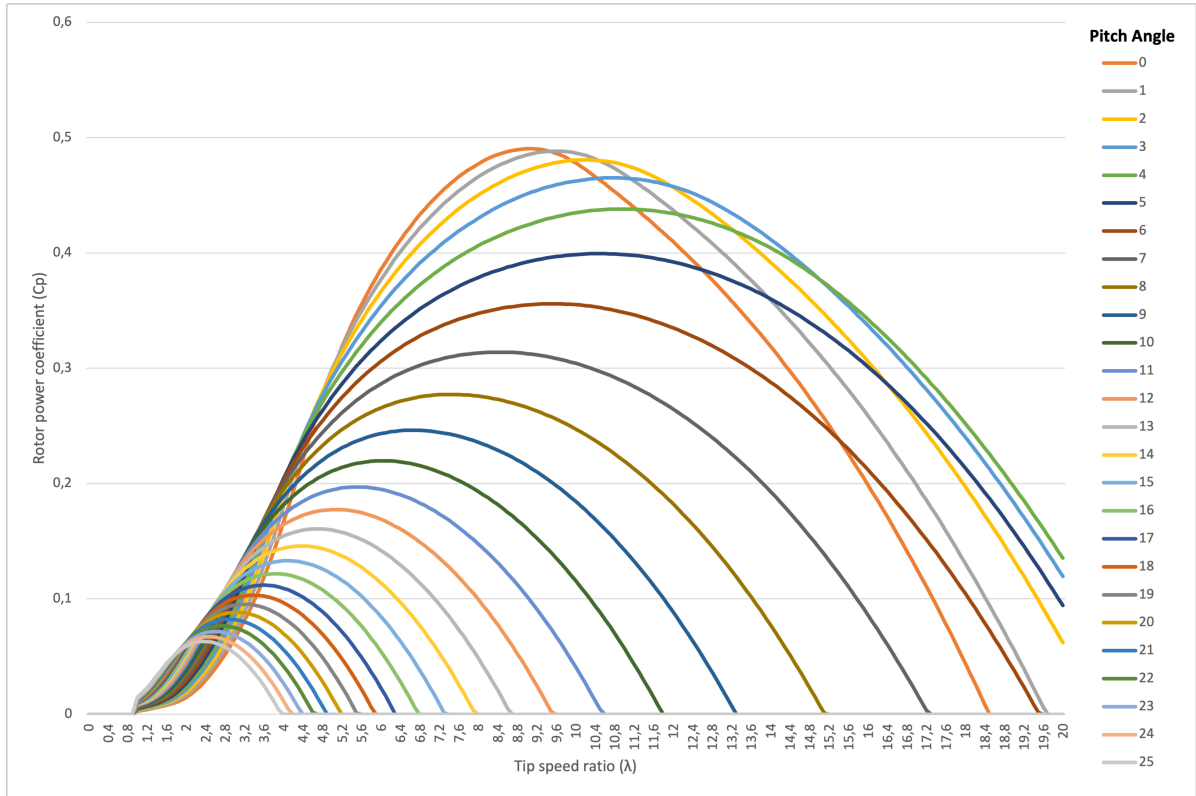
Figure 4.1: Power coefficient curve for different tip speed ratios showing the rotor performance at different pitch angles.

Besides these physical inputs for the wind turbine, the simulation model also needs inputs for both the pitch, torque and fore-aft damping controller. Part of the inputs, such as the maximum and minimum pitch angle and the torque limit and minimum torque are available in the documentation. However, the other inputs, such as the scheduled gains for the pitch controller and the optimal mode gain for the torque controller, still need to be determined. The torque, pitch and fore-aft controller will be elaborated upon in section 4.1.2, section 4.1.3 and section 4.1.4 respectively.

4.1.2. Torque Control

As was already introduced in section 3.3.2, the baseline control below rated wind speed is fully controlled by the torque controller. For this reason, the torque control in the baseline controller will not incorporate a scheduled pitch at low wind speeds as in [25], but will stay at the fine pitch angle (0 for the baseline controller) and follow a sub-optimal line over the torque-speed curve. This can be found in figure 4.2 below.
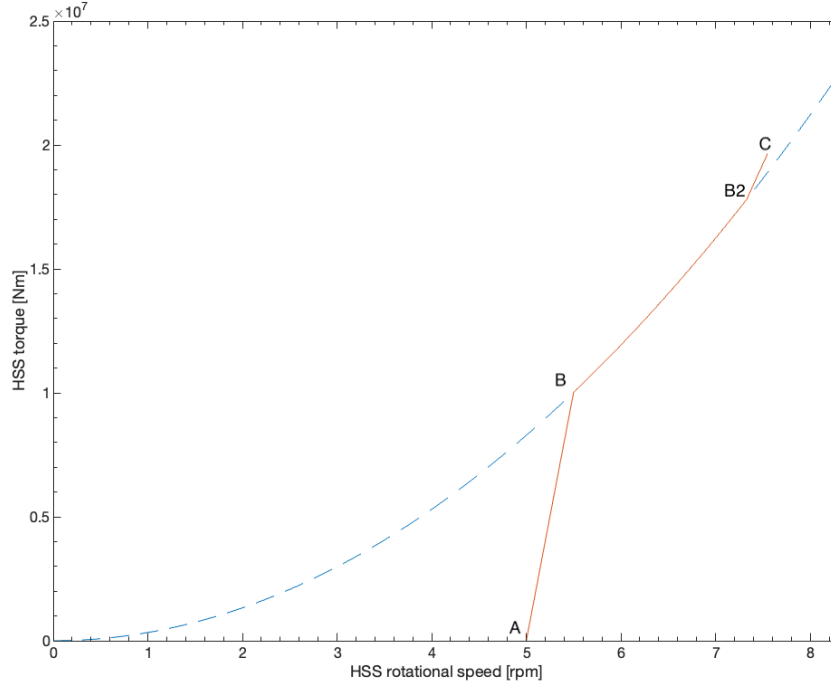
Figure 4.2: Torque-Speed curve of the basic wind turbine model.

Because the torque controller uses this simplified control, the torque-speed curve has a steep curve from point A, the minimum rotational speed which is equal to 5 RPM, to point B, the first point from where the torque controller follows the optimum generator torque line which is 5.5 RPM.

Between point B and B2 on the torque-speed curve, 5.5 RPM and 7.33 RPM respectively, the torque controller follows the optimum generator torque curve which is related to the generator rotational speed. This relationship is determined based on the following equation:

$$\tau_{gen} = K_{opt}\omega_{gen}^2 \tag{4.1}$$

where τ_{gen} is the generator torque, K_{opt} is the optimal mode gain and ω_{gen} is the generator rotational speed. K_{opt} for the 15MW wind turbine has been determined to be **30221628** $Nm/(rad/s)^2$.

Above rated wind speed, the torque controller sets a constant torque, which is point C in figure 4.2. Besides the torque, also the generator speed remains constant at point C. This is done using the pitch controller, which will be elaborated upon in the next section.

4.1.3. Pitch Control

The pitch controller implemented in FASTTool is a gain scheduled PI controller. The pitch controller is active above rated wind speed. The PI controller is a controller consisting of a proportional and an integral part. In general the transfer function of a PI controller is given by [40]:

$$C(s) = K_p + \frac{K_i}{s} \tag{4.2}$$

where K_p is the proportional gain and K_i is the integral gain. Because of the non-linear nature of a wind turbine, a linearised model is needed to design the pitch controller. The pitch control is highly non-linear since the rotor aerodynamic torque is non-linearly dependent on the rotor blade pitch angle and wind

speed [41]. To design the gain scheduling for the pitch controller, the wind turbine is linearised for all wind speeds above rated wind speed with wind speed steps of 1 m/s. The linearisation is performed using the linearisation tool in FASTTool. For each step in the linearisation, a pitch angle is determined. In order for the controller to quickly converge to the right pitch angle, the gain values of the PI controller are adjusted for each pitch angle present in the linearised model of the wind turbine.

In general, the gains are chosen such that the controller meets three main criteria related to the gain margin, phase margin and crossover frequency. To properly understand these criteria, the gain margin, phase margin and crossover frequency will firstly be explained using the final loop gain corresponding to a pitch angle of 3.897, which can be seen in figure 4.3.
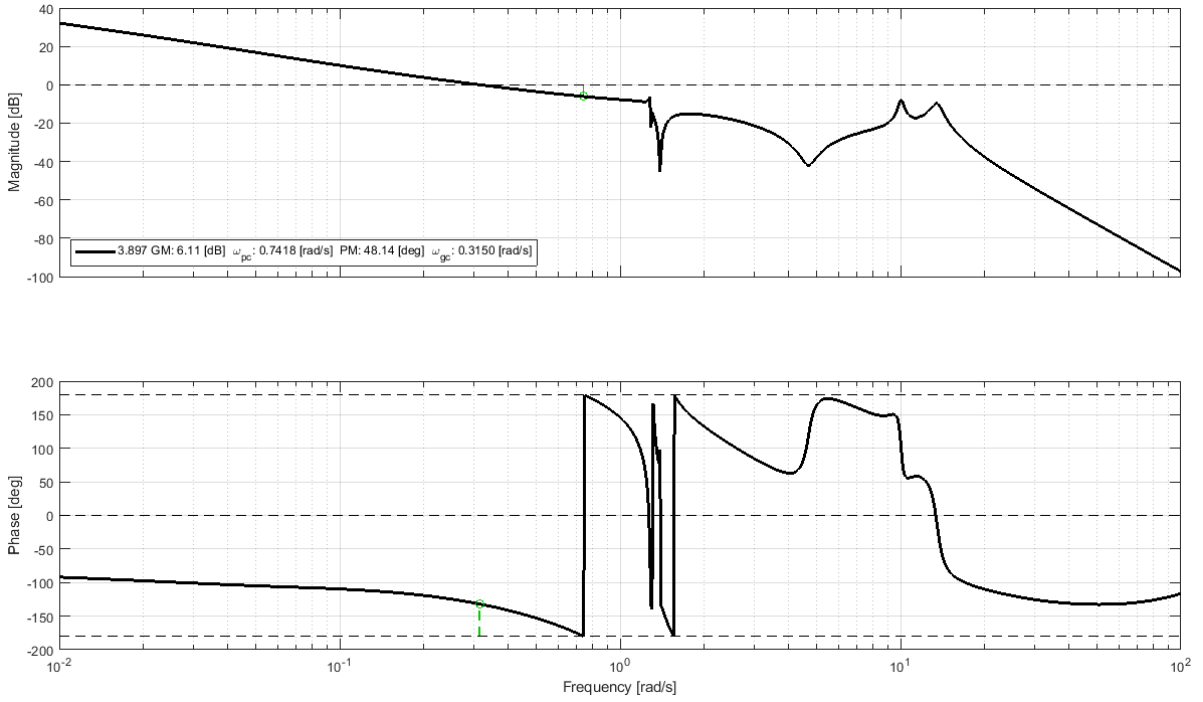
Figure 4.3: Bode diagram showing the tuned loop gain for a pitch angle of 3.897 degrees.

The gain and phase margin are used in control to ensure that there are certain stability margins that describe how stable the system is and how robust it is to disturbances [40]. The phase and gain margin can be extracted from the bode plot. The gain margin is the difference between the 0 dB line at the point of the phase crossover frequency. This is the frequency where the phase reaches -180 degrees. The gain margin gives information on the stability of the closed loop system in the sense that it can be seen as the factor by which the open loop gain can be increased while the closed loop system maintains stable [42]. The gain margin in figure 4.3 can be seen in the top part at the green line. For the bode diagram at a pitch angle of 3.897 degrees, the gain margin is equal to 6.11 dB. Next, the phase margin is the difference between the -180 dB line at the point of the gain crossover frequency. This is the frequency where the gain crosses the 0 dB line. The phase margin also gives information on how close the system, in this case the controller, is to unstable behavior [42]. However, the phase margin does not provide direct information on how much the gain can be increased while ensuring stability [42]. The phase margin in figure 4.3 can be seen in the bottom part, at the green line. The phase margin here is 48.14 degrees. Lastly, the crossover frequency of interest is the frequency at which the gain crosses the 0 dB line. The crossover frequency determines the tracking response of the controller. In figure 4.3, the crossover frequency is 0.3150 rad/s.

The first criterion the controller should meet is that the phase margin should be between 30 and

60 degrees [40]. However, a higher phase margin will ensure that the response of the controller is less oscillatory. Secondly, the lowest acceptable gain margin is usually between 1.6 and 3.5 dB [42]. For the design of this pitch controller, a minimum of 3 dB would be acceptable to ensure a stable response of the controller. The third and final criterion used is to ensure an acceptable crossover frequency. As the crossover frequency of the IEA 15MW turbine is not yet known, it is derived from another reference turbine, the NREL 5MW [43], where the crossover frequency is set to 0.6 rad/s. As it is not possible at low pitch angles to satisfy both the phase and gain margin criteria while maintaining a crossover frequency of 0.6 rad/s, the crossover frequency is scaled by $\frac{1}{R}$, where R is the rotor radius of the wind turbine. This is considered acceptable, as with increasing rotor radius it is considered acceptable for the pitch controller to have a slightly slower response. We then get the following crossover frequency:

$$
\begin{aligned}
\frac{\omega_{new}}{\omega_{ref}} &= \frac{R_{ref}}{R_{new}} \\
\frac{\omega_{new}}{0.6[rad/s]} &= \frac{63[m]}{120[m]} \\
\omega_{new} &= 0.315[rad/s]
\end{aligned}
\tag{4.3}
$$

where ω_{new} is the new crossover frequency for the IEA 15MW turbine, ω_{ref} is the reference crossover frequency of the NREL 5MW turbine, R_{ref} is the reference of radius of the NREL 5MW turbine and R_{new} is the rotor radius of the IEA 15MW turbine.

A minimum crossover frequency of 0.315 rad/s is therefore used for this controller. An important change compared to the NREL 5MW turbine is that the crossover frequency is no longer a constant value, but increases linearly as at higher pitch angles it is possible to have stable gain and phase margins while also having a crossover frequency closer to 0.6 rad/s.

Next to the PI controller, both a low-pass filter and two notch filters are used. The low-pass filter and the notch filters are used to filter the reference generator speed, which is used to calculate the generator speed error which is fed into the PI-controller. The low-pass filter is used to reduce the output at high frequencies. The low-pass filter used for each pitch angle is a first order low-pass filter with a cut-off frequency of 3 rad/s. This was found to be sufficient in ensuring stability. The low-pass filter frequency response can be seen in figure 4.4.
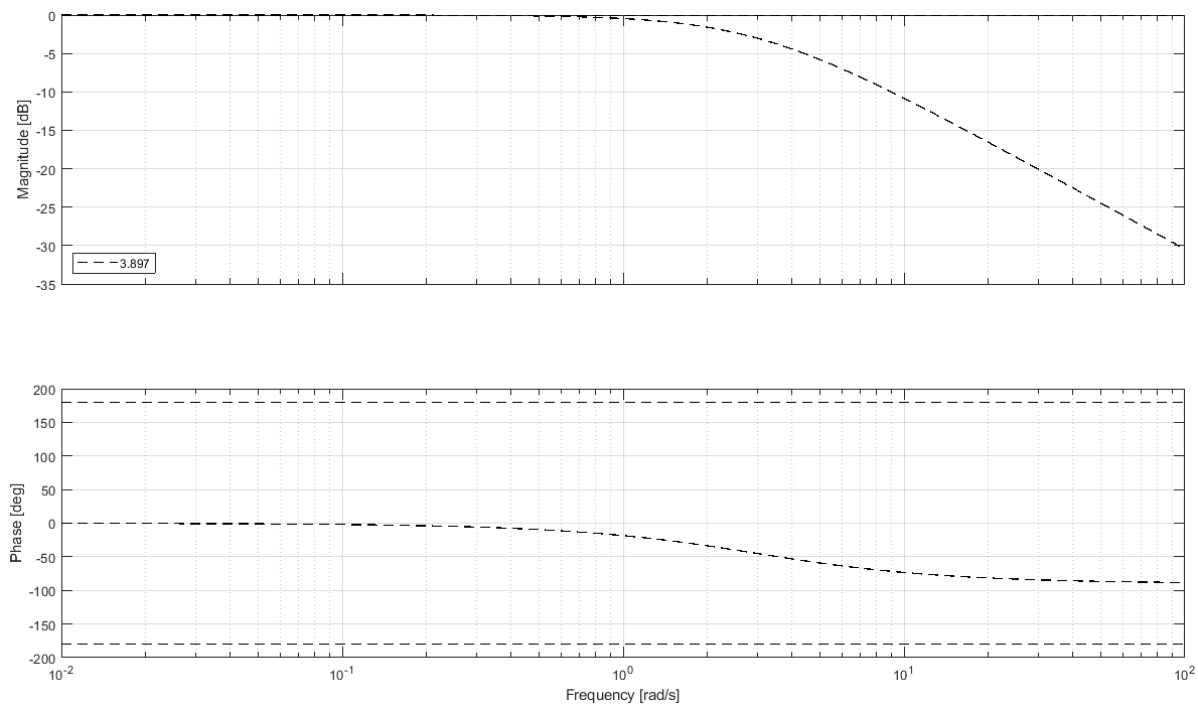
Figure 4.4: Low-pass filter of 3 rad/s.

The notch filters are used to filter out specific peaks which may lead to instability. To show the need for a notch filter in the pitch controller, the bode plot of the loop gain corresponding to a pitch angle of 3.897 degrees will be shown similar to figure 4.3. However, in this figure the notch filters are not included. The loop gain without the notch filters can be found in figure 4.5.
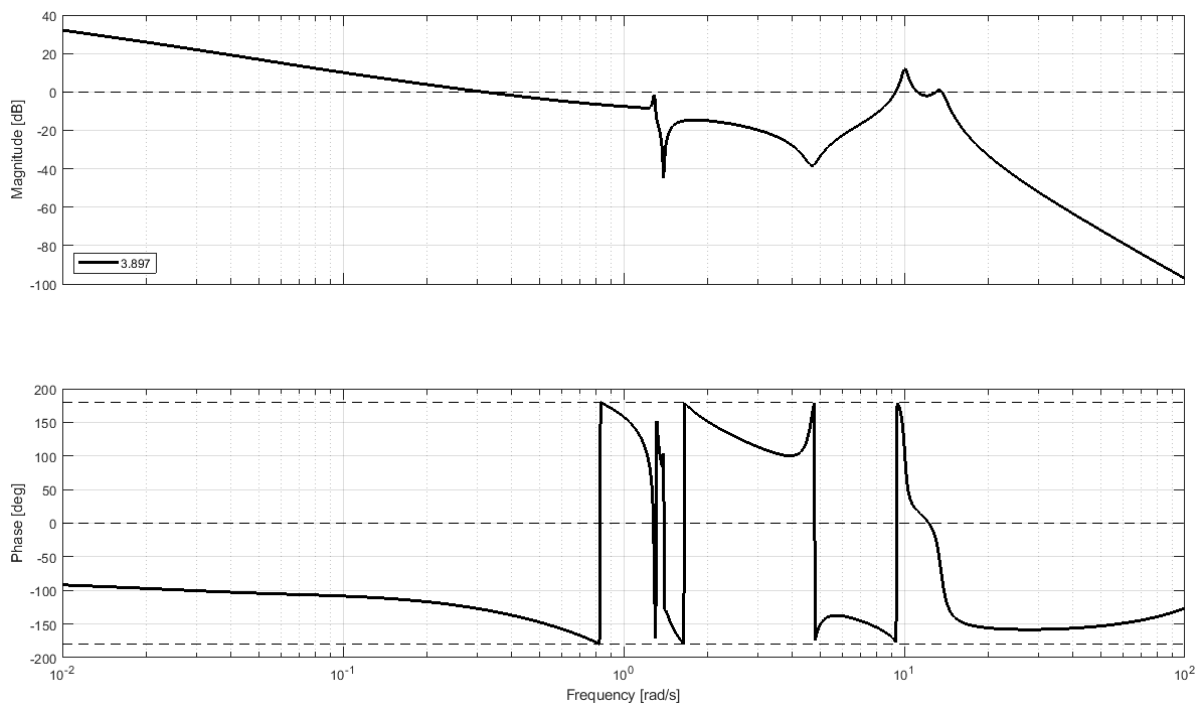
Figure 4.5: Bode diagram showing the loop gain at a pitch angle of 3.897 degrees without notch filters.

As can be seen in the figure, the bode plot shows two peaks that show a gain either approaching the 0 dB line very close, or even crossing the 0 dB line at multiple locations. The first peak is located at 1.289 rad/s. This is a very narrow peak; for this reason the notch filter coefficients have been chosen as $\beta_1 = 0.001$ and $\beta_2 = 0.01$. The second peak, which could also be seen as two peaks, is located around 10.07 rad/s and is much wider than the first peak. For this filter the notch coefficients which are used are $\beta_1 = 0.1$ and $\beta_2 = 1$. Combining these two notch filters gives the bode plot as in figure 4.6.
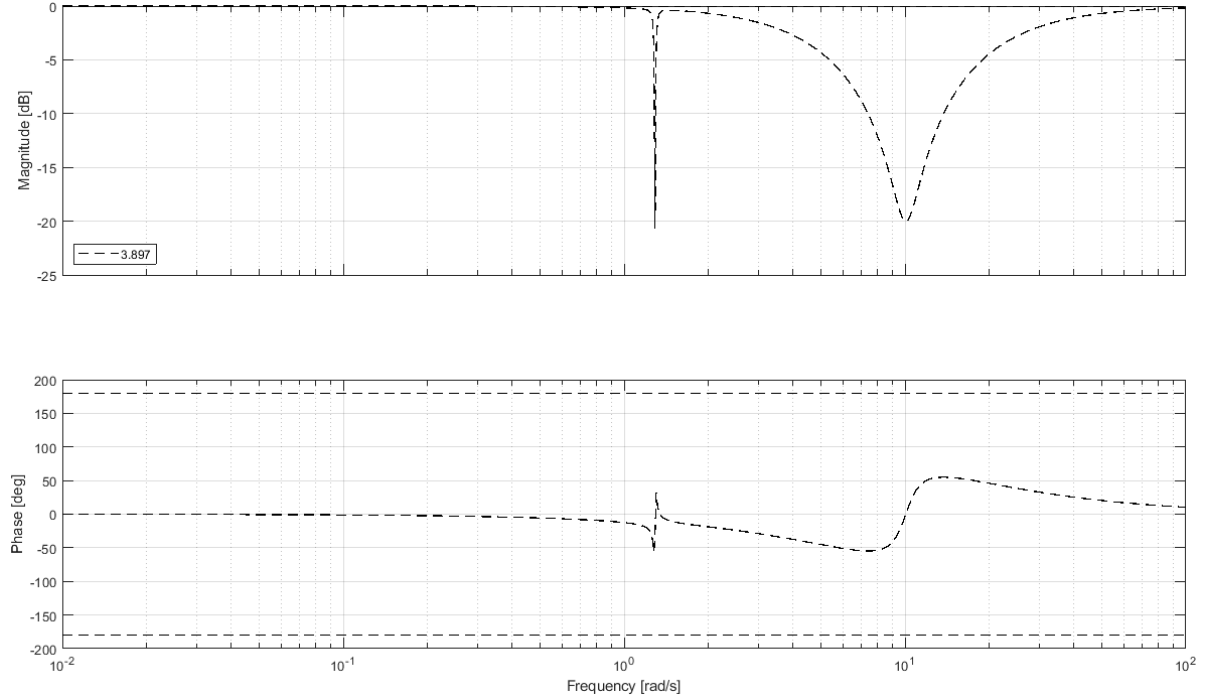
Figure 4.6: Notch filter at 1.289 rad/s, with coefficients $\beta_1 = 0.001$ and $\beta_2 = 0.01$, and at 10.07 rad/s, with coefficients $\beta_1 = 0.1$ and $\beta_2 = 1$.

The proportional and integral gain are scheduled for each pitch angle such that the criteria for the gain margin, phase margin and crossover frequency are complied with. The final gain scheduled pitch controller can be found in table 4.1 below, where K_p is the proportional gain, K_i is the integral gain, GM is the gain margin, PM is the phase margin and ω_c is the crossover frequency.

Pitch	K_p	K_i	GM [dB]	PM [deg]	ω_c [rad/s]
3.8970	-1.7018	-0.1000	6.11	48.14	0.3150
6.6650	-1.1095	-0.1050	8.78	52.48	0.3300
8.6640	-0.8860	-0.1100	9.85	53.42	0.3450
10.3600	-0.7590	-0.1150	10.42	54.08	0.3600
11.8700	-0.6776	-0.1200	10.73	54.88	0.3750
13.2600	-0.6190	-0.1250	10.88	55.78	0.3900
14.5600	-0.5752	-0.1300	10.94	56.76	0.4050
15.7900	-0.5416	-0.1350	10.89	57.84	0.4200
16.9700	-0.5172	-0.1400	10.80	59.07	0.4350
18.1000	-0.4960	-0.1450	10.61	60.27	0.4500
19.1800	-0.4764	-0.1500	10.42	61.51	0.4650
20.2400	-0.4637	-0.1550	10.18	62.86	0.4800
21.2600	-0.4580	-0.1600	9.85	64.30	0.4951
22.2600	-0.4501	-0.1650	9.58	65.77	0.5100
23.2300	-0.4448	-0.1700	9.30	67.21	0.5250

Table 4.1: Scheduled gain for the PI controller of the basic wind turbine.

The PI control, low-pass filter and notch filters are combined and result in the bode diagram which can be seen in figure 4.7.
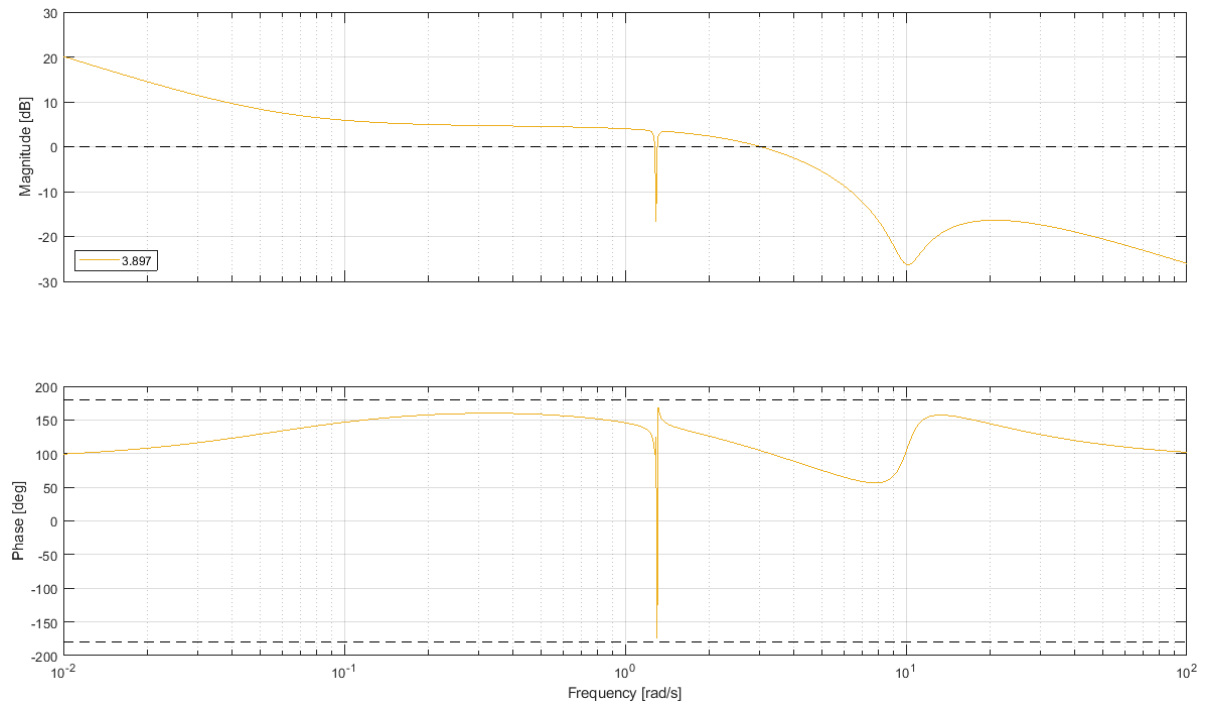
Figure 4.7: Combination of the PI controller, low-pass filter and two notch filters.

Combining this with the plant, which is the wind turbine model, in order to see what the frequency response of the combined system with the gain scheduled controller is. This results in the loop gain of figure 4.8. This can be used to evaluate the frequency response of the entire system. In the green lines in the top part of this figure, it can be seen that the gain margins are all close together. As it is hard to read of, the exact values can also be seen in table 4.1. Next, the green lines in the bottom half of the

figure show the phase margins. The phase margins also show the location of the crossover frequencies, which are linearly increasing.
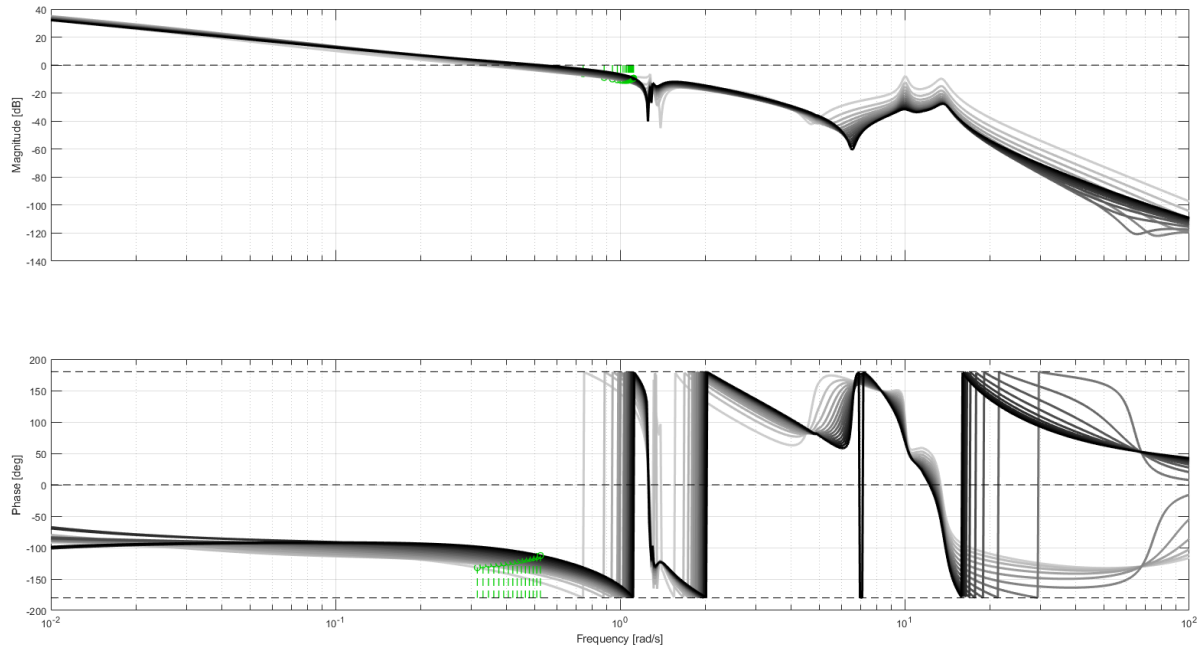
Figure 4.8: Loop gain after applying the scheduled gain.

4.1.4. Fore-Aft Control

Additionally to the torque and pitch control, the baseline controller also includes a fore-aft damping controller. In FASTTool, the fore-aft tower acceleration is integrated to get the speed. This speed is then multiplied with the gain of the fore-aft controller, which determines the change in pitch angle. This change in pitch angle damps the tower movement.

The gain of the fore-aft controller is the only variable in this controller. In order to evaluate the gain of the fore-aft damping controller, different gains are compared in both the time and the frequency domain. For each gain, a stepped simulation is performed for the above rated wind speeds (10 to 25 m/s). This is done for the gain values of 0, 0.01, 0.025, 0.05, 0.075, 0.1, 0.125, 0.2 and 1. This has shown that a higher gain results in more damping of the tower. This is valid until a certain point, as the damper will at some point run into the maximum pitch rate of the wind turbine. These simulations clearly show that a gain of 1 does not show desired behavior. However, for the other gains the simulations do not show a clear difference between the gains 0.05, 0.075, 0.1, 0.125 and 0.2. The responses are therefore also evaluated in the frequency domain. The simulation output of the tower acceleration can be found in figure A.1, and the output of the pitch angles can be found in figure A.2.

To get to the frequency domain for the tower acceleration spectrum, the square of the absolute value of the Fast Fourier Transform is taken. For the pitch angle spectrum, only the absolute of the Fast Fourier Transform is taken. It was seen that a gain of 0.125 shows the preferred response as this gain ensures the lowest damping amplitudes which is around $5 \cdot 10^5 \ m^2/s$. The pitch angle spectrum does not show any difference, and therefore no objections, for a gain of 0.125 compared to the lower gains. The tower acceleration spectrum can be found in figure A.3, whereas the pitch angle spectrum can be found in figure A.4.

4.2. Synthetic Inertia Controller

To emulate the inertia of the wind turbine as synthetic inertia, the kinetic energy stored in the rotating mass needs to be utilised. The power available in the rotors of the wind turbine can be calculated by taking the derivative of the kinetic energy at any rotational speed ω[9]:

$$P = \frac{dE_k}{dt} = I \cdot \omega \cdot \frac{d\omega}{dt} \tag{4.4}$$

where E_k is the kinetic energy, I the total inertia of the wind turbine and ω the mechanical rotational speed of the generator. In electrical power engineering, the inertia constant H is used [44]:

$$H = \frac{I\omega_s^2}{2S} \tag{4.5}$$

in which S is the nominal apparent power of a certain generator. By substituting this in the above equation, we get:

$$\frac{P}{S} = 2H \cdot \frac{\omega}{\omega_s} \cdot \frac{d[\frac{\omega}{\omega_s}]}{dt} \tag{4.6}$$

If $\overline{P}$ and $\overline{\omega}$ are the per-unit quantities of power and rotational speed, we can derive $\overline{P}$ as:

$$\overline{P} = 2H \cdot \overline{\omega} \cdot \frac{d\overline{\omega}}{dt} \tag{4.7}$$

And the per-unit torque can be written as:

$$\overline{T} = 2H \cdot \frac{d\overline{\omega}}{dt} \tag{4.8}$$

In a wind turbine, the torque controller maximises the power output at a certain generator rotational speed (ω_{gen}). To mimic inertia, a value is added to the torque set-point proportional to the RoCoF of the grid frequency. This value could corresponds to equation 4.8, as this is the torque that can be extracted from the rotating mass of the wind turbine. This will cause the rotors to slow down and thus extract the kinetic energy. However, because the rotational speed of the wind turbine generator is decoupled from the grid, the addition to the torque control in equation 4.8 is not calculated proportional to the rotational speed of the generator, but to the RoCoF of the grid frequency.

A problem which then arises with using function 4.8 to calculate the change in torque, is that due to the constant gain of 2H the power extracted from the rotors is not dependant on the rotor speed of the wind turbine. Because of this there is a trade-off between a high value for 2H with the risk of stalling the wind turbine, and a low value for 2H in which the torque addition could be low compared to the amount of kinetic energy available in the rotors of the wind turbine. To solve this problem, this research uses the gain K as proposed in [22] and [45]. By using this approach, the change in torque demand is dependant on the rotational speed of the wind turbine. As a result the wind turbine releases more synthetic inertia at higher rotor speeds and less at lower rotor speeds.
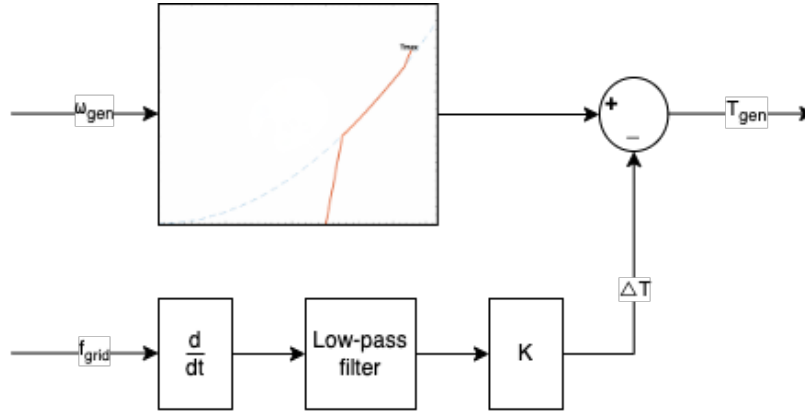
Figure 4.9: Control scheme of the synthetic inertia controller.

The control scheme for the inertial controller is given in [9] and can be found in figure 4.9. As can be seen in the control scheme in figure 4.9, the torque controller, in the top part of the control scheme, follows the optimum torque curve on the torque-speed curve as explained in section 4.1.2. Additionally, the synthetic inertia controller reacts proportionally to the RoCoF of the grid frequency with an addition to the torque controller. This addition to the torque control will be referred to as ΔT. ΔT is then calculated using the following equation [22], [45]:

$$\Delta T = -K_{in} \cdot \frac{df_{grid}}{dt} \tag{4.9}$$

where K_{in} is the inertial gain and f_{grid} is the measured grid frequency.

In order to limit the mechanical drive train loads, a first-order low pass filter is included in the control [9]. The low-pass filter used has a cut-off frequency of 1 rad/s. Next, the inertial gain K_{in} used in this approach is dependent on ω_{gen} which is calculated as:

$$K_{in} = K_0(\omega_{gen}^2 - \omega_{min}^2) \tag{4.10}$$

where K_0 is a proportional constant which can be set to different values according to the amount of synthetic inertia the wind turbine needs to supply, ω_{gen} is the measured generator speed (per unit) and ω_{min} is the minimum generator speed (per unit). K_0 is used as a variable in the case studies and will therefore be specified later. ω_{min} is set to 0.57 based on comparable values in [22] and [45].

4.3. Fast Frequency Response Controller

4.3.1. De-loading Strategies

In order for the wind turbine to actively supply energy as primary frequency control, the de-loaded operation of the wind turbine is needed. De-loading of the wind turbine can be done by either overspeeding the wind turbine or by adjusting the active output power by pitching the blades. Overspeeding the wind turbine is best below rated power, whereas de-loading by pitching is done at and above rated power [46].
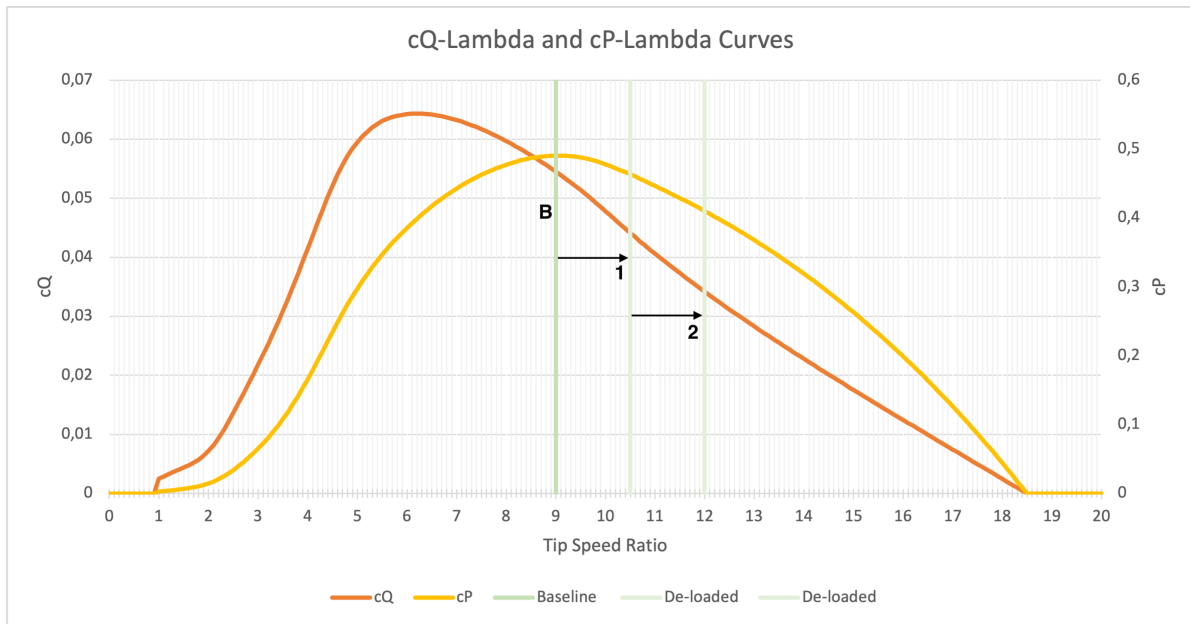
Figure 4.10: C_P-λ and C_Q-λ curves for the IEA 15MW turbine showing the baseline operation at a design tip speed ratio of 9, as well as two de-loaded operations.

During overspeeding, the operating point at the torque-speed curve is translated to the right hand side of the nominal curve. This is depicted in figure 4.10. This figure shows both the power coefficient (C_P) - tip speed ratio (λ) curve, and the torque coefficient (C_Q) - tip speed ratio (λ) curve for the IEA 15MW wind turbine at a pitch angle of 0 degrees. In the baseline operation, the wind turbine operates at its optimal tip speed ratio. This is at a tip speed ratio of 9, which is denoted with line B in figure 4.10. The points where line B crosses the power coefficient and torque coefficient curve shows the operating points at these curves. When the wind turbine is de-loaded, its torque demand is decreased. Due to the decreased torque demand, the torque coefficient drops and the wind turbine operates at a point to the right of the baseline operation. Because of this shift to the right, the tip speed ratio increases. In the graph, two de-loaded operations are highlighted. These correspond to line 1 and line 2. As the tip speed ratio increases, the operating point at the power coefficient curve also shifts to the right. The result of this is that the wind turbine operates at a lower power coefficient and thus at a lower power. As can be seen in figure 4.10, a bigger decrease in torque (and thus in the torque coefficient) results in a higher tip speed ratio and subsequently in a lower power coefficient. Hence, the power coefficient at line 2 in the graph is lower than the power at line 1. It is clear from this behavior that the operating point on the torque curve can be influenced by the torque controller.

In figure 4.11 the torque-speed curves for the IEA15MW reference turbine can be found for different wind speeds. The figure shows both the maximum power curve, as well as the operation of the turbine operating points corresponding to a de-loading to 90% of the nominal output power. Next sections will show how the calculations are done to achieve this deloading of 90%. Due to the over speeding, the maximum rotational speed of 7.55 RPM is reached not at a wind speed of 10.55 m/s, but somewhere between 8 and 9 m/s.
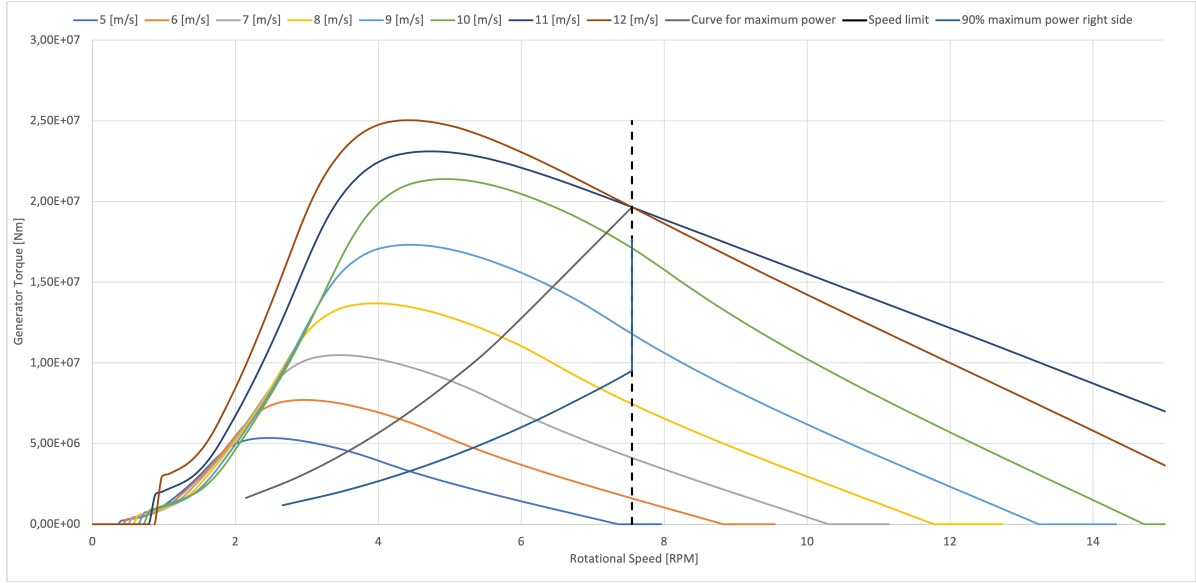
Figure 4.11: Torque-Speed curve of the IEA15MW Reference Turbine showing the maximum power curve as well as the de-loaded operation at 90% power by over speeding the turbine for different wind speeds.

Two strategies for de-loading the wind turbine in FASTTool are investigated and will be elaborated upon in the rest of this section. It should be noted that for each de-loading strategy the scheduled gains for the pitch controller should be determined again for the lower demanded torque at the newly designed point C. The adjusted gains for the 10% de-loaded wind turbine can be found in table 4.2.

Pitch	Kp	Ki	GM [dB]	PM [deg]	omega [rad/s]
5.2610	-1.7708	-0.1000	6.02	46.37	0.4000
7.5810	-1.3117	-0.1050	7.77	50.91	0.4170
9.4050	-1.0882	-0.1100	8.64	52.86	0.4330
10.9900	-0.9567	-0.1150	9.11	54.16	0.45
12.4300	-0.8646	-0.1200	9.38	55.20	0.4670
13.7600	-0.7959	-0.1250	9.56	56.27	0.4830
15.0200	-0.7435	-0.1300	9.64	57.23	0.5000
16.2100	-0.7032	-0.1350	9.65	58.19	0.5170
17.3600	-0.6679	-0.1400	9.59	59.12	0.5331
18.4600	-0.6399	-0.1450	9.47	60.01	0.5500
19.5200	-0.6171	-0.1500	9.33	60.94	0.5670
20.5500	-0.5935	-0.1550	9.19	61.90	0.5830
21.5600	-0.5792	-0.1600	8.96	62.83	0.6000
22.5400	-0.5631	-0.1650	8.79	63.78	0.6170
23.5000	-0.5519	-0.1700	8.58	64.85	0.6330

Table 4.2: Scheduled gain for the PI controller of the IEA 15MW wind turbine de-loaded to 90%

De-loading Strategy 1

The first option for de-loading the wind turbine is to lower the demanded torque at rated power on the torque-speed curve. By combining this with a changed mode gain, the overall torque-speed curve is translated down. The de-loaded power can be calculated as:

$$P_{De-loaded} = (1 - \alpha_{De-load}) \cdot P_{Rated} \tag{4.11}$$

where $P_{De-loaded}$ is the new de-loaded power, $\alpha_{De-load}$ is the de-loading factor for the wind turbine (for example a factor of 0.1 means 10% de-loading of the turbine) and P_{Rated} is the rated power of the wind turbine. Next, the demanded torque for the de-loaded operation can be calculated:

$$\tau_{De-loaded} = \frac{P_{De-loaded}}{\omega_{Rated} \cdot \eta_{gen}} \tag{4.12}$$

in which $P_{De-loaded}$ of equation 4.11 is used, ω_{Rated} is the rated generator speed and η_{gen} is the efficiency of the generator. For the 10% de-loading of the IEA 15MW turbine this results in a de-loaded power of 13.5 MW and a demanded torque of 17685034 Nm.

As was shown in figure 4.10, to de-load the wind turbine, the torque demand is lowered resulting in a higher tip speed ratio and a lower power coefficient. To calculate the mode gain for the de-loaded operation, the de-loaded power coefficient is needed. This can be calculated using the following equation:

$$C_{P,de-loaded} = C_{P,max} \cdot (1 - \alpha_{De-load}) \tag{4.13}$$

in which $C_{P,de-loaded}$ is the de-loaded power coefficient achieved by overspeeding the wind turbine to reach the de-loaded operating point to the right of the optimal operating point as shown in figure 4.10, $C_{P,max}$ is the maximum power coefficient for the turbine at the design tip speed ratio and $\alpha_{De-load}$ is again the de-loading factor. The de-loaded power coefficient is then used to calculate the de-loaded mode gain for the torque controller. The de-loaded mode gain, $K_{De-loaded}$, is calculated as:

$$K_{De-loaded} = \frac{0.5 \cdot \rho \cdot C_{P,De-loaded} \cdot \eta_{gearbox} \cdot \pi \cdot R^5}{r_{gearbox}^3 \cdot \lambda_{overspeed}} \tag{4.14}$$

in which ρ is the air density, $\eta_{gearbox}$ is the efficiency of the gearbox, R is the rotor radius, $r_{gearbox}$ is the gearbox ratio and $\lambda_{overspeed}$ is the new tip speed ratio due to overspeeding of the wind turbine. This results into a de-loaded power coefficient for the IEA 15MW wind turbine of 0.441 and a de-loaded mode gain of 15238030 $Nm/(rad/s)^2$.
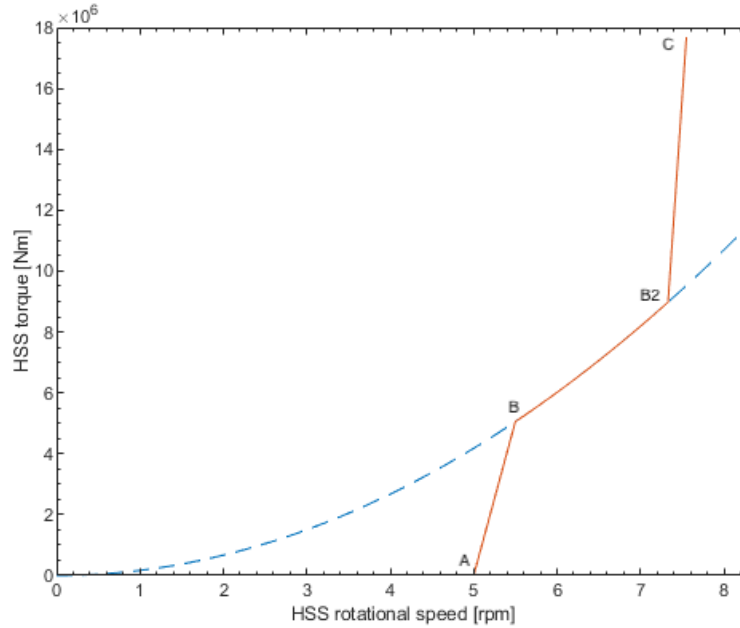
Figure 4.12: Torque-speed curve of the IEA15MW reference turbine 10% de-loaded using de-loading strategy 1.

In an ideal situation the wind turbine would over-speed to the maximum rotational speed (7.55 RPM), and would then stay on this rotational speed while increasing the power to the desired de-loaded point. The wind turbine would then for example follow the de-loaded 90% operating line in figure 4.11. However, to do this, a PI controller is needed for the torque controller. This is not implemented in the used model, as FASTTool implements a feed-forward controller. Because of this the slope from point B2 to point C cannot be a completely vertical line, but has to follow a slope which can be used to assess where at the curve the turbine is operating. Therefore, the IEA15MW reference turbine at 10% de-loading will not follow the torque-speed curve of figure 4.11, but rather the curve in figure 4.12.
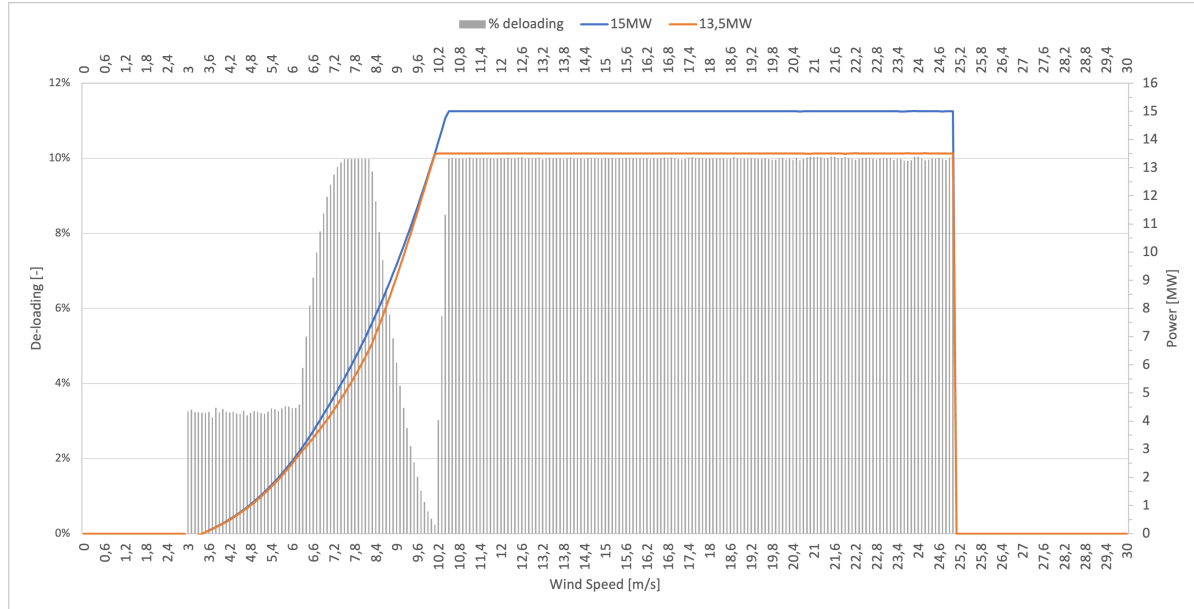
Figure 4.13: Power curve of the baseline 15MW output compared to the 13.5 MW output (10% de-loading using de-loading strategy 1) showing the percentage of de-loading for different wind speeds.

To asses the effectiveness of the de-loading strategy, the power curve is plotted; the power curve can be found in figure 4.13. Firstly, the normal operation corresponding with the baseline controller of section 4.1 is plotted. Secondly, the power curve corresponding to the 10% de-loaded turbine is plotted in the same figure. Lastly, the difference between these two outputs has been portrayed for each wind step as a percentage. If the wind turbine would have been perfectly de-loaded, this percentage would of course be 10% along the entire curve. However, from this graph it can be seen that the wind turbine is only properly de-loaded between points B and B2 and above rated power. Between points A and B and points B2 and C the wind turbine operates around its optimal power coefficient due to the steep lines in the torque-speed curve; this results in an output very close to the baseline operation. This can firstly be explained by looking at figure 4.11. Because of the speed limit, the de-loading of the torque cannot pass the vertical line at a generator speed of 7.55 RPM. As a result the torque demand gradually increases, and gets closer to the optimal operating point. This reduces the effectiveness of the de-loading. Additionally, as the baseline torque controller deviates from the optimal line on the torque-speed curve between points B2 and C as shown in figure 4.2 and point C in the de-loaded curve is much higher compared to the curve between point B and B2 as in figure 4.12, the operating points just below rated wind speed for the baseline and de-loaded turbine are very close together.

Similar behavior can be seen for the cut-in wind speeds. The lines between point A and B for the baseline controller in figure 4.2 and for the 10% de-loaded operation in figure 4.12 are comparable. A difference can be seen in the height of point B and the slope of the line. Because of this difference the wind turbine is de-loaded, but not to 10% as can be seen in figure 4.13.

De-loading Strategy 2

In the second de-loading strategy, both the demanded torque and mode gain are lowered to decrease the torque-speed curve. An important addition for strategy 2 compared to strategy 1, is that the wind turbine also operates at a different fine pitch angle. By increasing the fine pitch angle, the power coefficient at which the turbine operates is lowered; this increases the de-loading performance around rated wind speed.
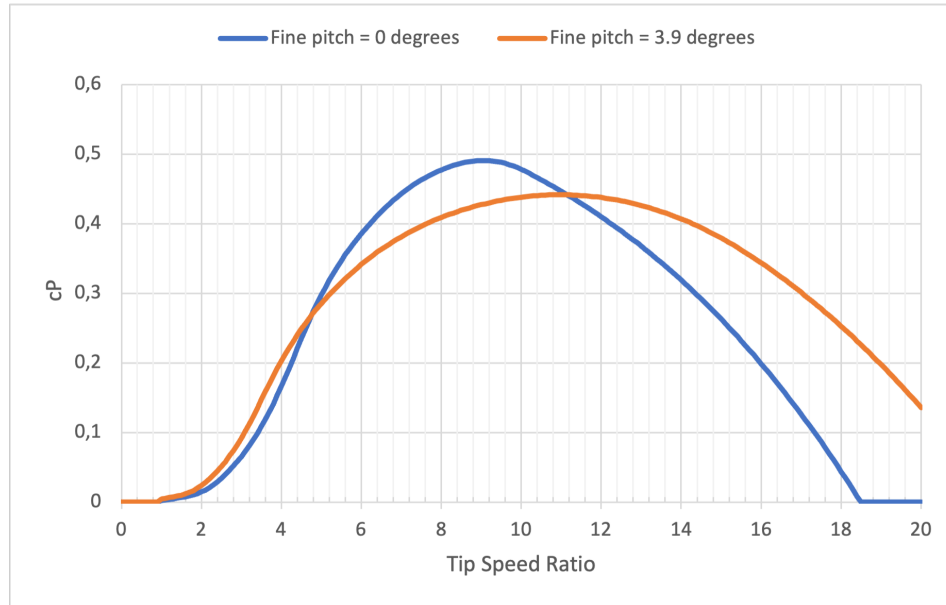
Figure 4.14: $C_P - \lambda$ curves for a fine pitch angle of 0 and 3.9 degrees.

The de-loaded power, demanded torque and de-loaded power coefficient are calculated using the same equations as for de-loading strategy 1. This is with equation 4.11, equation 4.12 and equation 4.13 respectively. Differently from de-loading strategy 1, the de-loaded power coefficient is not only used to calculate the de-loaded mode gain, but also to determine the pitch angle at which this de-loaded power coefficient is the maximum value. By using this pitch angle as the fine pitch angle, the whole power coefficient curve is lowered. An example of this can be seen in figure 4.14. How this new power coefficient curve is reached will be elaborated on next.

To find the de-loaded pitch angle, the de-loaded power coefficient is matched with the corresponding fine pitch angle and tip speed ratio. This is done by outputting the rotor performance from FASTTool using the proper inputs for the IEA15MW turbine. In doing so, a matrix is created in which the power coefficient is determined for all pitch angles from 0 to 20 degrees with steps of 0.1 degrees, at tip speed ratios from 0 to 20 with steps of 0.1. For each pitch angle in this matrix, the maximum power coefficient is highlighted. The de-loaded power coefficient is then matched with the closest highlighted power coefficient in the matrix, and the associated pitch angle and tip speed ratio. This is done for the de-loaded operation of the IEA 15MW reference turbine with 10%, similar to the de-loading with strategy 1, which gives a de-loaded power coefficient of 0.441, a new fine pitch angle of 3.9 degrees and a tip speed ratio, λ, of 11. The power coefficient curves for both the power coefficient curve for a fine pitch of 0 degrees and for a fine pitch of 3.9 degrees can again be seen in figure 4.14.
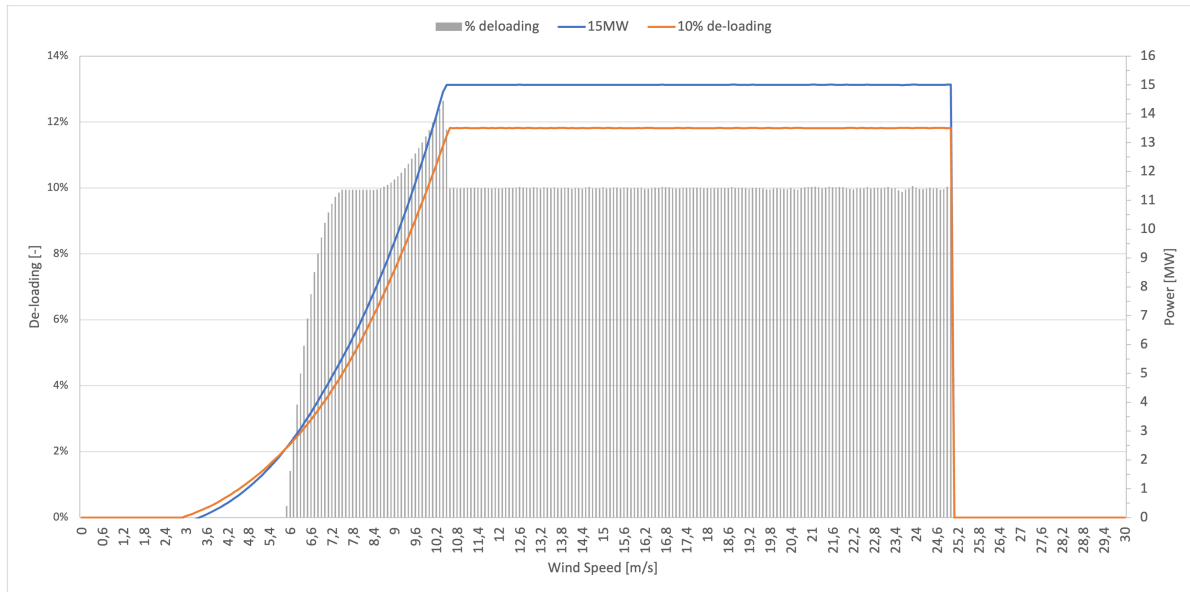
Figure 4.15: Power curve of the baseline 15MW output and the 10% de-loaded output (using de-loading strategy 2) showing the percentage of de-loading for different wind speeds.

The de-loaded power coefficient and the de-loaded tip speed ratio are used to calculate the de-loaded mode gain similar to de-loading strategy 1 using equation 4.14. This gives a de-loaded mode gain for the 10% de-loaded IEA 15MW turbine of 15867964 $Nm/(rad/s)^2$. The power curve corresponding to these inputs can be found in figure 4.15. As the figure shows, using de-loading strategy 2 results in a better de-loading output compared to strategy 1, as it does not return to the maximum power coefficient of 0.490 around rated wind speed.

However, there are two interesting areas to highlight in the power curve. Firstly, at low wind speeds, just above the cut-in wind speed, the de-loaded wind turbine has a higher power output compared to the baseline wind turbine. This is an unwanted effect of using a fine pitch angle of 3.9 degrees. Between points A and B on the torque-speed curve (as for example in figure 4.12), the torque setpoint is below the optimum generator torque line. This lower torque setpoint results in a higher tip speed ratio. As the wind turbine operates at a different power coefficient curve as shown in figure 4.14, the power produced at an operating point deviating from a tip speed ratio of 11 will differ for the baseline controller and the controller using de-loading strategy 2. As can be seen in figure 4.14, a higher tip speed ratio at a fine pitch of 3.9 degrees results in a higher power coefficient compared to the baseline operation. This explains a higher power at low wind speeds for the de-loaded controller using strategy 2 compared to the baseline controller as in figure 4.15.

Next, close to rated wind speed the de-loading shows opposite behavior and de-loading goes up. This is the result of the steep curve between points B2 and C. Contrary to the wind speeds close to cut-in wind speed, the tip speed ratio close to rated wind speed goes down. This is a response to the torque demand between point B2 and C on the torque speed being above the optimum generator torque line. The power coefficient curves in figure 4.14 show that for a lower tip speed ratio at a fine pitch angle of 3.9 degrees, the power coefficient drops below the power coefficient for a fine pitch angle of 0 degrees which is the fine pitch of the baseline controller. As a result, the wind turbine de-loads a bit more.

4.3.2. Controller Design
As explained in section 4.2, when supplying synthetic inertia, the wind turbine supplies or absorbs energy proportional to the RoCoF. However, the wind turbine can also supply frequency response in

different ways by reacting to the frequency deviation. FFR is the controlled contribution of electrical torque and therefore power as a response to frequency difference [7]. FFR can either react proportionally to the frequency deviation, as with the DROOP controller, or react according to a pre-defined schedule.

The DROOP control is a widely suggested controller to be used as a proportional response to frequency deviation [5], [7], [44], [45], [47]. This control is similar to the primary frequency control strategy which is used by conventional power plants [44]. The DROOP control scheme regulates the active output power of the wind turbine based on the difference between the measured grid frequency and the reference frequency (50 Hz). The DROOP controller as suggested in these papers are all in line with the control scheme as portrait in figure 4.16.
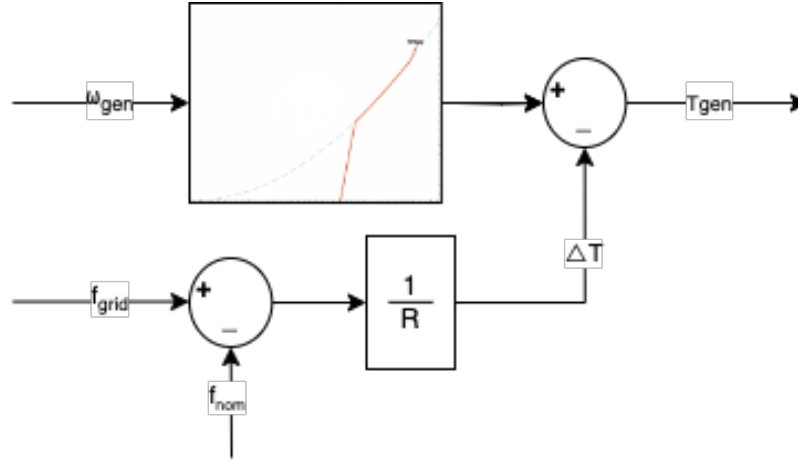
Figure 4.16: Control Scheme DROOP controller.

Here, the difference in per-unit torque is calculated using formula 4.15

$$\Delta T = -\frac{1}{R}(f_{grid} - f_{nom}) \tag{4.15}$$

where f_{grid} is the measured grid frequency, f_{nom} is the nominal grid frequency and R is the droop constant. Similar to the synthetic inertia controller, the gain is calculated as in [22] and [45]. In these papers it is proposed for R to be proportional to the square of the measured rotor speed ω_i. R can then be calculated as:

$$R = R_0 \frac{(\omega_{max}^2 - \omega_{min}^2)}{(\omega_{gen}^2 - \omega_{min}^2)} \tag{4.16}$$

where R_0 is the proportional droop constant of the wind turbine operating at the maximum rotor speed, ω_{max} is the maximum generator speed (per unit), ω_{min} is the minimum generator speed (per unit) and ω_i is the measured generator speed (per unit). R_0 is suggested to be 2%, which is also used in this study [45]. Additionally, ω_{min} is set to 0.56 and ω_{max} to 1.25, based on comparable values in [22] and [45].

As can be seen in figure 4.16, the DROOP controller outputs an additional torque set point which is directly added to the torque controller. In FASTTool, the torque set point below rated wind speed is determined by the mode gain of the torque control, whereas above rated wind speed the torque set point is determined by the demanded torque. The DROOP controller should therefore be active on both these parameters.

An important understanding which should be kept in mind is that a FFR is increasing the de-loaded power in a proportional or scheduled reaction to the frequency deviation. If the wind turbine is de-loaded using only the torque controller as in de-loading strategy 1, this is also the only controller the

FFR should react on. However, if the wind turbine is also de-loaded by means of the pitch controller as in de-loading strategy 2, the FFR should also revert the pitch angle (partially). If this is the case, the DROOP controller should also change the pitch set point, which can be done in a similar control scheme as for the DROOP controller active on the torque controller. The change in the per-unit pitch angle is calculated similar to the per-unit torque as:

$$\Delta\beta = -\frac{1}{R}(f_{grid} - f_{nom}) \tag{4.17}$$

where $\Delta\beta$ is the change in pitch angle. This change in pitch angle is subtracted from the pitch angle determined by the pitch controller as in figure 3.2.

4.4. Model Validation

As the results from the case study can be strongly influenced by unexpected behavior in the simulation, the first step in the validation is to investigate the performance of the wind turbine during its normal and de-loaded operation. In the baseline operation and while supplying synthetic inertia, the wind turbine will operate normally. On the other hand, the de-loaded operation is used when supplying FFR. After investigating the normal and de-loaded performance, the synthetic inertia and FFR controller responses will be evaluated to see if these controllers respond as expected.

To validate the normal operation of the wind turbine, it should first be checked whether the torque and pitch controller are functioning as is expected. In figure 4.17, the operation of the baseline controller is plotted for a stepped wind input over all the wind speeds in the operating range of the turbine, which is from 3 to 25 m/s. In this figure the pitch angles are shown to see if the pitch controller properly converges to the desired pitch angle. This should cause the rotor speed to quickly converge to its maximum rotor speed, which can also be seen in the figure. The power and torque are shown to see if the the torque is constant above rated power, and if this results in a stable output power. Finally, the tower fore-aft and side-side accelerations are plotted to see if no large oscillations occur.
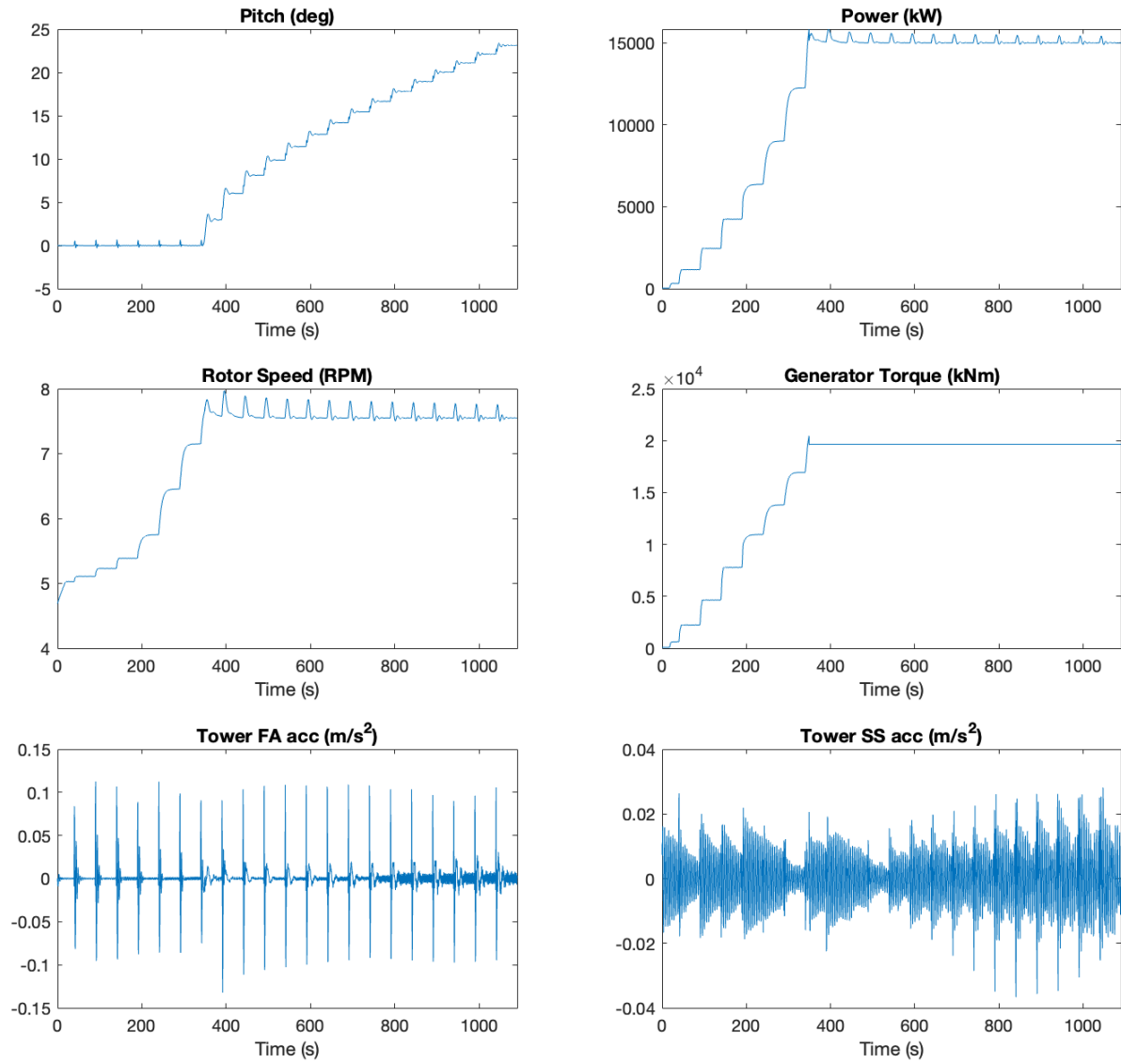
Figure 4.17: Stepped operation of the baseline controller for a stepped wind input of 3 to 25 m/s with a wind step of 1 m/s.

As can be seen in figure 4.17, the wind turbine shows desired behavior both in partial and in full load. The torque controller converges to the desired torque and results in a smooth increase in rotational speed and power. Above rated wind speed the pitch controller quickly converges to the correct pitch angle and only causes a small overshoot in the rotational speed. Thus, the pitch controller shows a quick convergence to zero error. Additionally, no particularities are seen in the tower fore-aft and side-side acceleration.

Next, the same is done for the de-loaded operation of the wind turbine. Figure 4.18 shows the de-loading of the wind turbine using de-loading strategy 1 with a stepped wind input from 3 to 25 m/s.
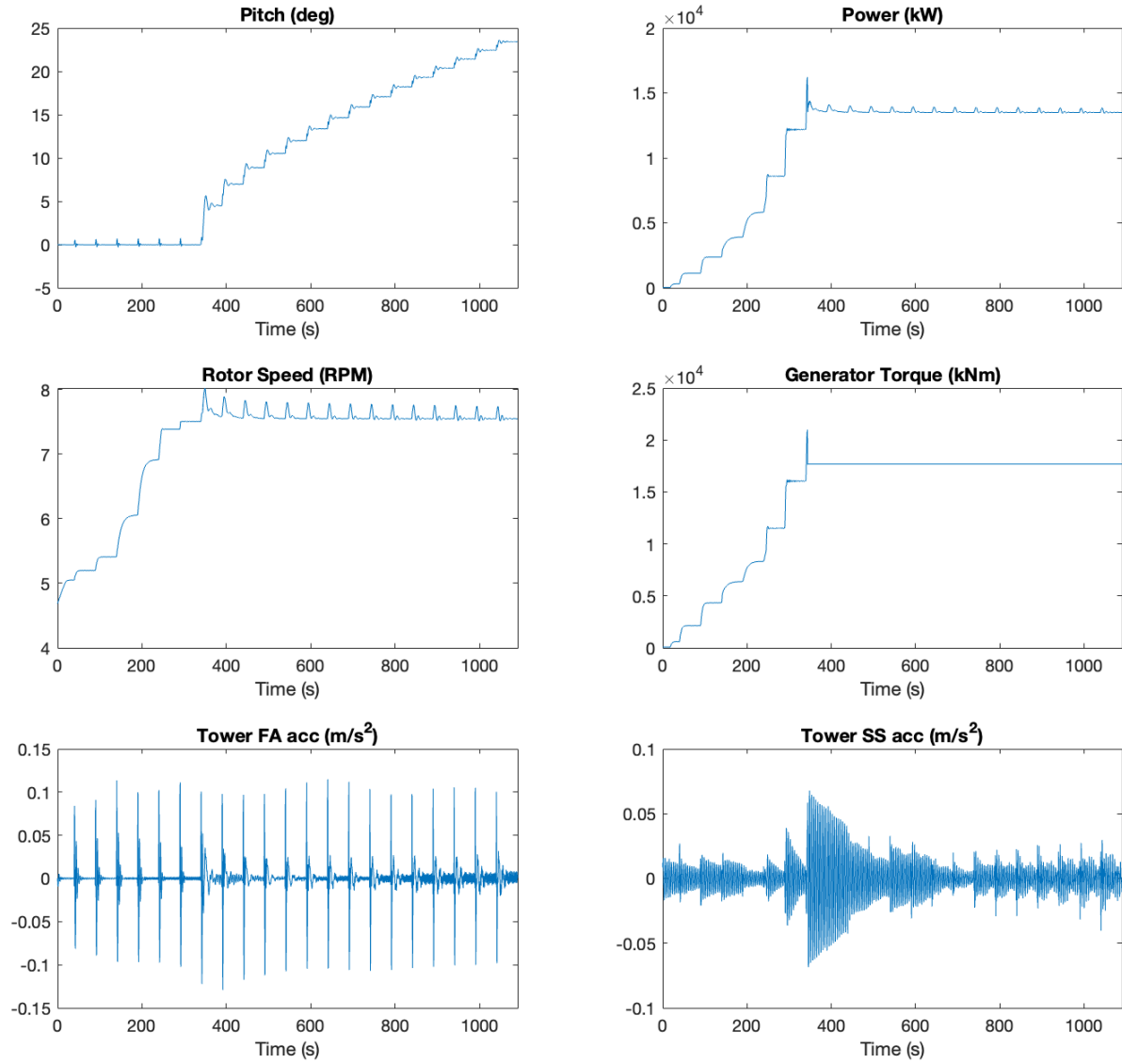
Figure 4.18: Stepped operation of the 10% de-loaded wind turbine using de-loading strategy 1, with a stepped wind input from 3 to 25 m/s with a wind step of 1 m/s.

The figure shows that the pitch and torque control mostly respond as expected. Only just below rated power some oscillations can be seen in the generator torque induced by the steep line on the torque-speed curve. Additionally, because of the steep line in the torque-speed curve, the torque controller shows a bigger overshoot compared to the normal operation. This overshoot could be a point of attention for the power electronics. However, as the torque does not pass the maximum allowable torque of the wind turbine, this will not be further investigated in this research. De-loading of the wind turbine is in order, and can be best seen above rated wind speed. This is as would have been expected based on the power curve for de-loading strategy 1.

The figure shows a fore-aft acceleration similar to the acceleration in the normal operation. On the contrary, the side-side acceleration does show a significant difference around rated wind speed. For the normal operation this is in the range of $0.02 \ m/s^2$, whereas this is in the range of $0.075 \ m/s^2$ around rated power for de-loading strategy 1. To further dive into this, the side-side acceleration around rated wind speed is studied in the frequency domain. Figure 4.19 shows the tower side-side acceleration for the stepped wind input from 9 to 12 m/s in the frequency domain for the normal operation and the

operation using de-loading strategy 1. This single sided spectrum is constructed using a Fast Fourier Transform. It can be seen that because of de-loading the amplitude of the peak around 0.205 Hz increased from about 0.0078 m/s to 0.02 m/s. This peak is very close to the first natural frequency of the tower, which is 0.22 Hz. At 0.22 Hz the amplitude increased from 0.0019 m/s to 0.0036 m/s, and thus almost doubled. The oscillations observed just below rated power and the overshoot at rated wind speed are likely contributing factors to the amplified amplitudes. These torque variations exert rotational forces on the tower top, thus exciting side-side motion of the tower. Because of this behavior around the nominal wind speed, the results when using this de-loading strategy should be interpreted with caution and will therefore be studied in more depth later in this validation section. The natural frequency of the tower was found by constructing the Campbell diagram using FASTTool. The diagram can be found in figure B.1 in appendix B.
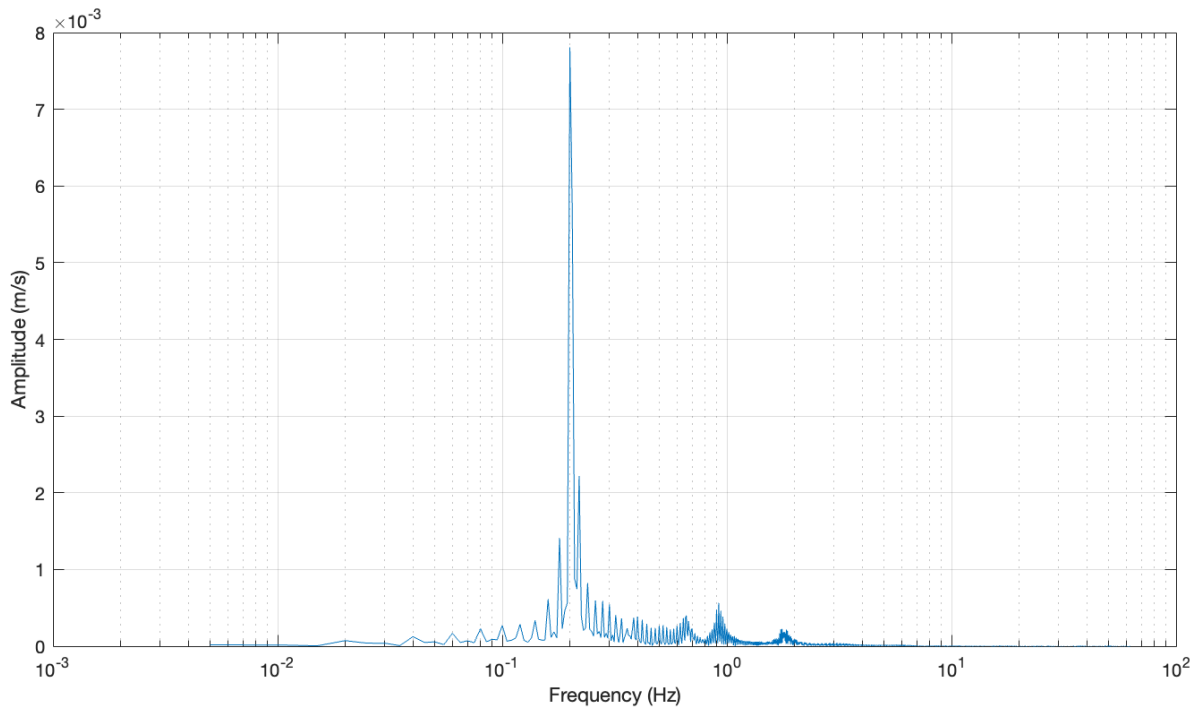
(a) Tower side-side acceleration for the normal operation, shown in the frequency domain for a stepped wind input from 9 to 12 m/s with a wind step of 1 m/s.
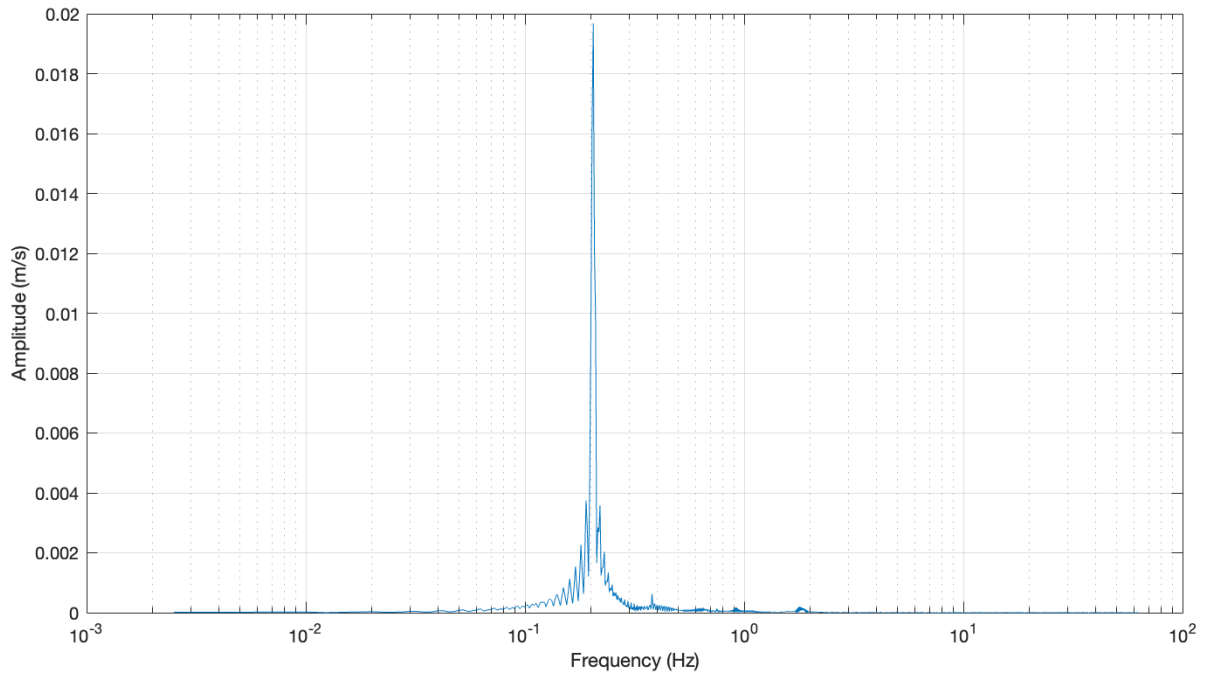
(b) Tower side-side acceleration for the de-loaded operation using de-loading strategy 1, shown in the frequency domain for a stepped wind input from 9 to 12 m/s with a wind step of 1 m/s.

Figure 4.19: Frequency domain plots of the tower side-side acceleration for the normal operation and the de-loaded operation using de-loading strategy 1.

Figure 4.20 shows the operation of the wind turbine at 10% de-loading using de-loading strategy 2. At low wind speeds, the operation of the de-loaded turbine behaves similar to de-loading strategy 1, only the fine pitch angle is no longer 0, but 3.9 degrees. The figure shows similar behavior to de-loading strategy 1 for the torque. The same oscillations just below rated power can be seen in the torque

of the wind turbine. Additionally, it can be seen that for this de-loading strategy the torque at rated wind speed is not yet set to a constant value. This has to do with the way the torque controller is modelled in FASTTool. The generator torque is set stable after the pitch angle is 1 degrees above its fine pitch angle. In this de-loaded operation with de-loading strategy 2, this is not yet the case at rated wind speed.
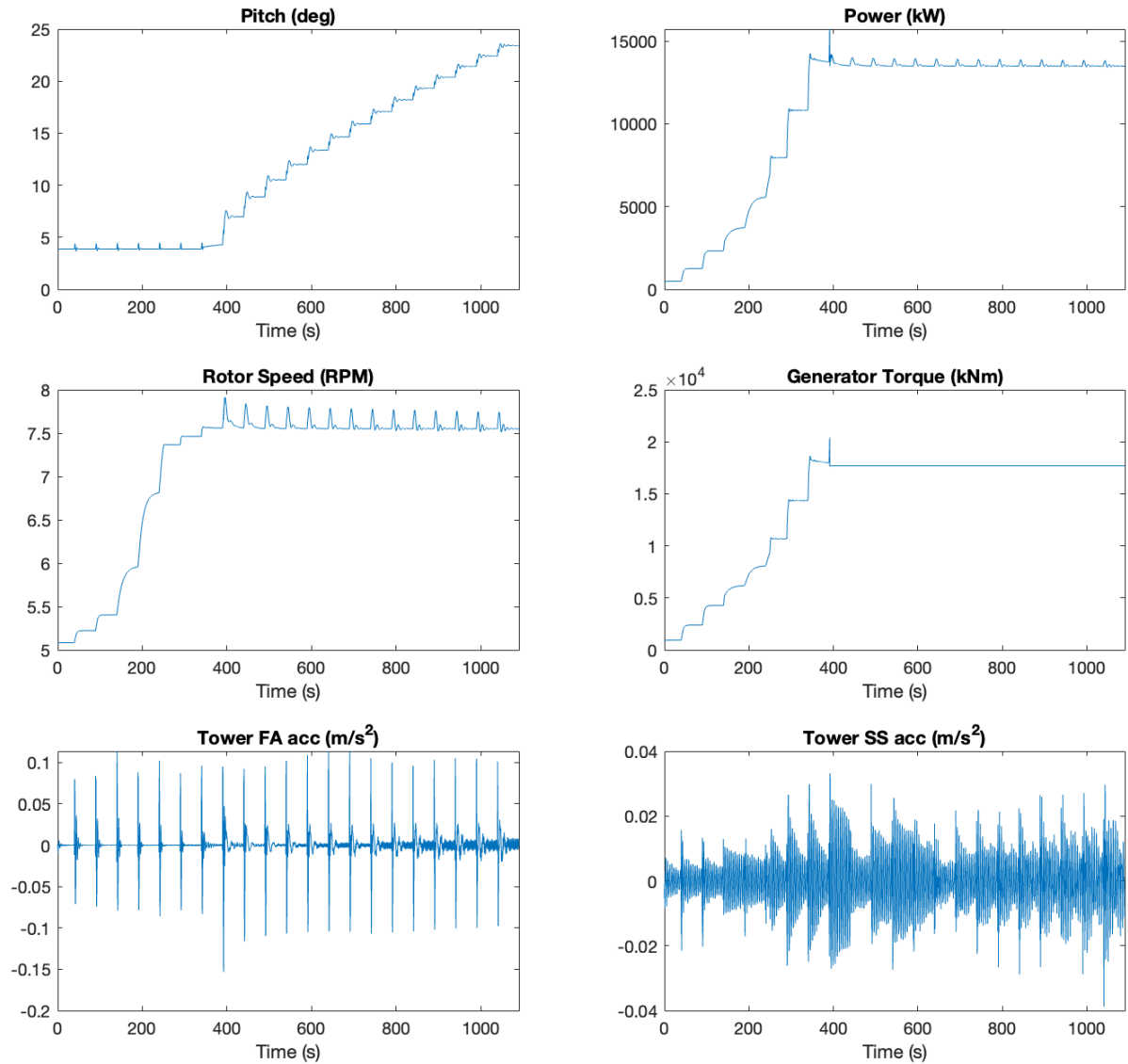
Figure 4.20: Stepped operation of the 10% de-loaded wind turbine using de-loading strategy 2 for a stepped wind input of 3 to 25 m/s with a wind step of 1 m/s.

Similar to de-loading strategy 1, strategy 2 shows no changes for the fore-aft acceleration of the tower. Nevertheless, strategy 2 does also show a change in side-side acceleration of the tower. The change is slightly lower compared to de-loading strategy 1, as it shows peaks around 0.035 m/s^2 opposed to 0.075 m/s^2 for de-loading strategy 1. Similarly to de-loading strategy 1, the tower side-side acceleration is also studied in the frequency domain for de-loading strategy 2, which can be found in figure 4.21. For de-loading strategy 2 the amplitude at 0.205 Hz only increased slightly to about 0.01 m/s. Additionally, the peak did get wider. The peak at the first natural frequency of the tower increased to about 0.0055 m/s.
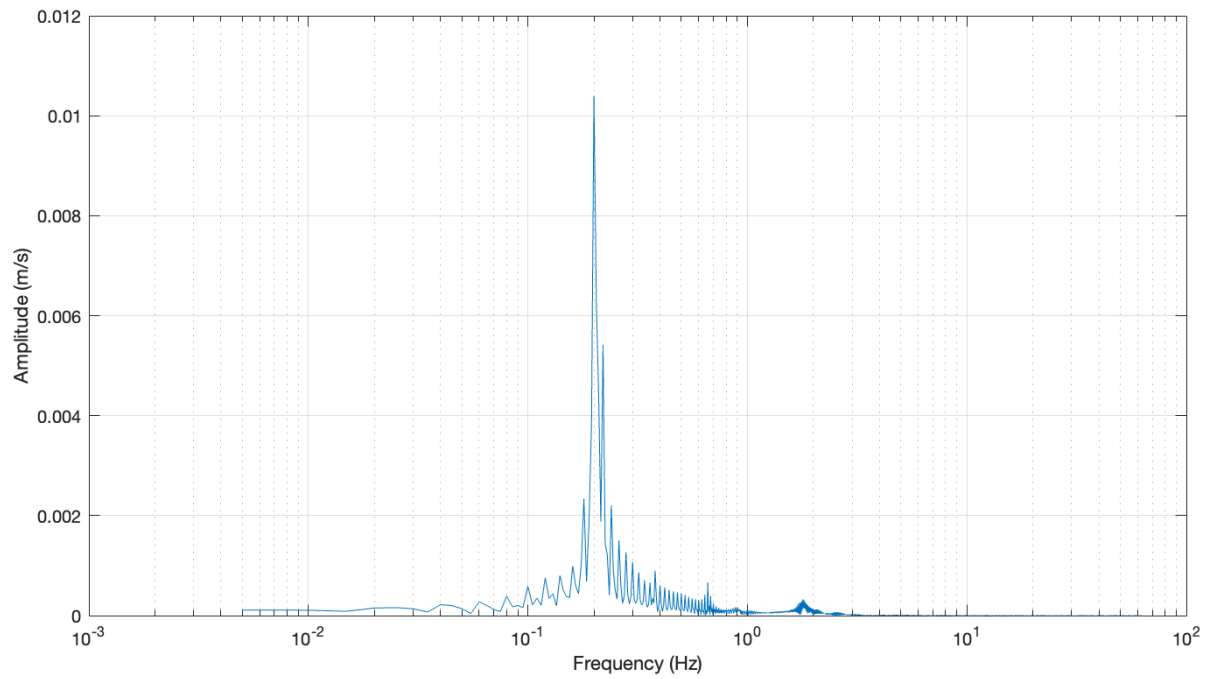
Figure 4.21: Tower side-side acceleration for the de-loaded operation using de-loading strategy 2, shown in the frequency domain for a stepped wind input from 9 to 12 m/s with a wind step of 1 m/s.

To ensure that the wind turbine also operates as expected in turbulent wind conditions, the operation of the normal operations and of the two de-loading strategies is also checked for a normal turbulence wind model as described by the IEC standard [31]. The turbine shows expected behavior for the normal operation for all operational wind speeds. For the two de-loaded operations, the turbine shows normal behavior for all wind speeds except for those around rated power. An example of this can be seen in figure 4.22.
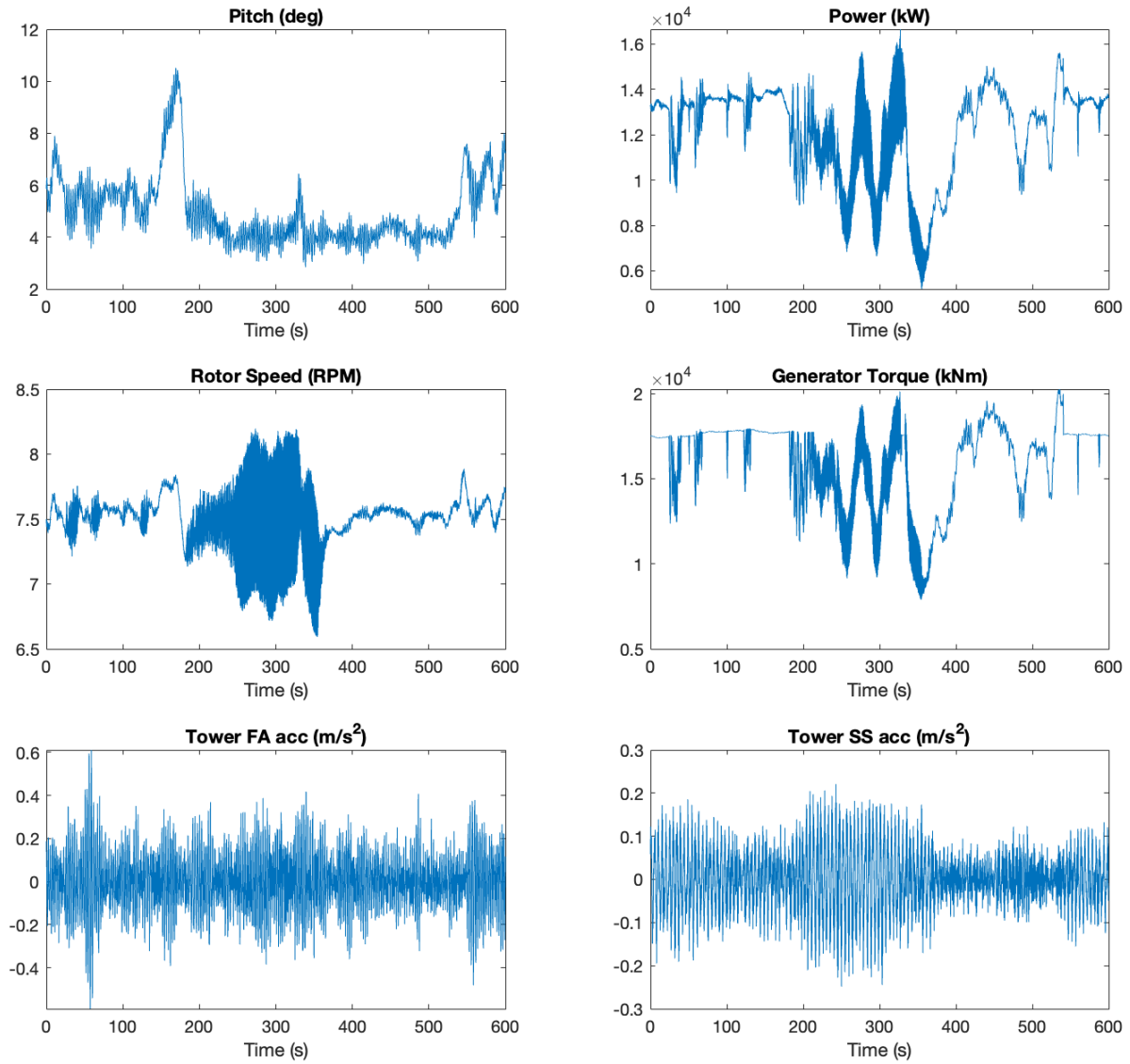
Figure 4.22: Wind turbine operation using de-loading strategy 2 with a normal turbulence wind input with a mean wind speed of 11 m/s.

Large oscillations are seen in the rotor speed of the wind turbine at both de-loading strategies around rated wind speed. The rotor speed of the operation is also plotted in the frequency domain in figure 4.23. From this figure it can be seen that the rotor speed of the wind turbine resonates with the second natural flap-wise frequency of 1.57 Hz and with the second edge-wise natural frequency of the blades at 2.23 Hz. The response corresponding to the second edge-wise natural frequency is much smaller compared to the response corresponding to the flap-wise natural frequency.
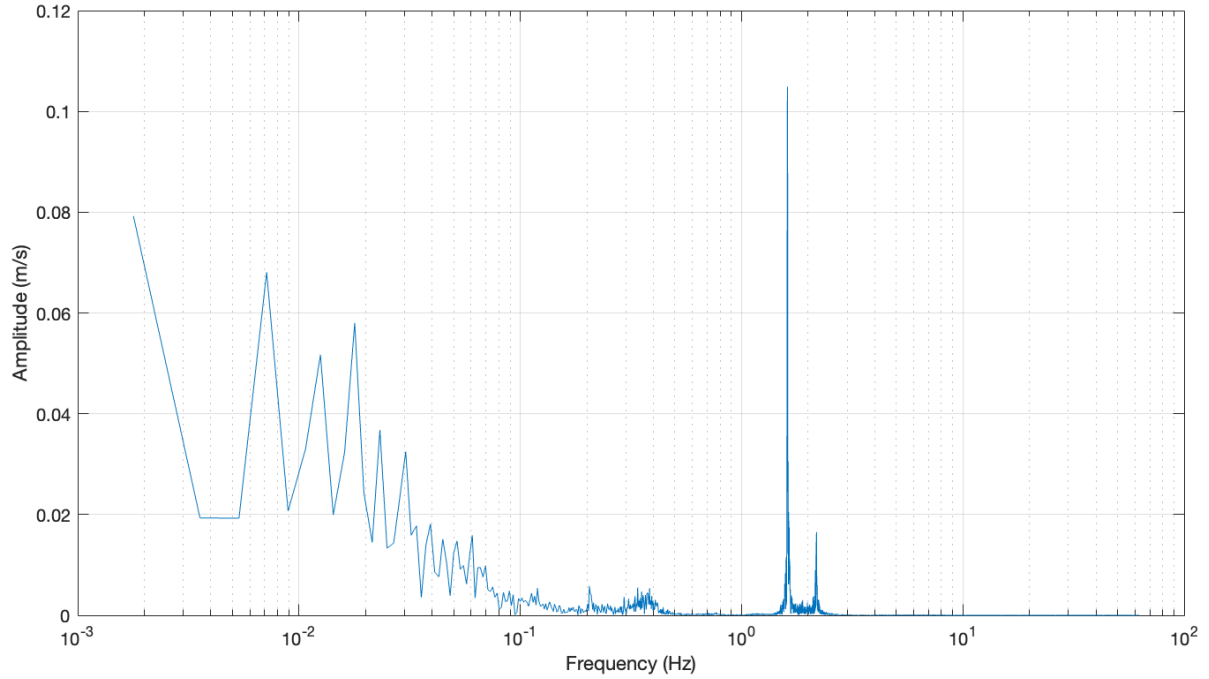
Figure 4.23: Rotational speed for the de-loaded operation using de-loading strategy 2, shown in the frequency domain for a normal turbulence model wind input with a mean wind speed of 11 m/s.

Similar to the rotor speed, the generator torque also shows peaks at 1.57 Hz and 2.23 Hz. This is as expected, as the torque below rated wind speed is determined using the rotational speed of the generator. Due to time constraints of the research, and the goal of the research being to show the difference in fatigue and ultimate loads and not to design perfect de-loading for the wind turbine, the problem of this resonance will not further be addressed. However, results around rated wind speed using a de-loaded wind turbine should either not be used, or be used with great care.

Combining the de-loading performance found for both de-loading strategies in section 4.3.1 with the results from this validation section, it can be concluded that de-loading strategy 2 shows the most desired de-loading capabilities. Specifically, de-loading strategy 2 showed the best de-loading performance, particularly near rated wind speed. Additionally, this de-loading strategy resulted in a lower increase in the amplitude of the side-side acceleration of the tower in the frequency domain. Based on these findings, de-loading strategy 2 will be used to de-load the wind turbine in the case study.

Now the operation of the baseline and de-loaded wind turbine have been studied, both the synthetic inertia controller response and the FFR controller response should be inspected. The synthetic inertia controller is an addition to the wind turbine's normal operation, while the FFR controller needs the wind turbine to be de-loaded. Since de-loading strategy 2 is chosen to be used in the case study, this de-loading strategy will be investigated further. The wind turbine will be studied while it is de-loaded using de-loading strategy 2 to 90% of the nominal power.

Firstly, the synthetic inertia controller will be discussed at a proportional gain of 46.6, which is the same gain as used in [22] and [45]. To compare the controller to literature, a controlled frequency drop is used from 50Hz to 49.5Hz. This frequency drop will be imposed on the synthetic inertia controller for both partial load, at 8 m/s, and full load, at 20 m/s. To study the response, the components plotted are the frequency drop, the output power, the rotor speed and the generator torque. These can be found in figure 4.24 for the partial load response and in figure 4.25 for the full load response.
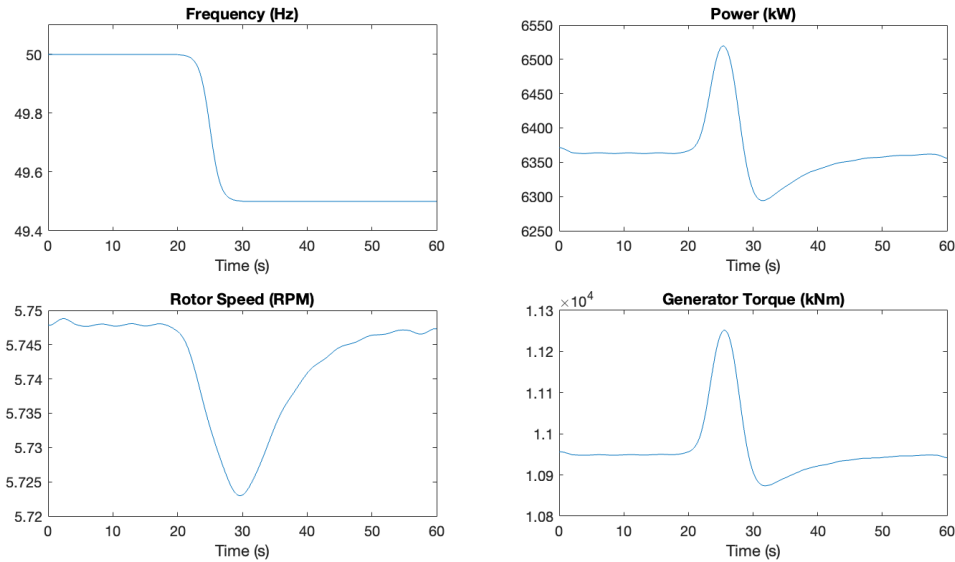
Figure 4.24: Response of the wind turbine using the inertial controller with a proportional constant of 46.6 to a grid frequency drop at a constant wind speed of 8 m/s.
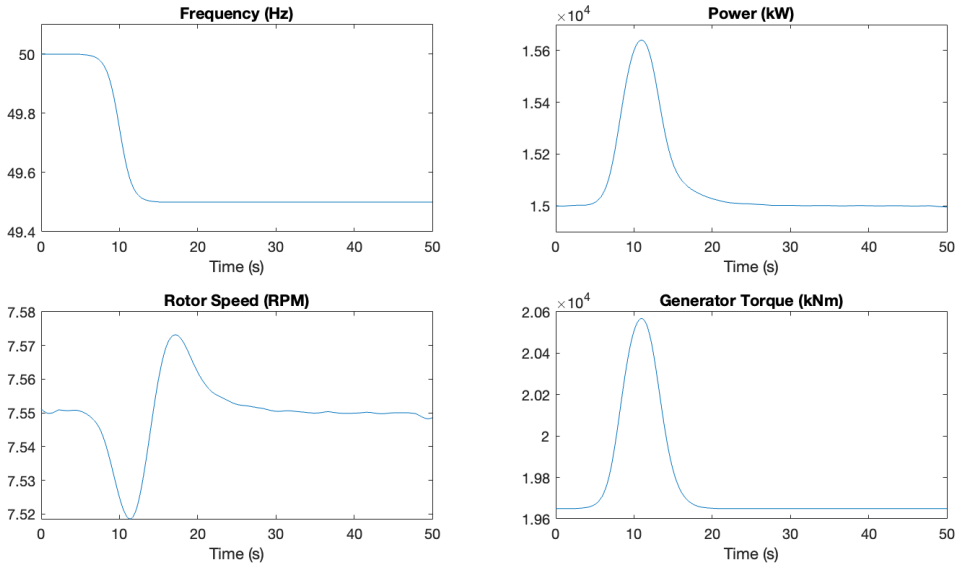
Figure 4.25: Response of the wind turbine using the inertial controller with a proportional constant of 46.6 to a grid frequency drop at a constant wind speed of 20 m/s.

In response to the frequency drop, the generator torque is increased proportionally as expected. This yields an increase in power, but also results in a drop in rotor speed. The effect of this rotor speed drop in partial load is that a small drop in output power can be seen after the inertial response. The drop resolves when the rotor speed is back to its pre-response value. However, during full load, a decrease in rotor speed does not lead to a drop in power since the torque is not determined based on rotational speed but is instead set constant. However, as in full load the pitch controller is active, the rotor speed overshoots a little bit above 7.55 RPM, which is the rated rotor speed. This is similar to the small overshoot which was observed in the stepped response of both the baseline and de-loaded wind turbine.

Overall, the response is in line with the expected behavior of the wind turbine to the inertial controller. Moreover, the response is also in line with the response seen in existing research [46]. In this

study, a similar frequency dip from 50 to 49.5 Hz over a 10-second period was used as in this validation section.

Since the wind turbine studied in [46] is a 2 MW doubly fed induction generator wind turbine using a different proportional gain for the synthetic inertia controller, direct comparisons of numerical values, such as the overshoot of the rotor speed and dip in rotor speed, torque and power, are not applicable. Nonetheless, the shapes and duration of the behaviors seen can be compared. For instance, the dip in rotor speed in partial load has a similar duration of around 25 seconds before returning the its pre-disturbance rotational speed. Consequently, the drop in torque and power has a similar duration. It should be noted that the shapes of the responses show the same behavior. Furthermore, at full wind speed, the synthetic inertia controller demonstrates the same shape and duration as seen in [46]. Since no figure was provided for the rotor speed at full load, this cannot be compared. However, the rotor speed for the IEA 15 MW wind turbine at a wind speed of 20 m/s behaves as would have been expected, due to which differences are not likely.

Next, the FFR controller is discussed. Similar to the inertial controller, the FFR controller will be studied for its response to a frequency drop from 50Hz to 49.5 Hz. This will be done for constant wind speed, both at partial and full load, using the DROOP controller. The output for the FFR controller at partial load can be found in figure 4.26 and the response for full load can be found in figure 4.27.
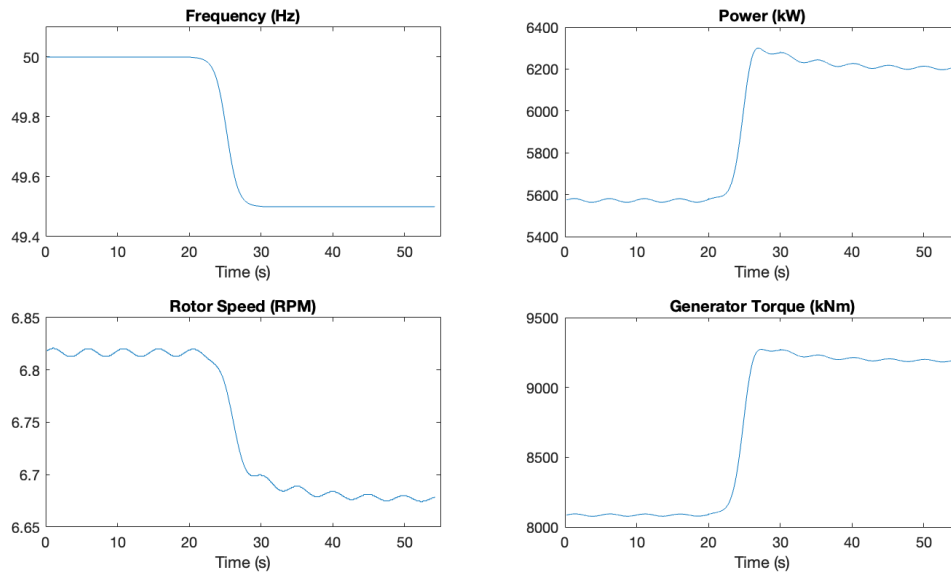
Figure 4.26: Response of the wind turbine using the FFR controller with a proportional constant of 0.02 to a frequency drop at a constant wind speed of 8 m/s.
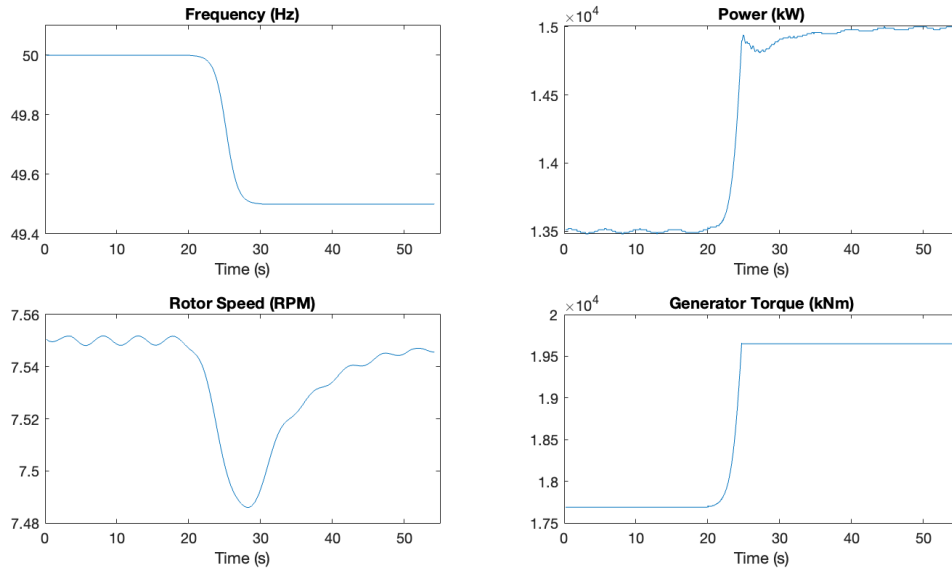
Figure 4.27: Response of the wind turbine using the FFR controller with a proportional constant to a frequency drop at a constant wind speed of 15 m/s.

Since the FFR controller does not respond to the RoCoF, but to the difference in grid frequency, the generator torque set point as a reaction to the drop in frequency will stay high. This is as expected, as the frequency signal does not return to 50 Hz, but stays at 49.5 Hz.

In partial load the rotor speed converges to a new stable level, which is lower than the initial rotor speed. This is because the wind turbine was de-loaded using a lower torque and a higher fine pitch. Because of this the wind turbine was over speeding compared to the normal operation. As the output power of the wind turbine should increase as a reaction to the lower grid frequency, the de-loading is reversed and as a result the wind turbine operates at a lower rotor speed.

Differently, in full load the wind turbine is de-loaded by operating at a lower demanded torque and at its rated rotor speed. The pitch controller is active to limit the rotor speed to the rated speed, namely 7.55 RPM. Here, the FFR controller increases the generator torque to a higher set point as a response to the decrease in grid frequency. Due to this, the rotor speed decreases. But, as the pitch controller is active the decrease in rotor speed is only temporally, and converges to 7.55 RPM again.

Similarly to the synthetic inertia controller, the wind turbine's behavior is as expected from the modelling. Additionally, it is also similar to reactions found in literature [46].

In line with the evaluation of the synthetic inertia controller, the numerical values cannot directly be compared. However, the shape and duration of the responses show similar patterns when comparing the FFR controller response with the findings in the mentioned research. While the comparison can only be made for partial load, as the response for full load is not shown in the study, the FFR controller response in full load is in line with expectations.

The only difference between the response of the FFR controller in partial load and the repsonse described in [46] is the absence of a substantial overshoot in torque and power for the FFR controller. This can be explained to the fact that the controller in this research relies on the rotational speed, which decreases, and thus the response is decreased. Nonetheless, even though the response in full load cannot be compared to this study, the response demonstrates expected behavior.

It should be noted that the frequency dip of 0.5 Hz is larger than would be expected from the average grid frequency behavior in a large grid. The normal responses the synthetic inertia and FFR controllers

using similar proportional gains will give are therefore expected to be considerably smaller compared to the examples given. Therefore, it may be beneficial to increase the response of the synthetic inertia and FFR controller. To study this larger response to a smaller change in grid frequency, the proportional gains of the controllers will also be validated at values 100 times larger than those in the normal scenario given before. The grid drop will therefore be smaller and is equal to a controlled frequency drop from 50 to 49.9 Hz.

Firstly, the synthetic inertia controller response will be studied at a proportional gain K_0 equal to 4660. The response of the wind turbine to this controller setting at a wind speed of 8 m/s can be found in figure 4.28. As can be seen in the figure, the torque demand is higher compared to figure 4.24, while the size and duration of the decrease in grid frequency is much smaller. It should be noted that this also causes a larger dip in the rotor speed, which could induce a second frequency dip. However, the increased proportional constant does allow the wind turbine to supply more synthetic inertia to the grid.
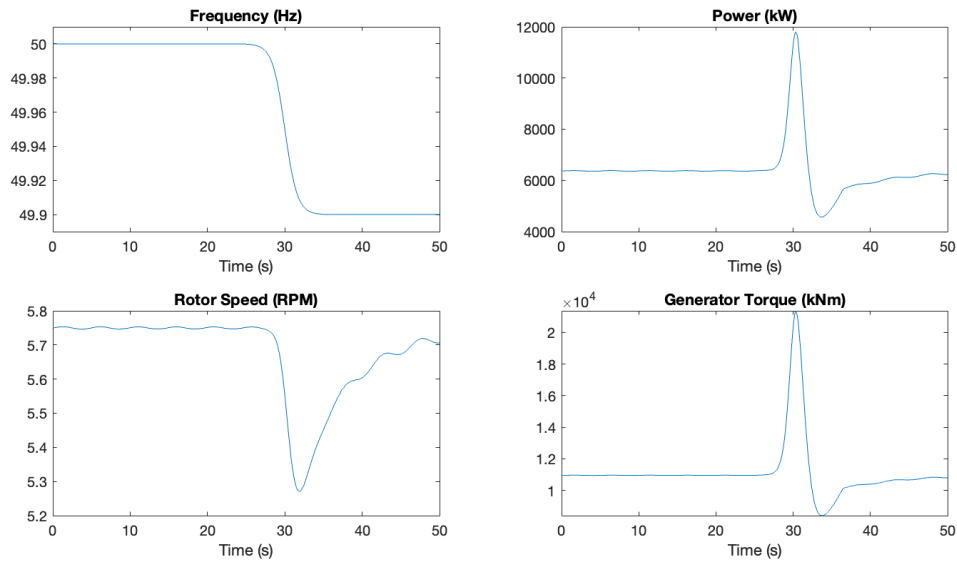
Figure 4.28: Response of the wind turbine using the synthetic inertia controller with a proportional gain of 4660 to a frequency drop of 0.1 Hz at a constant wind speed of 8 m/s.
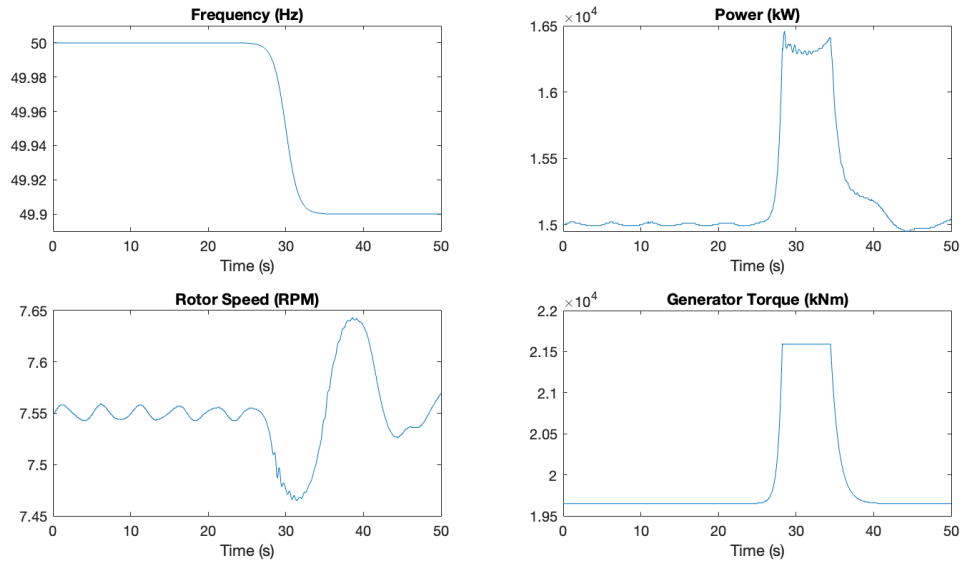
Figure 4.29: Response of the wind turbine using the synthetic inertia controller with a proportional gain of 4660 to a frequency drop of 0.1 Hz at a constant wind speed of 20 m/s.

Next, the response of the wind turbine to the synthetic inertia controller with a high proportional gain in full load can be found in figure 4.29. The response is shown at a constant wind speed of 20 m/s. The figure shows that the additional power due to the synthetic inertia controller doubled compared to the response at a proportional gain of K_0 is 46.6. This does cause a slightly larger dip and overshoot in the rotational speed of the wind turbine. It can be seen that the torque demand reaches the torque limit of the wind turbine which is $2.158 \cdot 10^7 Nm$. This therefore shows the limit of the wind turbine concerning the supply of synthetic inertia with this controller. The proportional gain should thus be well matched with the RoCoF of the grid the wind turbine is positioned in.

The response of the FFR controller will also be studied at a proportional gain 100 times larger. The proportional gain, R_0, will therefore be set to 2. The response of the wind turbine with this controller setting to a frequency drop from 50 to 49.9 Hz can be seen in figure 4.30 at a wind speed of 8 m/s and in figure 4.31 at a wind speed of 20 m/s.
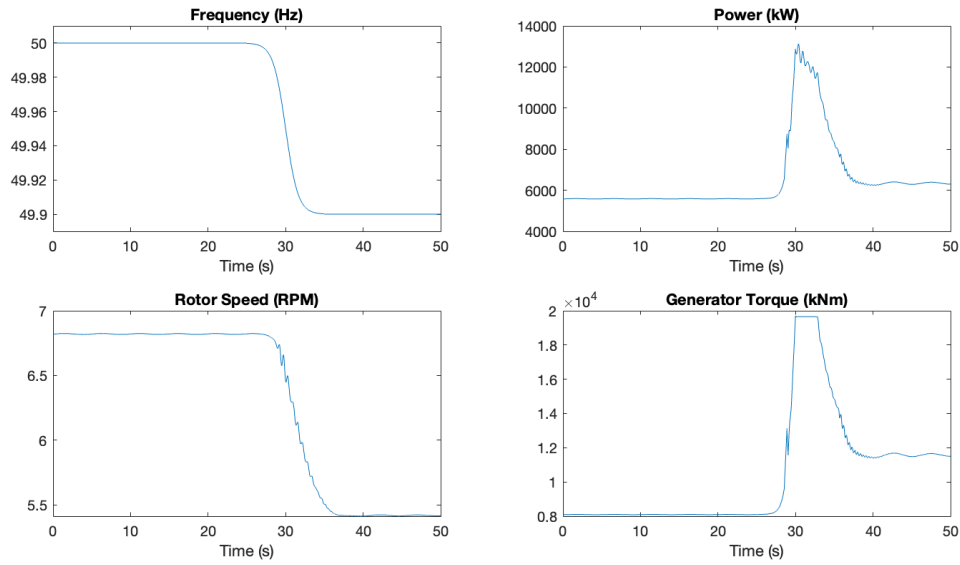
Figure 4.30: Response of the wind turbine using the FFR controller with a proportional gain of 2 to a frequency drop of 0.1 Hz at a constant wind speed of 8 m/s.
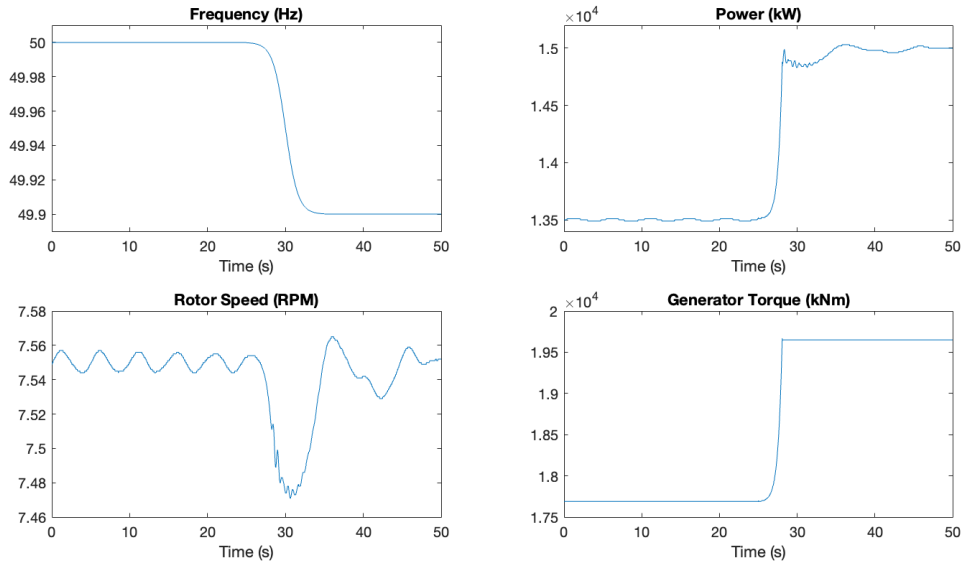
Figure 4.31: Response of the wind turbine using the FFR controller with a proportional gain of 2 to a frequency drop of 0.1 Hz at a constant wind speed of 20 m/s.

At partial load, the FFR response shows a larger overshoot in torque and power compared to the response at the lower proportional gain in figure 4.26. This is caused by the quick increase in torque demand and the slower decrease in pitch angle. Due to the large increase in torque the rotor speed decreases. This decrease in rotor speed determines a new and lower operating point for the torque controller. It can be seen that due to the 0.1 Hz decrease of the grid frequency, the FFR controller already reaches the torque limit of the wind turbine. Some minor fluctuations in the rotor speed and output power can be seen because of this.

At full load, the response of the wind turbine shows a good response to the frequency drop. The torque and power show a similar increase to the maximum power point compared to the response at lower proportional gain in figure 4.27. Furthermore, the rotor speed shows a quick convergence to the

maximum rotor speed of 7.55 RPM after the short dip.

In conclusion, both the synthetic inertia controller and FFR controller show satisfactory performance, making them viable options for implementation in the case study. Nevertheless, it should be stressed again that the results obtained from the FFR controller, particularly around rated wind speed, should be taken with care. The de-loading of the wind turbine during this phase shows undesired oscillations in the rotor speed, which should be taken into account when analysing and processing the FFR controller outputs. Furthermore, de-loading strategy 2 will be used in the case study to de-load the wind turbine due to its better de-loading performance and lower side-side tower acceleration amplitude in the frequency domain compared to de-loading strategy 1.

5

Case Study

In this chapter, different cases will be studied to gain knowledge about the behavior of the wind turbine when supplying synthetic inertia and FFR in different design cases as well as to study the ultimate and fatigue loads imposed on the wind turbine. First, the development of the cases will be explained. This will start with an outline of which design load cases from the IEC standard will be used in the case studies. Next, the external conditions affecting the case study will be elaborated upon. These include the location and associated Weibull parameters, and three grid frequency scenarios, including the normal grid frequency behavior and two more extreme grid frequency scenarios. After the case study is well outlined, the results of the individual cases will be given. This will start with the baseline case, then the synthetic inertia case and finally the FFR case. In these cases both fatigue analysis and ultimate load analysis will be performed. Finally, the results of these individual case studies will be compared to highlight differences and possibilities in delivering synthetic inertia and FFR.

5.1. Development of Cases

5.1.1. Parameter Overview Case Study

The case study in this research consists of three cases. The first case uses the baseline controller and therefore acts as the baseline case. In the other two cases, the synthetic inertia controller and FFR controller are studied. The baseline case establishes a reference point for the ultimate loads and FDEL in various load scenarios. Meanwhile, the synthetic inertia and FFR cases investigate the impact of providing these ancillary services on wind turbine loads.

To develop the cases and to be able to compare them, the general conditions need to be determined. The first important condition for the cases is the wind-inflow. The wind-inflow is determined by the DLCs which are studied. Besides the wind-inflow itself, the location of the wind turbine impacts the wind climate. The location determines the Weibull parameters used for translating the 10-minute FDEL to the lifetime FDEL.

Besides the weather conditions, the grid frequency input has a major impact on the output of the synthetic inertia and FFR case. The grid frequency input determines the response shape, while the size of the proportional constant determines the magnitude of the response of the controllers. This proportional constant will be elaborated upon as a controller setting within the cases.

The following subsections will elaborate on the choices made concerning the DLCs, wind-inflow conditions and grid frequency inputs.

5.1.2. Design Load Cases Studied

The IEC [31] outlines many DLCs which can be studied. Important states of the turbine in these cases are power production, startup of the wind turbine, shutdown of the wind turbine, idling, faults, emergency shutdowns and finally transport and assembly. These load cases are divided into fatigue and ultimate load cases.

As there are many cases to be considered, it is not possible to run all DLCs for every case. Therefore, the focus in this case study is on situations where the wind turbine provides a response to the grid frequency. This choice was made because in other situations the loads on the wind turbine do not differ from the normal situation and no comparison can be made. The situations assessed correspond to situations of normal power generation, power generation plus the occurrence of a fault or loss of electrical connection to the grid, startup of the wind turbine and finally an emergency shutdown. An emergency shutdown is considered as it may occur together with the delivery of a frequency or inertial response.

A summary of all DLCs studied for the case study can be found in table 5.1. In the rest of this section, the DLCs chosen will be elaborated upon and the general steps performed in the DLCs will be explained.

Design situation	DLC	Wind condition	Other conditions	Type of analysis
1) Power production	1.2	NTM $3m/s < V_{hub} < 25m/s$	-	Fatigue
	1.3	ETM V_{hub} = 9.5, 10.5 and 25 m/s	-	Ultimate
2) Power production plus occurrence of fault	2.1	NTM V_{hub} = 9.5, 10.5 and 25 m/s	Control system fault after 360 seconds	Ultimate
3) Start up	3.2	EOG V_{hub} = 3, 8.5, 12.5 and 25 m/s	Start up after 200 seconds, EOG after 260 seconds	Ultimate
5) Emergency shut down	5.1	NTM V_{hub} = 8.5, 12.5 and 25 m/s	Emergency shut down after 360 seconds	Ultimate

Table 5.1: Overview of the DLCs investigated in the case study. Modified from [31].

For normal power production, both a fatigue and ultimate load case is studied. The fatigue load case studied is DLC 1.2. This load case is simulated for every wind speed with steps of 1 m/s in the operational range of the wind turbine. This is thus between 3 and 25 m/s. In DLC 1.2, the normal turbulence model is used for the wind condition. The ultimate load cases studied for normal power production is DLC 1.3. Differently from DLC 1.2, for this load case the extreme turbulence model is used for the wind condition. The ultimate loads for DLC 1.3 are studied at 9.5 m/s, rated wind speed of 10.5 m/s and cut-out wind speed of 25 m/s.

The power generation plus the occurrence of a fault is analysed using DLC 2.1. This DLC uses the normal turbulence model for the wind condition. This load case is also studied at wind speeds of 9.5 m/s, 10.5 m/s and 25 m/s. The fault in this situation takes place after 360 seconds in the simulation. For this load case the ultimate loads are studied. Next, the start up of the wind turbine is analysed for ultimate loads using DLC 3.2. This load case studies the start up of the wind turbine together with an extreme operating gust. The start up takes place after 200 seconds in the simulation, whereas the

extreme operating gust happens after 260 seconds. This load case is studied at 3 m/s, 8.5 m/s, 12.5 m/s and 25 m/s. Finally, the ultimate loads during an emergency shutdown of the wind turbine are studied using DLC 5.1. This DLC uses the normal turbulence model for the wind condition. The emergency shutdown takes place after 360 seconds in the simulation. The ultimate loads are studied at wind speeds of 8.5 m/s, 12.5 m/s and 25 m/s.

For the ultimate load analysis, simulations are thus performed for DLC 1.3, 2.1, 3.2 and 5.1. These DLCs use different wind conditions, which vary between the normal turbulence model, extreme turbulence model and the extreme operating gust. Examples of these can be found in figures 5.1a, 5.1b and 5.1c respectively. As the wind profile is different for each simulation, the exact simulations can not be done twice. This guarantees that the results found in the load calculations are independent.

To ensure some statistical reliability of the results, each simulation is performed six times. This is in line with guidelines from the IEC [31]. Each of these six simulations is done for 660 seconds, of which the first 60 seconds are not taken into account. This is done to ensure that the initial conditions do not have an effect on the simulation results.

The outputs of the simulations are processed as described in section 2.4.3. This is done for both the blade root and the tower base of the wind turbine. The properties of the wind turbine blades and tower used in the calculations can be found in table 5.2. Most parameters are taken from the IEA documentation of the wind turbine [25] and the GitHub database [30]. Only the ultimate compressive strength of the blades is different, as this is not given for the blade root in the documentation. It is assumed that the ultimate compressive strength for the blades is 600 MPa. However, if the ultimate loads approach the ultimate strength of the triax glass fibre reinforced epoxy, which is the main material of the blade root, extra attention should be given to this. The ultimate compressive strength of this material is 448.9 MPa [25].

	Blades	**Tower**
Stiffness [Nm^2]	$1.525 \cdot 10^{11}$ [30]	$3.185 \cdot 10^{12}$ [25]
Young's Modulus [MPa]	$28.7 \cdot 10^9$ [25]	$200 \cdot 10^9$ [25]
x / y [m]	2.6 [25]	5 [25]
Ultimate stress [MPa]	600	450 [25]

Table 5.2: Properties of the IEA 15MW wind turbine used for the load calculations.
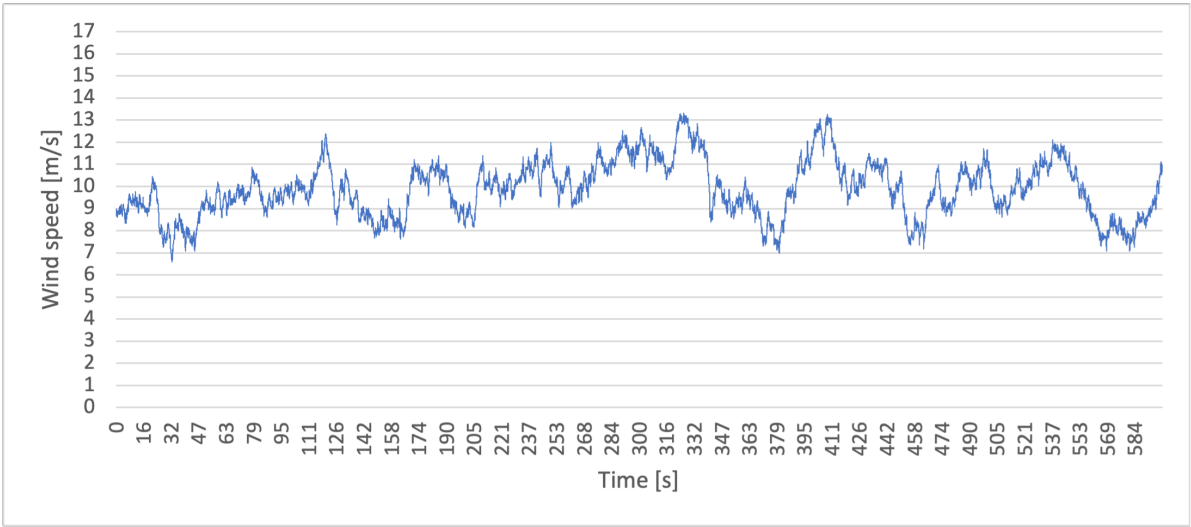
(a) Wind condition based on the normal turbulence model with a mean wind speed of 10 m/s.
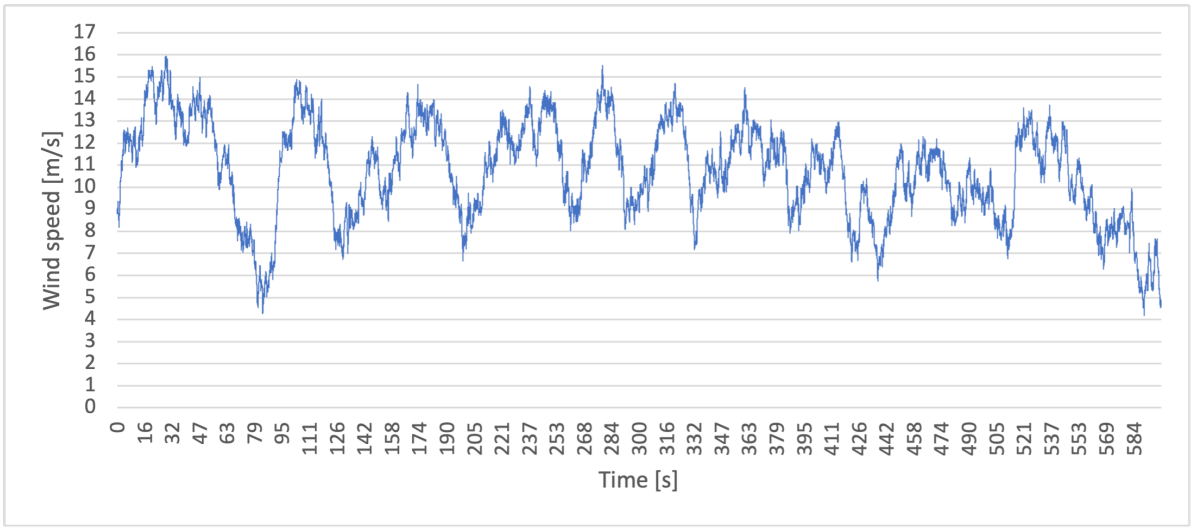
(b) Wind condition based on the extreme turbulence model with a mean wind speed of 10.5 m/s.
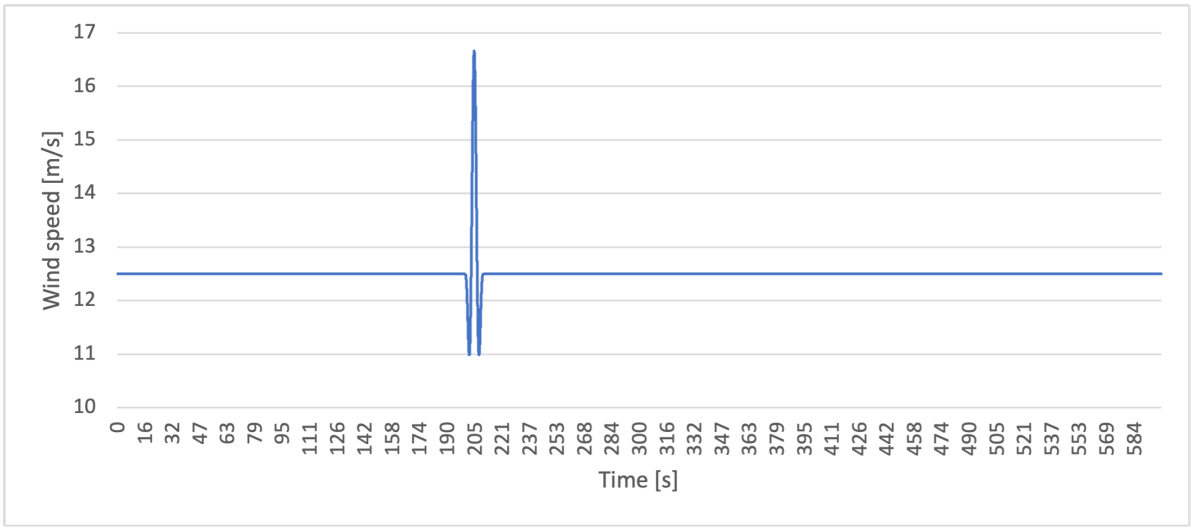
(c) Wind condition based on the extreme operating gust model with a mean wind speed of 12.5 m/s.

Figure 5.1: Wind conditions used in the cases.

Next, DLC 1.2 is thus the only load case where a fatigue load analysis is performed. In this scenario the wind condition is determined by the normal turbulence model as in figure 5.1a.

For the fatigue analysis, firstly two simulations are performed for each wind speed from 3 to 25 m/s with steps of 1 m/s. Only two simulations are performed for the fatigue analysis due to time constraints. However, differently from the ultimate load analysis, in the fatigue load analysis the entire simulation is used instead of just the maximum moments. This makes the analysis more reliable statistically.

Next, the moments imposed on the blade root and the tower base in the simulations are converted to stresses. The stresses are calculated similarly as for the ultimate load analysis, again using the properties as stated in table 5.2. This is done in the flap-wise and edge-wise direction for the blade root, and in the fore-aft and side-side direction for the tower base. The stress cycles are extracted from these stresses using the rainflow counting method. From these stress cycles the FDEL and the damage for the 10-minute simulation can be calculated.

As the FDEL will be used to compare the baseline case to the other two cases, this is the main parameter that will be determined for the fatigue load analysis. The FDEL is firstly determined for the 10-minute simulations using equation 2.16. To use this equation, the Wöhler exponent m is needed. For the blades, a Wöhler constant m = 9 is used [48]. For the tower a Wöhler constant m = 4 is used [49], [50]. This gives a FDEL for each wind speed in the operational range of the wind turbine. The number of reference equivalent load cycles is set such that the FDEL represents the load which would cause the same damage as all load cycles combined, if it were applied with a frequency of 1 Hz. To do this, the reference equivalent load cycles is set to 600 for the 10-minute simulations.

From the FDEL per wind speed, the lifetime FDEL can be determined as explained in section 2.4.4. The lifetime FDEL will be used to compare the fatigue damage in each case based on only one number. The number of reference equivalent load cycles used is 10512000, which is the amount of seconds in 20 years. This gives the lifetime FDEL with a reference frequency of 1 Hz.

Lastly, the fatigue damage is calculated for both the blade root and the tower base using Miner's rule. To calculate the fatigue damage using Miner's rule, firstly the maximum allowed load cycles is calculated. For the blades this can be done using the ultimate compressive strength from table 5.2 and the Wöhler constant m = 9 [48], as the Wöhler curve for the blades of the wind turbine has a single slope. However, the Wöhler curve of steel has two slopes. The exact Wöhler curve, and therefore the fatigue endurance limit, is not documented for the steel used in the tower of the IEA 15MW wind turbine. However, the same material, A572 Gr. 50 Steel, is studied in [51]. In this study a fatigue strength, which is the load range at the knee point of the Wöhler curve, of 131.72 MPa after 10^6 cycles has been determined. This fatigue strength is also used in the fatigue analysis of the tower of the IEA 15MW wind turbine. Similarly as for the FDEL, a Wöhler constant m = 4 is used for the tower [49], [50]. With this, the maximum allowed load cycles for the tower can be calculated, and subsequently the damage for each wind speed bin. Similarly as for the lifetime FDEL, the lifetime damage on the blades and tower of the wind turbine is calculated using the probabilities from the Weibull distribution. The Weibull distribution is dependent on the location of the wind turbine, which will be discussed in the next section.

5.1.3. Location Case Study
As introduced in section 3.1, the wind turbine studied is located close to the shore of the Netherlands. Besides the grid the wind turbine is connected to, the location is of importance for the wind distribution. The location used is near existing or future wind farms off the shore of the Netherlands [52]. The exact location used can be seen in figure 5.2.
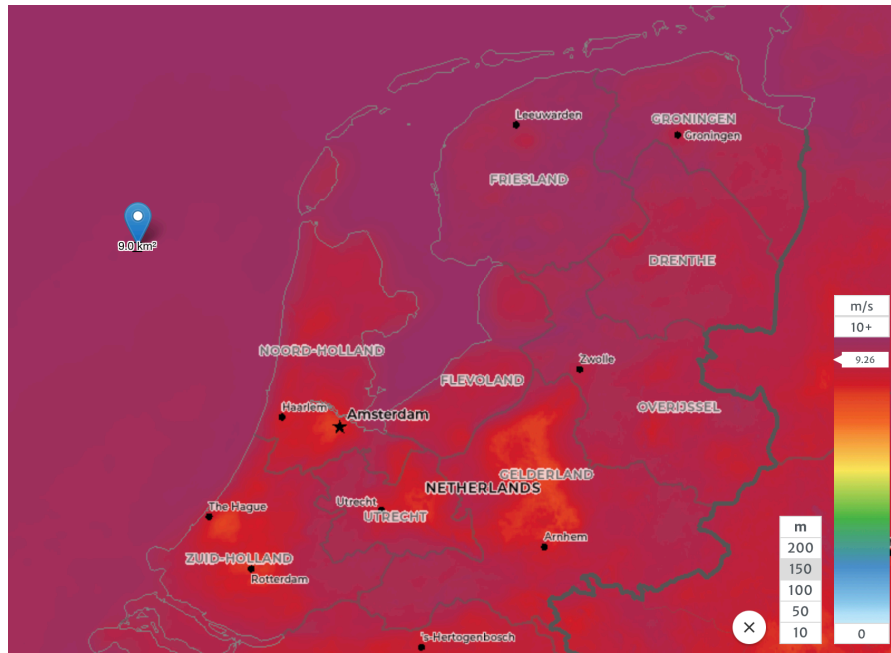
Figure 5.2: Location used in the case studies for the wind turbine. Figure from Global Wind Atlas [53].

The probability distribution of the wind speed is based on a Weibull distribution. For this distribution a shape parameter of 2.18 and a scale parameter of 10.54 are used [53]. As mentioned in section 5.1.1, the probabilities obtained from the Weibull curve will be used to determine the lifetime FDEL. Besides the Weibull parameters, location also affects grid frequency. The data sets used for the grid frequency are discussed in the next section.

5.1.4. Grid Frequency Data Sets Used

Using the method as described in section 2.3.2 and the data-set introduced in section 3.2, three individual data-sets have been developed to use as grid frequency inputs in the case study. These include a data-set portraying the normal behavior of the grid frequency, the grid frequency including the maximum RoCoF and the grid frequency including the maximum deviation from 50 Hz. "Maximum" here means: the maximum RoCoF and the maximum frequency deviation present in the entire annual grid frequency data-set of 2021 as recorded in Flensburg, Germany.
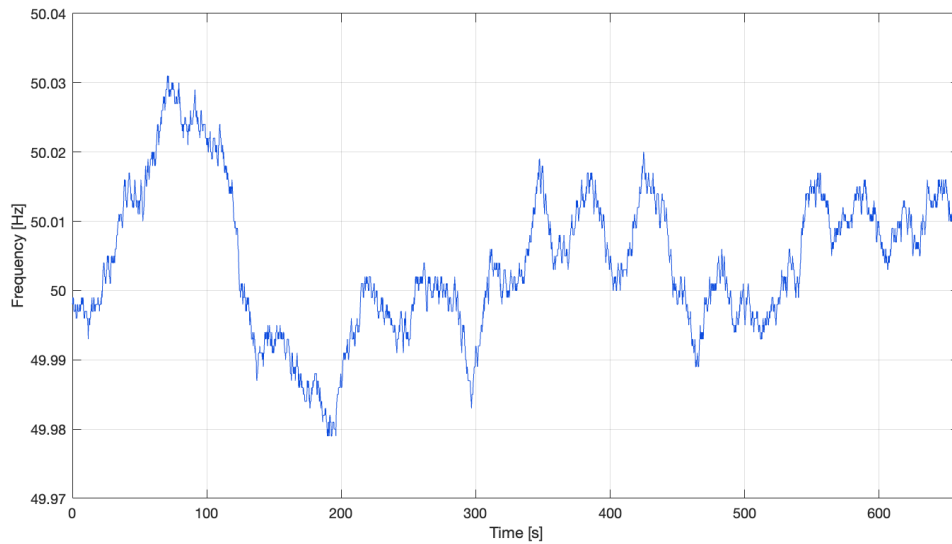
Figure 5.3: Normal grid frequency behavior extracted from the annual data set.

The normal behavior of the grid frequency can be found in figure 5.3. As can be seen in this figure, the frequency deviates normally around 50 Hz, representing the normal frequency behavior that the controllers would need to respond to.
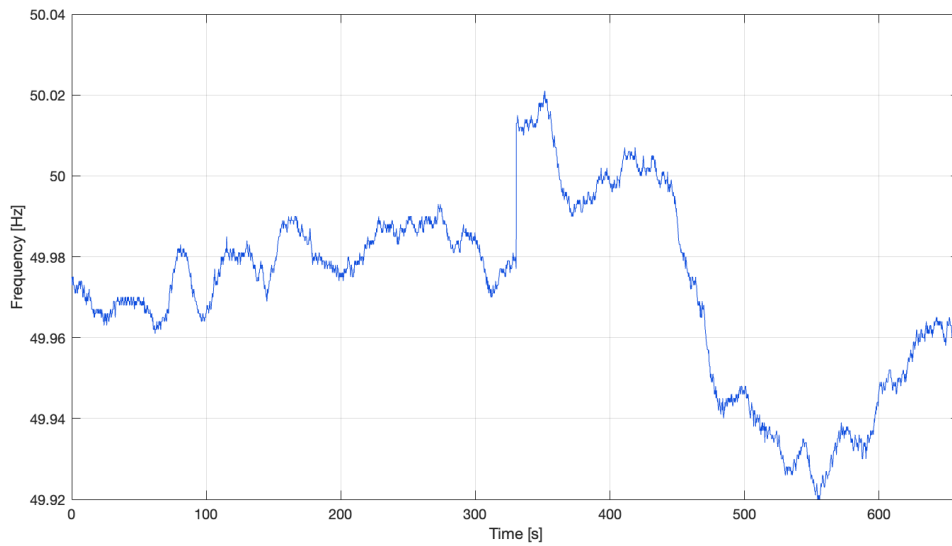
Figure 5.4: Grid frequency showing the highest RoCoF extracted from the annual data set.

The grid frequency including the maximum RoCoF can be found in figure 5.4. The maximum RoCoF in the data set is found to be 0.2195 Hz/s. This can be seen in the figure at 330 seconds. For the maximum RoCoF it is especially of interest to see how the synthetic inertia controller will react, and how the loads will behave as this will trigger the largest reaction from this controller.
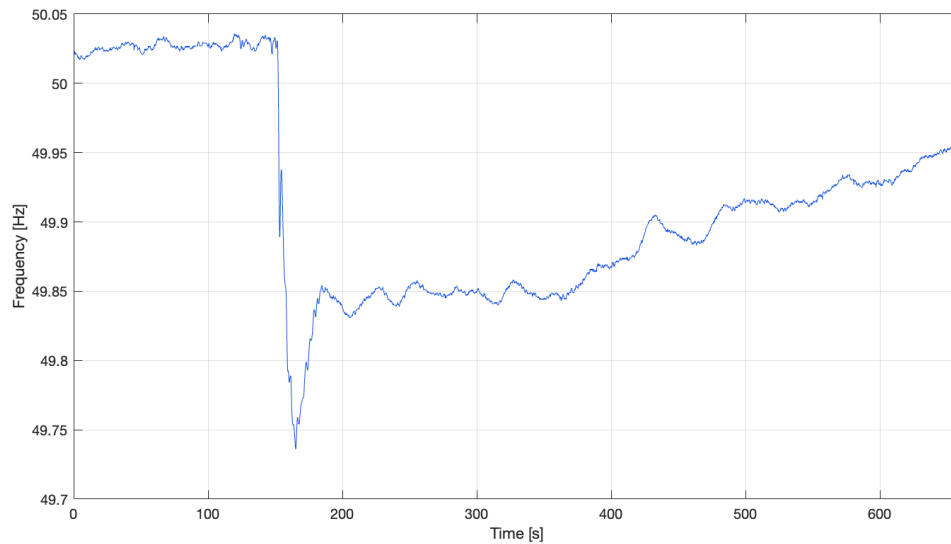
Figure 5.5: Grid frequency showing the maximum deviation from 50 Hz extracted from the annual data set.

Finally, the grid frequency including the maximum deviation from 50 Hz can be found in figure 5.5. While the maximum deviation can be found in this data set, the maximum RoCoF identified here is only 0.1402 Hz/s, evident at approximately 150 seconds in the figure. For this frequency the most interesting response is expected from the FFR controller, as this controller responds to the frequency deviation. Consequently, the controller will have the biggest overall response.

5.2. Case Study Analysis and Findings

5.2.1. Case 1: Baseline Case

The baseline case is the normal operation of the wind turbine using the baseline controller. For this case, all load cases as described in section 5.1.2 are analysed. This section is divided into two parts, the ultimate load analysis and the fatigue analysis.

Ultimate Load Analysis

Load Case	Wind Speed [m/s]	$\sigma_{Flap,max}$ [MPa]	$\sigma_{Edge,max}$ [MPa]	$y_{tip,max}$ [m]	$\sigma_{FA,max}$ [MPa]	$\sigma_{StS,max}$ [MPa]
DLC 1.3	9.5	51.9	21.1	25.7	166.1	26.5
DLC 1.3	10.5	53.5	21.1	26.5	170.1	29.1
DLC 1.3	25	41.7	20.1	14.4	118.9	64.9
DLC 2.1	9.5	48.8	21.9	23.8	155.9	28.6
DLC 2.1	10.5	49.2	22.1	24.5	159.7	29.7
DLC 2.1	25	36.4	19.9	10.9	101.7	57.2
DLC 3.2	3	17.2	16.8	6.0	14.6	23.6
DLC 3.2	8.5	30.0	16.0	15.7	91.2	11.7
DLC 3.2	12.5	47.2	16.8	23.1	173.1	20.0
DLC 3.2	25	27.6	15.2	7.9	104.5	43.4
DLC 5.1	8.5	42.8	18.5	21.3	138.6	21.0
DLC 5.1	12.5	48.4	18.8	24.1	152.1	29.7
DLC 5.1	25	37.5	18.7	11.8	105.8	57.6

Table 5.3: Results ultimate load analysis case 1: baseline case

The results for the ultimate load analysis can be found in table 5.3. The table firstly shows the maximum flap wise stress ($\sigma_{Flap,max}$) and edge wise stress ($\sigma_{Edge,max}$) for the blades. Additionally, the table also shows the maximum tip deflection of the blades ($y_{tip,max}$). Furthermore, the table shows the maximum stresses on the tower in the fore-aft ($\sigma_{FA,max}$) and side-side direction ($\sigma_{StS,max}$). The maximum stress and maximum tip deflection in this table have already been corrected with the appropriate partial safety factors from section 2.4.2. The maximum stresses for each case can also be found in figure 5.6.
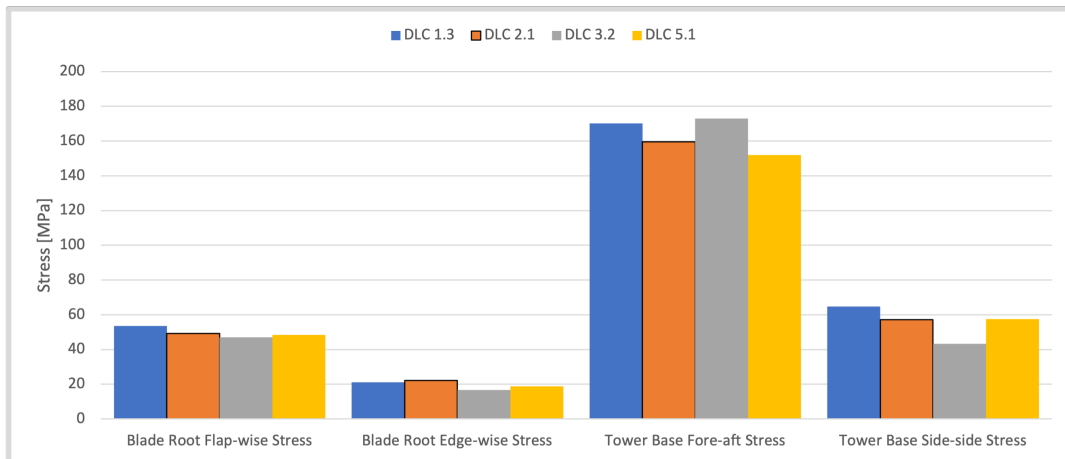
Figure 5.6: Maximum stress of each ultimate load case in case 1: baseline case. The figure shows the stresses in the flap-wise and edge-wise direction for the blades, and in the fore-aft and side-side direction for the tower.

Because the moment of inertia, and subsequently also the stress, is calculated using uniform conditions and does not take into account stress concentrations, the results from this ultimate load analysis do not give direct conclusions on the integrity of the wind turbine. This can be justified, as the main goal for the loads is to compare the loads in the baseline case, case 1, to those in case 2 and case 3.

The ultimate stresses can however give an indication on which loads might be design driving. For this reason the maximum stresses in both the flap-wise and the edge-wise direction for the blades and in the fore-aft and Side-Side direction for the tower are compared to: $\frac{1}{\gamma_n \cdot \gamma_m} \cdot \sigma_{ultimate}$. Based on this relation, the maximum stresses on the blades should remain lower than or equal to 500 MPA, whereas the maximum stresses on the tower should remain below 346.2 MPa. The results from the baseline scenario have shown that the maximum loads stay well below these values.

Lastly, the maximum tip deflections are checked in order to see if these stay below the maximum tip deflection before hitting the tower. The maximum tip deflection is equal to the unbent blade tip distance to the tower, which is 30 meters [25]. The maximum tip deflection in the DLCs is 26.5. This tip deflection already incorporates the total safety factor for the tip deflection.

Fatigue Load Analysis

The results for the flap-wise and edge-wise FDEL on the blades can be found in figure 5.7, and for the fore-aft and side-side FDEL in figure 5.8.
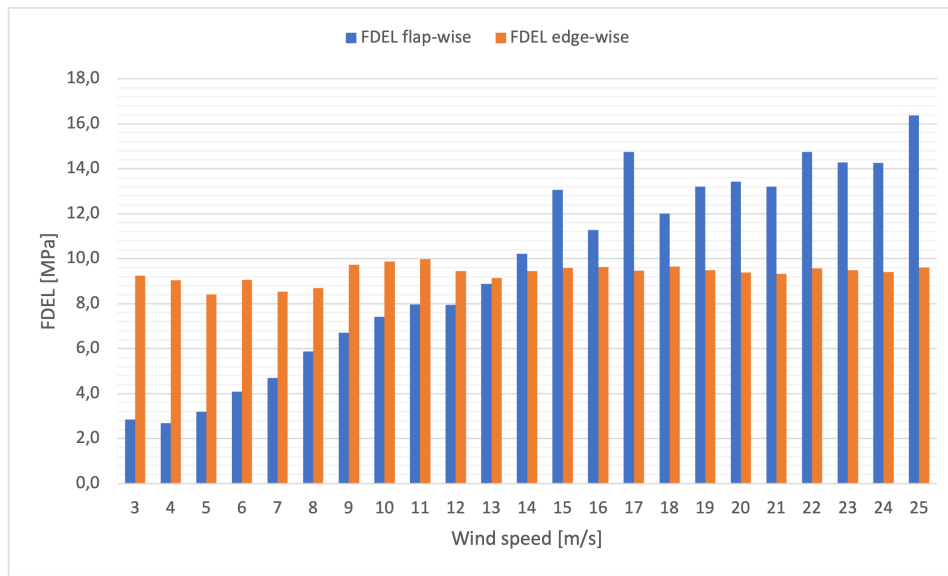
Figure 5.7: FDEL of the baseline case in the flap-wise and edge-wise direction for the wind turbine blades at each wind speed.
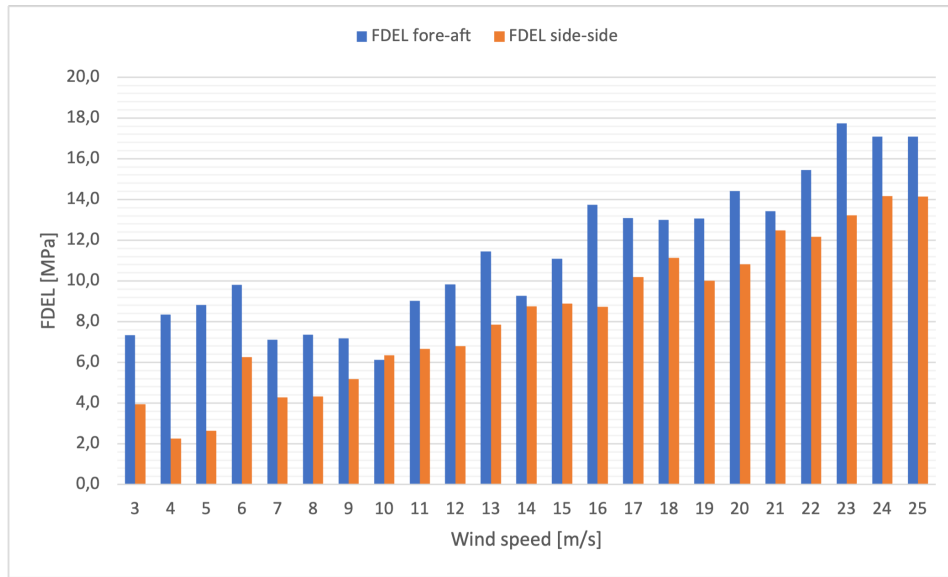
Figure 5.8: FDEL of the baseline case in the fore-aft and side-side direction for the wind turbine blades at each wind speed.

The FDEL on the blades in the flap-wise direction increases as the wind speed increases. On the other hand, the FDEL in the edge-wise direction remains stable between about 8 MPa and 10 MPa. The FDEL on the tower of the wind turbine shows a mainly increasing trend for both the fore-aft and the side-side direction. The increase in FDEL at higher wind speed for the flap-wise, fore-aft and side-side direction is as would be expected at higher aerodynamic loads. The fact that the stresses in the edge-wise direction on the blades stay rather constant could suggest that the blades have been optimised to withstand the loads in this direction. This could be true, as this would be a problem to address with wind turbine blades of this size. It should be noted that this is not explicitly mentioned in the documentation of the reference turbine. Additionally, the edge-wise stiffness of the blades of the IEA 15MW reference turbine is on average about 2 times higher compared to the flap-wise stiffness of the blades [25].

Next, the lifetime FDEL is determined. This results in a lifetime FDEL on the blades in the flap-wise direction of 11.3 Mpa, and of 9.4 MPa in the edge-wise direction. Furthermore, this gives a lifetime FDEL on the tower of 10.0 MPa in the fore-aft direction, and of 7.3 MPa in the side-side direction.

Additionally, the damage on the blades and tower of the wind turbine is calculated using Miner's rule. This gives a flap-wise lifetime damage of $3.9 \cdot 10^{-10}$ on the blades and an edge-wise lifetime damage of $6.8 \cdot 10^{-11}$. Additionally, this gives a fore-aft lifetime damage on the tower of 0.001 and an edge-wise lifetime damage of 0.0004.

A remark should be made again at this point that the reader should keep in mind that the main purpose for these numbers is to compare the different cases. As the FDEL and the damage calculated does not take into account the mean of the load cycle, it is not intended to use these numbers to see if the actual fatigue damage of the lifetime would exceed the allowable threshold in its lifetime.

5.2.2. Case 2: Synthetic Inertia Case

The second case studied is the synthetic inertia case. In this case the wind turbine is operated using the synthetic inertia controller as described in section 4.2. This section is divided into three parts. Firstly, the settings used for the proportional constant will be chosen and motivated. After this, the results of the ultimate load analysis and fatigue load analysis will be given and further discussed.

Proportional Constant

The only parameter used in the synthetic inertia controller which should be highlighted at this point, is the proportional constant K_0. This proportional constant determines the magnitude with which the torque demand is changed. Studying the effect of different proportional constants gives an insight on the scale on which synthetic inertia can be provided. The proportional constant K_0 is firstly used similar to how it is constructed in [22] and [45]. In these papers, the proportional constant is set to 46.6. This part of the synthetic inertia case will be referred to as case 2A.

Due to the small RoCoF of the grid frequency in a large grid, a proportional constant of 46.6 results in a change in torque demand ranging from 10^4 to 10^5 Nm. This is a relatively small response compared to the normal operational points of the torque controller, which at rated power is just below $2 \cdot 10^7$. Therefore, it is also of interest to see what happens to the ultimate and fatigue loads on the wind turbine if the response of the synthetic inertia controller would be much larger. To study this effect, the wind turbine is studied while supplying synthetic inertia with a proportional constant 100 times larger then in case 2A. This case will be referred to as case 2B. The proportional constant for case 2B is therefore set to 4660. This results in a change in torque demand ranging from 10^6 to 10^7 Nm. Case 2A and 2B will both be evaluated in the ultimate and fatigue load analysis in the next section.

Ultimate Load Analysis

Similar to case 1, the ultimate load analysis is performed for DLCs 1.3, 2.1, 3.2 and 5.1. However, in case 2 the load cases are analysed for all three grid frequency inputs as shown in figure 5.1. This is done for both case 2A and case 2B.

Firstly, the results of case 2A will be discussed. The maximum loads for each load case can be found in figure 5.9. This figure shows the maximum stresses for each load case at the three different grid frequency inputs. What can be seen from this figure is that in terms of the different grid frequency inputs, the stresses on the blades and tower do not show any significant change.
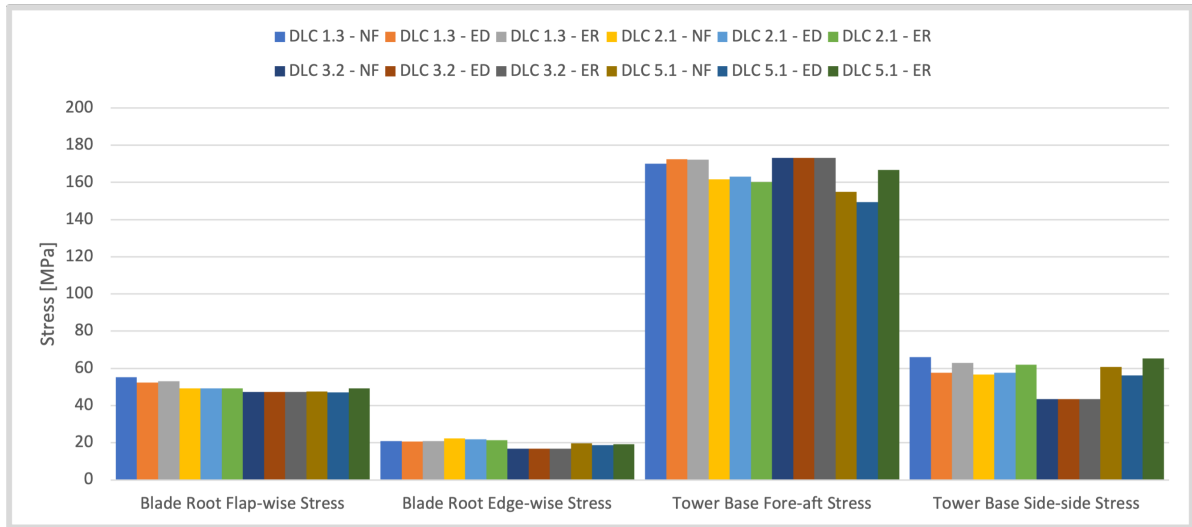
Figure 5.9: Maximum stress on the blade roots and tower base for each ultimate load case in case 2A for all grid frequency inputs. The grid frequency inputs are denoted as NF for the normal grid frequency, ED for the extreme deviation grid frequency and ER for the extreme RoCoF.

The maximum loads for each load case in case 2B can be found in figure 5.10. As the figure shows, case 2B overall shows similar behavior compared to case 2A considering the maximum stresses for each load case at the three different grid frequency inputs. The biggest difference can be found for

the side-side loads on the tower, which shows an increase of about 13% for the extreme deviation grid frequency input.
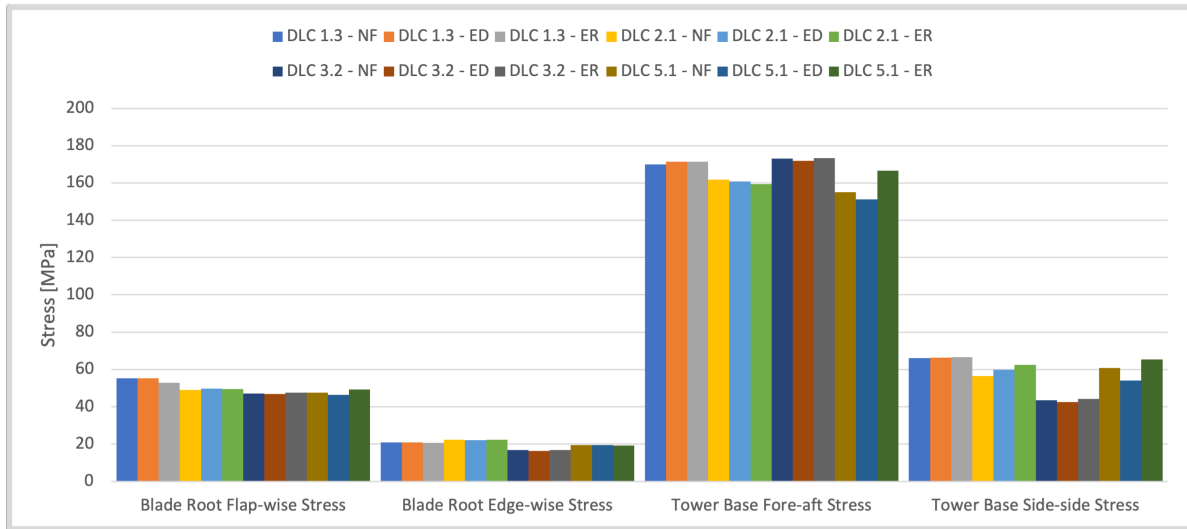
Figure 5.10: Maximum stress on the blade roots and tower base for each ultimate load case in case 2B for all grid frequency inputs. The grid frequency inputs are denoted as NF for the normal grid frequency, ED for the extreme deviation grid frequency and ER for the extreme RoCoF.

The last step in the ultimate load analysis is to determine the maximum tip deflection. The maximum tip deflection for each DLC can be found in figure 5.11. No major differences were found between case 2A and case 2B, as can be seen in the figure.
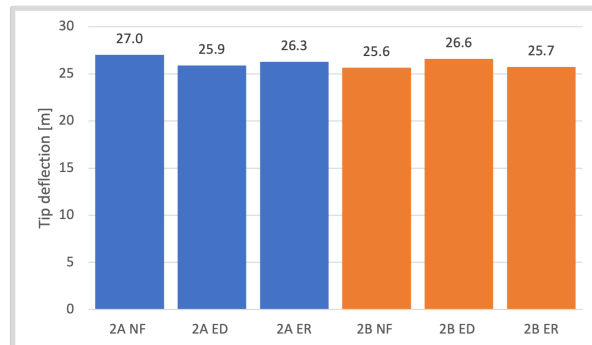
Figure 5.11: Maximum tip deflection for case 2. The grid frequency inputs are denoted as NF for the normal grid frequency, ED for the extreme deviation grid frequency and ER for the extreme RoCoF.

Fatigue Load Analysis

Next, the fatigue load analysis is performed for both case 2A and 2B. The analysis for each sub-case is performed for all three grid frequency inputs.

Firstly, the FDEL is calculated for each wind speed for both the tower and blades of the wind turbine in case 2A. The FDEL for all grid frequency inputs can be found in figure 5.12. Here, the FDEL in the flap-wise, edge-wise, fore-aft and side-side directions are plotted separately for all operational wind speeds with a step of 1 m/s.
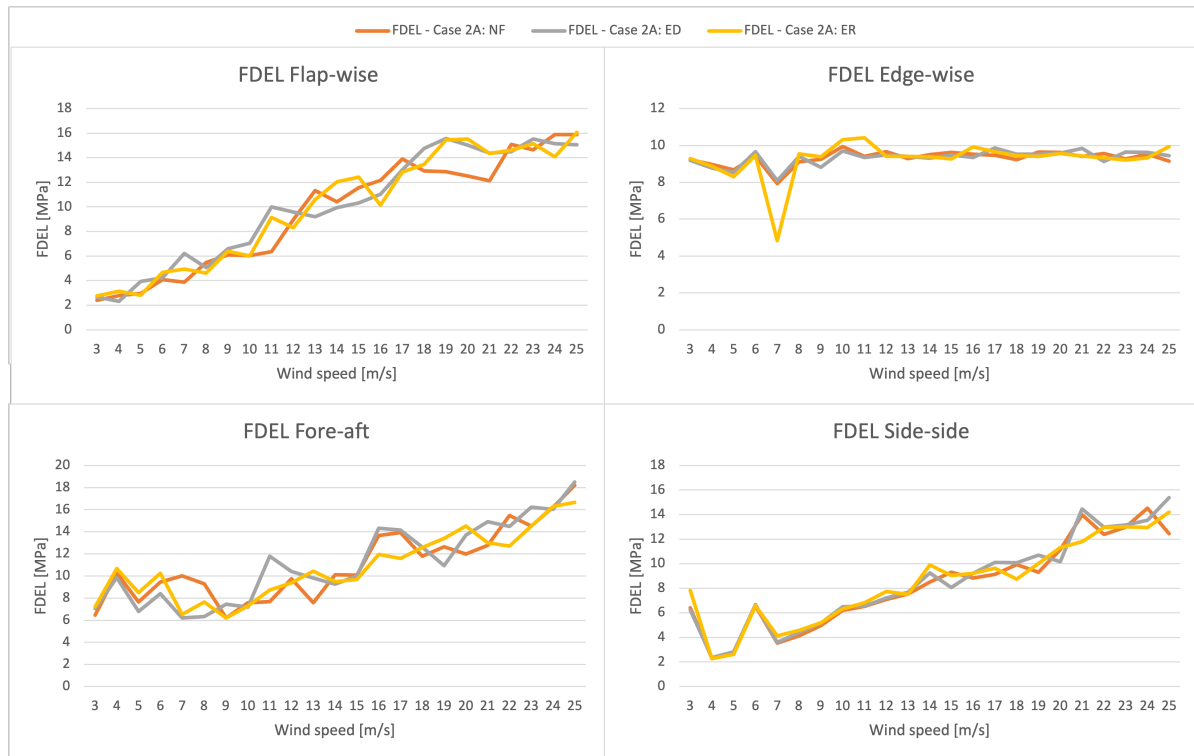
Figure 5.12: FDEL for wind speeds from 3 to 25 m/s for all scenarios in case 2A. The grid frequency inputs are denoted as NF for the normal grid frequency, ED for the extreme deviation grid frequency and ER for the extreme RoCoF.

The FDEL per wind speed shows similar values for all grid frequency inputs. The flap-wise FDEL on the blades gradually increase with increasing wind speeds, whereas the edge-wise FDEL stays between 8 and 10 MPa. An increase in FDEL for increasing wind speeds can also be seen for the fore-aft and side-side FDEL on the tower.

The lifetime FDELs can be found in table 5.4. The lifetime FDEL for all three grid frequency inputs show similar behavior as the FDEL per wind speed, as no substantial differences between the different grid frequency inputs are seen.

	Case 2A: NF	Case 2A: ED	Case 2A: ER
Flap-wise lifetime FDEL [MPa]	10.8	11.2	11.2
Edge-wise lifetime FDEL [MPa]	9.3	9.3	9.5
Fore-aft lifetime FDEL [MPa]	9.9	10.0	9.6
Side-side lifetime FDEL [MPa]	7.2	7.4	7.4

Table 5.4: Lifetime FDEL on the tower and blades in case 2A. The grid frequency inputs are denoted as NF for the normal grid frequency, ED for the extreme deviation grid frequency and ER for the extreme RoCoF.

Additionally, also the lifetime damages are calculated for case 2A. All lifetime damages calculated can be found in table C.1 in appendix C.

The FDELs for case 2B show an average increase of 5% in the edge-wise and 4% in the fore-aft direction, compared to case 2A. The FDELs on the blades in the flap-wise direction differ per grid frequency input, and show an average increase of 3% for the normal grid frequency input, generally stay the same for the extreme deviation input and show an average decrease of 3% for the extreme RoCoF input. However, a large average increase of about 20% is seen in the side-side direction of the

tower. This increase is shown in figure 5.13. In this figure the FDEL is shown for all wind speeds for all grid frequency inputs of case 2B. The overall largest increase is seen for a grid frequency input of the maximum RoCoF. This can again be explained by the increased response from the synthetic inertia controller due to a higher RoCoF.
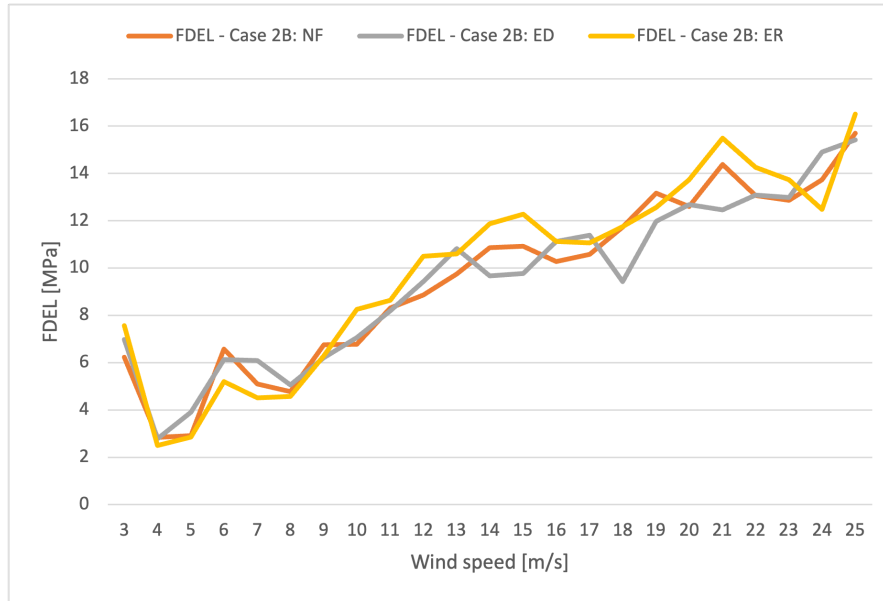
Figure 5.13: Side-side FDEL on the tower for case 1 and all scenarios in case 2B. The grid frequency inputs are denoted as NF for the normal grid frequency, ED for the extreme deviation grid frequency and ER for the extreme RoCoF.

This increase can also be seen when calculating the lifetime FDELs, as in table 5.5. The lifetime FDELs shows a small decrease in flap-wise FDEL, a small increase in edge-wise and fore-aft FDEL and lastly the much larger increase in side-side FDEL.

	Case 2B: NF	Case 2B: ED	Case 2B: ER
Flap-wise lifetime FDEL [MPa]	11.1	11.2	10.9
Edge-wise lifetime FDEL [MPa]	9.7	9.7	9.8
Fore-aft lifetime FDEL [MPa]	10.1	10.4	10.0
Side-side lifetime FDEL [MPa]	8.5	8.4	9.1

Table 5.5: Lifetime FDEL on the tower and blades in case 2B. The grid frequency inputs are denoted as NF for the normal grid frequency, ED for the extreme deviation grid frequency and ER for the extreme RoCoF.

Lastly, the damage on the blades and tower is calculated using Miner's rule. Because of the Wöhler exponent m in the calculation of the damage, the increase in FDEL is amplified in the increase in lifetime damage. The damage can again be found in table C.1 in appendix C.

5.2.3. Case 3: FFR Case

The third and last case is the FFR case. In this case, the wind turbine is operated using the FFR controller as described in section 4.3. To use this controller, the wind turbine must be de-loaded. This section is again divided into three parts. First, the proportional constant used in the FFR controller and the de-loading strategy used are chosen and further explained. After this, the results of the ultimate load analysis and fatigue analysis are given and further discussed.

De-loading Factor and Proportional Constant

To supply FFR in this case, the wind turbine needs to be de-loaded. As was explained in section 4.4, de-loading strategy 2 will be used in order to supply FFR in case 3. The wind turbine in this case is de-loaded with 10% such that it is operating at 90% of its nominal power. This is similar to the examples given in section 4.3.1.

The proportional constant used in the FFR controller is the DROOP constant R_0. Similar to case 2, case 3 will also be studied at two different proportional constants. This constant is firstly set to 2% (0.02), as suggested in [22] and [45]. This will be referred to as case 3A.

In line with case 2, the FFR controller will also be studied at a proportional constant which is 100 times as large as in case 2A. For the second part of case 3, the DROOP constant is thus set to 200% (2). This case will be referred to as case 3B.

Ultimate Load Analysis

Similar to case 2, the ultimate load analysis is performed for DLCs 1.3, 2.1, 3.2 and 5.1 for both case 3A and 3B at all three grid frequency inputs.

The results for case 3A can be found in figure 5.14. The overall slightly higher loads for results corresponding to the maximum deviation grid frequency input can be explained from the behavior of the FFR controller. As the controller reacts to a deviation in grid frequency from 50 Hz, the change in torque demand and pitch set point will be largest for this scenario. Because of this, the wind turbine will be de-loaded less, and the maximum stresses on the wind turbine go up.
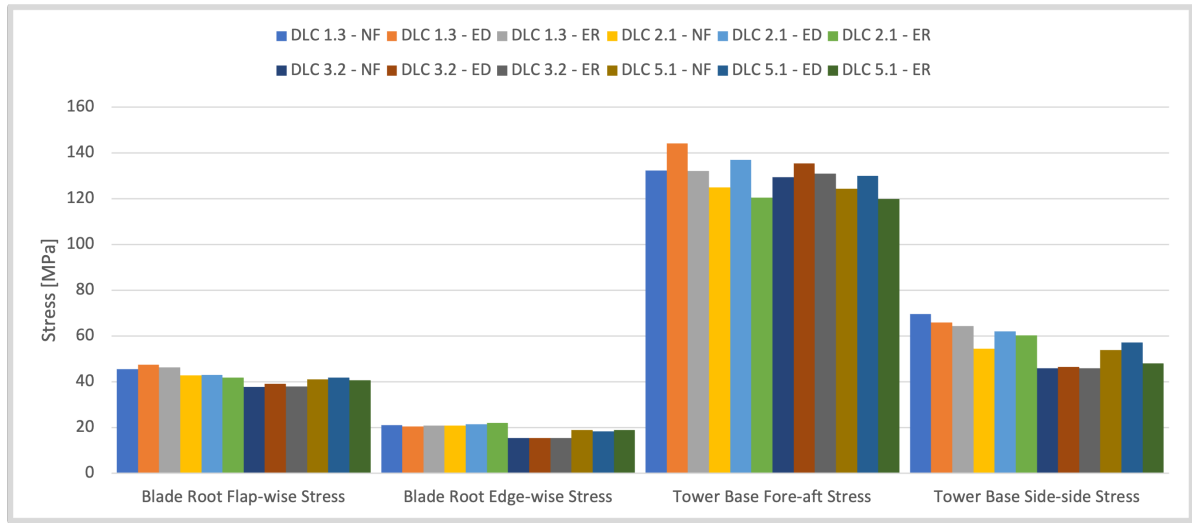
Figure 5.14: Maximum stress on the blade roots and tower base for each ultimate load case in case 3A for all grid frequency inputs. The grid frequency inputs are denoted as NF for the normal grid frequency, ED for the extreme deviation grid frequency and ER for the extreme RoCoF.

Next, the maximum stresses for case 3B are studied. The results for case 3B can be found in figure 5.15. The results for this case show that the maximum loads increased compared to case 3A. This can be explained by the fact that due to the increased proportional gain of this case, the wind turbine will be operating closer to its maximum power compared to case 3A.

The maximum stresses on the tower show no large changes for the side-side direction. On the other hand, the maximum stresses in the fore-aft direction do show some changes. Similar to the maximum fore-aft stresses in case 3A, the stresses using the maximum deviation grid frequency input shows higher maximum stresses compared to the two other grid frequency inputs.
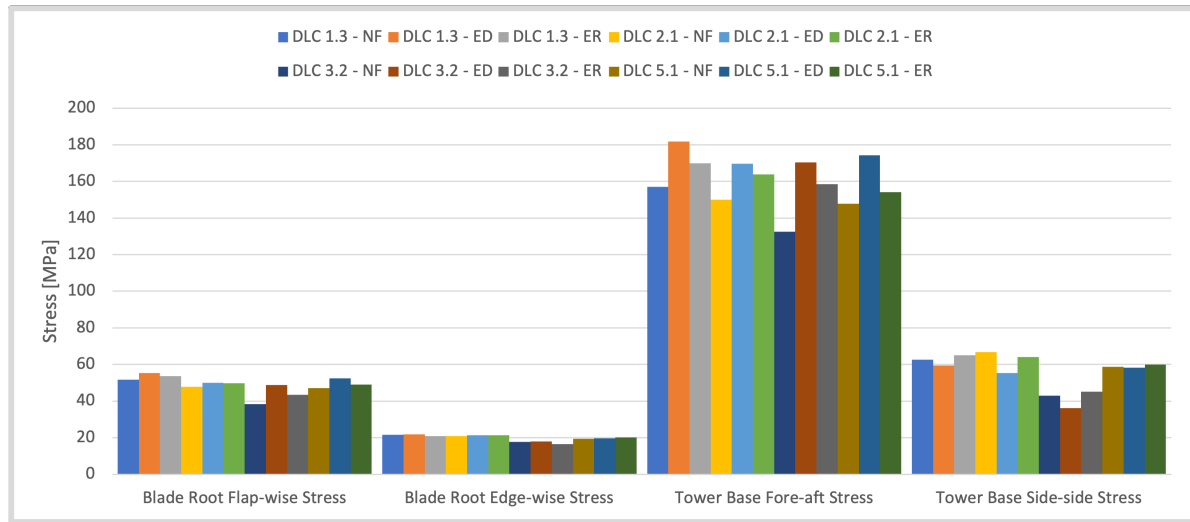
Figure 5.15: Maximum stress on the blade roots and tower base for each ultimate load case in case 3B for all grid frequency inputs. The grid frequency inputs are denoted as NF for the normal grid frequency, ED for the extreme deviation grid frequency and ER for the extreme RoCoF.

The last step in the ultimate load analysis for case 3 is to find the maximum tip deflection for each DLC. This can be found in figure 5.16. The tip deflections for case 3A are substantially lower compared to those in case 3B. This is as expected, as in case 3A the response of the FFR controller is much smaller compared to the response in case 3B. Because of this, the wind turbine operates much closer to the de-loaded point in case 3A, and to the maximum power operating point in 3B. Because of this the loads on the blades are higher in case 3B, which causes a higher tip deflection.
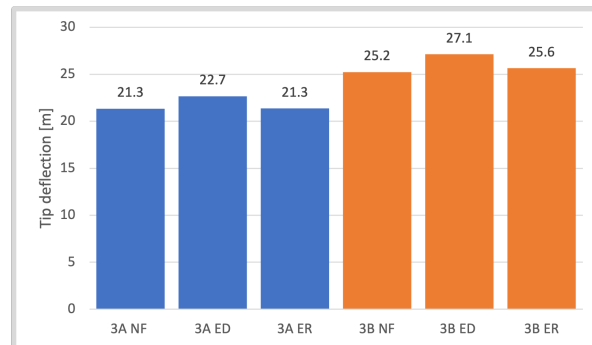
Figure 5.16: Maximum tip deflection for case 3. The grid frequency inputs are denoted as NF for the normal grid frequency, ED for the extreme deviation grid frequency and ER for the extreme RoCoF.

Fatigue Load Analysis

Figure 5.17 shows the FDELs corresponding to the fatigue analysis of case 3A. The FDELs in the edge-wise, fore-aft and side-side directions show no large deviations. The FDELs in the flap-wise direction do show some minor differences between the three grid frequency inputs.

Figure 5.17: FDEL for wind speeds 3 to 25 m/s for all scenarios in case 3A. The grid frequency inputs are denoted as NF for the normal grid frequency, ED for the extreme deviation grid frequency and ER for the extreme RoCoF.

The lifetime FDELs for case 3A can be found in table 5.6. The lifetime FDELs for case 3A show similar values for all three grid frequency inputs, except for the flap-wise lifetime FDEL. This lifetime FDEL is about 0.6 MPa higher for the extreme deviation grid frequency input compared to the other two grid frequency inputs. This can be attributed to the fact that the response of the controller is larger for this grid frequency input.

	Case 3A: NF	Case 3A: ED	Case 3A: ER
Flap-wise lifetime FDEL [MPa]	10.6	11.3	10.7
Edge-wise lifetime FDEL [MPa]	9.1	9.0	8.9
Fore-aft lifetime FDEL [MPa]	9.6	9.5	9.4
Side-side lifetime FDEL [MPa]	7.2	7.2	7.3

Table 5.6: Lifetime FDEL on the tower and blades in case 3A. The grid frequency inputs are denoted as NF for the normal grid frequency, ED for the extreme deviation grid frequency and ER for the extreme RoCoF.

Figure 5.18 shows the FDELs corresponding to case 3B. The results show that the FDELs increase for almost all directions compared to case 3A, except for the edge-wise FDELs on the blade. Due to the high proportional gain and the corresponding high response to the frequency deviation, the wind turbine does not operate at the 10% de-loaded operating point during large parts of the simulations. Because of this, less oscillations were seen in the rotor speed. However, the peaks between 10 and 12 m/s are not completely trustworthy because of the de-loading strategy used.

The results show that the responses to the maximum RoCoF and maximum deviation of the grid frequency are imposed to a significant increase in the flap-wise and fore-aft FDEL. The side-side FDEL also shows some large increases. However, these increases are mainly seen around rated wind speed

and should therefore be interpreted with care.
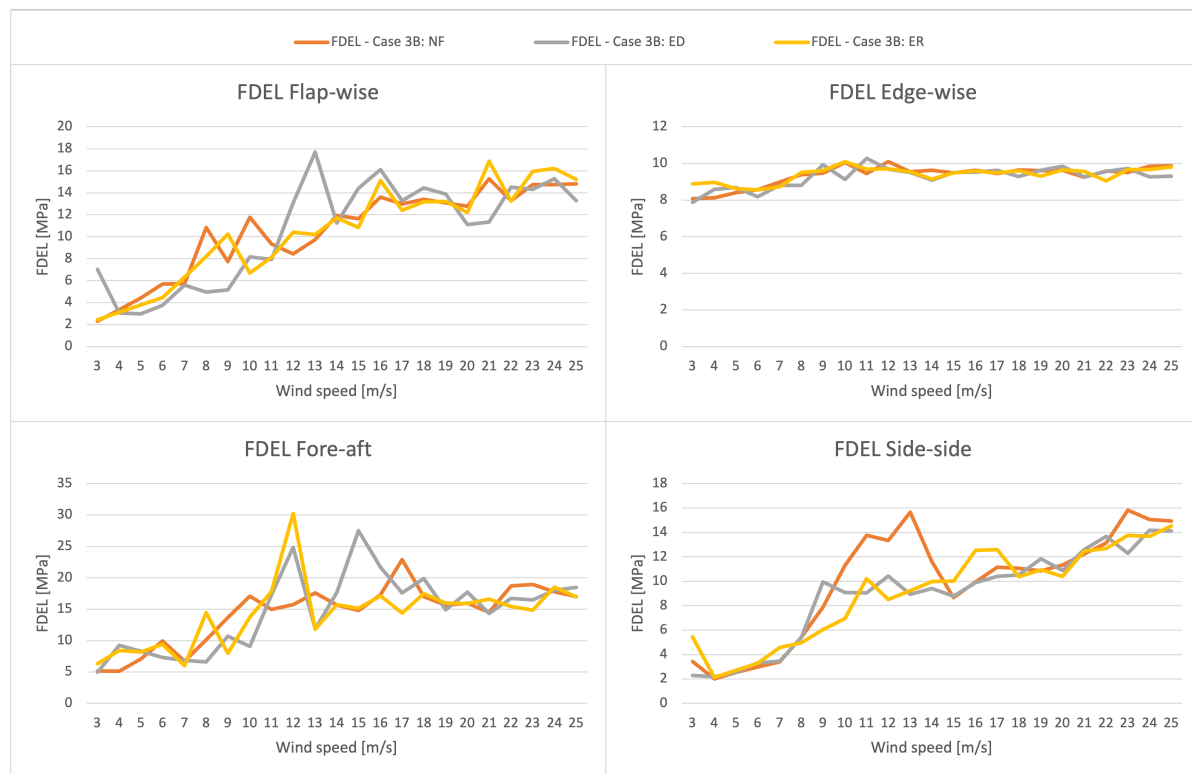
Figure 5.18: FDEL for wind speeds 3 to 25 m/s for all scenarios in case 3B. The grid frequency inputs are denoted as NF for the normal grid frequency, ED for the extreme deviation grid frequency and ER for the extreme RoCoF.

The lifetime FDELs for case 3B can be found in figure 5.7. A similar increase can be seen for the lifetime FDELs as was seen in the FDEL per wind speed, when compared to case 3A.

	Case 3A: NF	**Case 3A: ED**	**Case 3A: ER**
Flap-wise lifetime FDEL [MPa]	11.8	16.4	12.0
Edge-wise lifetime FDEL [MPa]	9.3	9.3	9.4
Fore-aft lifetime FDEL [MPa]	14.7	17.0	17.4
Side-side lifetime FDEL [MPa]	10.8	8.7	8.5

Table 5.7: Lifetime FDEL on the tower and blades in case 3B. The grid frequency inputs are denoted as NF for the normal grid frequency, ED for the extreme deviation grid frequency and ER for the extreme RoCoF.

Finally, the lifetime damages are calculated using Miner's rule. Due to the unwanted behavior of the wind turbine around rated wind speeds, these damages should be taken with care. The lifetime damages can again be found in table C.1.

5.2.4. Comparison of Cases

After all three cases were studied, a comparison could be made to point out possible opportunities and weaknesses to use a wind turbine as a source of inertia or FFR. The comparison in the rest of this section is divided into a comparison of the ultimate loads and a comparison of the fatigue loads. The comparison of the ultimate load analysis performed for all three cases will start with a comparison between case 2 and the baseline case. After this case 3 will be compared to case 2 and the baseline case. The comparison of the ultimate loads will be finalised with the maximum tip deflections. The fatigue

loads will be compared in a similar way, starting with a comparison between case 2 and the baseline case and finalising with a comparison between case 3 and the baseline case.

Ultimate Load Comparison

Figure 5.19 shows the percentage change between case 2 and the baseline case for the maximum stresses in the flap-wise and edge-wise direction for the blade root, and in the fore-aft and side-side direction for the tower base.

		Case 2A: NF	Case 2B: NF	Case 2A: ED	Case 2B: ED	Case 2A: ER	Case 2B: ER
DLC 1.3	Flap-wise -	3,3%	0,1%	-2,1%	3,4%	-0,9%	-1,0%
	Edge-wise -	-0,9%	-1,3%	-2,3%	-0,9%	-1,4%	-1,5%
	Fore-aft -	-0,1%	1,5%	1,3%	0,8%	1,3%	0,7%
	Side-side -	1,9%	0,7%	-11,3%	2,1%	-3,1%	2,6%
DLC 2.1	Flap-wise -	-0,2%	0,3%	0,0%	1,2%	0,2%	0,4%
	Edge-wise -	0,7%	0,0%	-0,9%	0,6%	-3,3%	0,7%
	Fore-aft -	1,3%	1,9%	2,2%	0,8%	0,4%	-0,2%
	Side-side -	-1,2%	4,7%	0,7%	4,7%	8,1%	9,3%
DLC 3.2	Flap-wise -	0,0%	0,8%	0,0%	-0,7%	0,0%	1,0%
	Edge-wise -	0,0%	5,0%	0,0%	-2,5%	-0,1%	-0,5%
	Fore-aft -	0,0%	0,8%	0,0%	-0,8%	0,0%	0,2%
	Side-side -	0,2%	8,5%	0,1%	-1,8%	0,1%	2,0%
DLC 5.1	Flap-wise -	-1,7%	0,7%	-3,0%	-4,3%	1,7%	-0,8%
	Edge-wise -	3,6%	2,7%	-0,7%	3,3%	1,8%	4,6%
	Fore-aft -	1,9%	2,9%	-1,8%	-0,6%	9,5%	4,5%
	Side-side -	5,3%	3,0%	-2,7%	-6,0%	13,4%	-10,9%

Figure 5.19: Percentage change maximum stresses in case 2 compared to baseline case. The grid frequency inputs are denoted as NF for the normal grid frequency, ED for the extreme deviation grid frequency and ER for the extreme RoCoF.

The results for the supply of synthetic inertia of case 2A show different results for different grid inputs. This is a logical outcome, as the grid frequency input determines the response of the synthetic inertia controller. Overall, the stresses on the blades and tower do not show a significant change when comparing case 2A to the baseline case. From this, it can be concluded that for the synthetic inertia controller with a normal proportional gain, the ultimate loads are dominated by the aerodynamic loads imposed on the turbine. The effect of the supply of synthetic inertia is not evidently noticeable.

Next, the stresses in case 2B show an overall increase for DLC 1.3 and 2.1 compared to case 2A. This increase is largest for the side-side stresses on the tower base, but also the other stresses on the tower and blades increase overall.

Differently from case 2A, the maximum stresses at wind speeds of 9.5 m/s and 10.5 m/s in case 2B show interesting behavior for the side-side stresses imposed on the tower of the wind turbine in DLCs 1.3 and 5.1. These stresses do not show when only looking at the maximum stresses in figure 5.19, as the maximum side-side stresses on the tower are dominated by the stresses at 25 m/s. These stresses can be found in figure 5.20, in which the stresses of case 2B are compared to the stresses in the baseline case.

As can be seen in the figure, the stresses of case 2B with a normal frequency grid input only show a small increase from case 1. This increase from the normal grid frequency input is about 10%. The effect of the controller on the stresses is more evident for the extreme RoCoF and extreme deviation grid frequency input. For these two grid frequency inputs, the increase is around 20%. This can be explained by the fact that the response of the synthetic inertia controller in these situations is larger. Because of this the stress curves are shifted up considerably more. An explanation for the fact that this behavior is only seen in DLCs 1.3 and 5.1, and not in 2.1 and 3.2, is that in DLC 2.1 and 3.2 the loads are still dominated by external conditions. In DLC 2.1 this is the sudden grid loss and in DLC 3.2 this is the extreme operating gust.
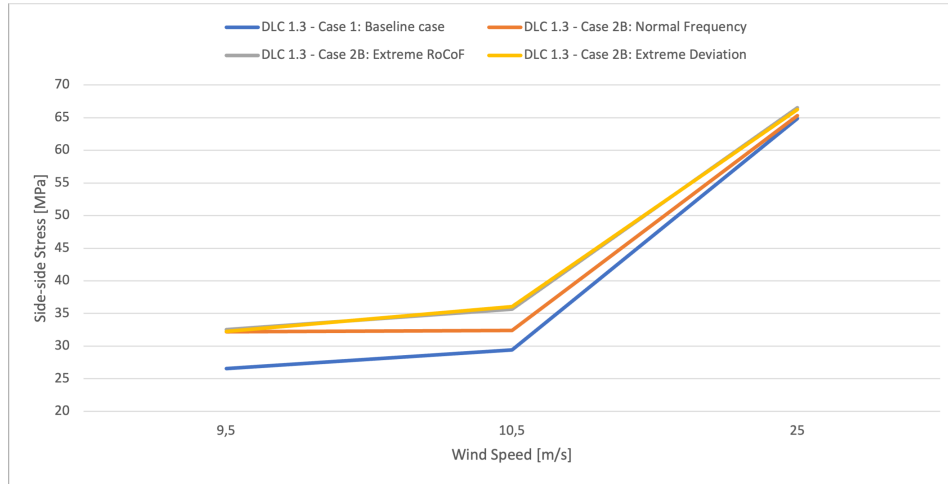
(a) Side-side maximum stress on the tower at different wind speeds for DLC 1.3 in case 2B.
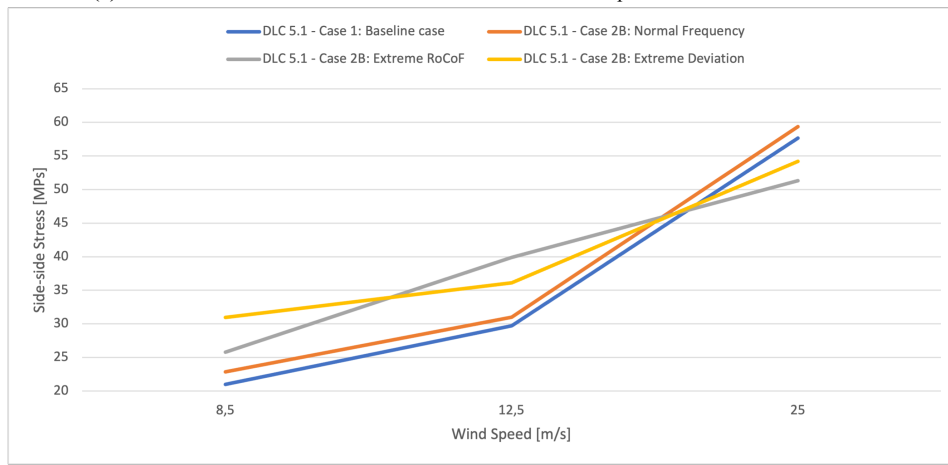
(b) Side-side maximum stress on the tower at different wind speeds for DLC 5.1 in case 2B.

Figure 5.20: Side-side stress trend in DLCs 1.3 and 5.1 for case 2B. The grid frequency inputs are denoted as NF for the normal grid frequency, ED for the extreme deviation grid frequency and ER for the extreme RoCoF.

The side-side stresses for DLC 1.3 in case 2B with a grid frequency input including the maximum RoCoF at a mean wind speed of 10.5 m/s are also plot in the frequency domain in figure 5.21a, where the single sided spectrum is constructed using a Fast Fourier Transform. A comparison is made with the frequency domain plot of the side-side stresses for DLC 1.3 of case 1 at a mean wind speed of 10.5 m/s. This plot can be seen in figure 5.21b.
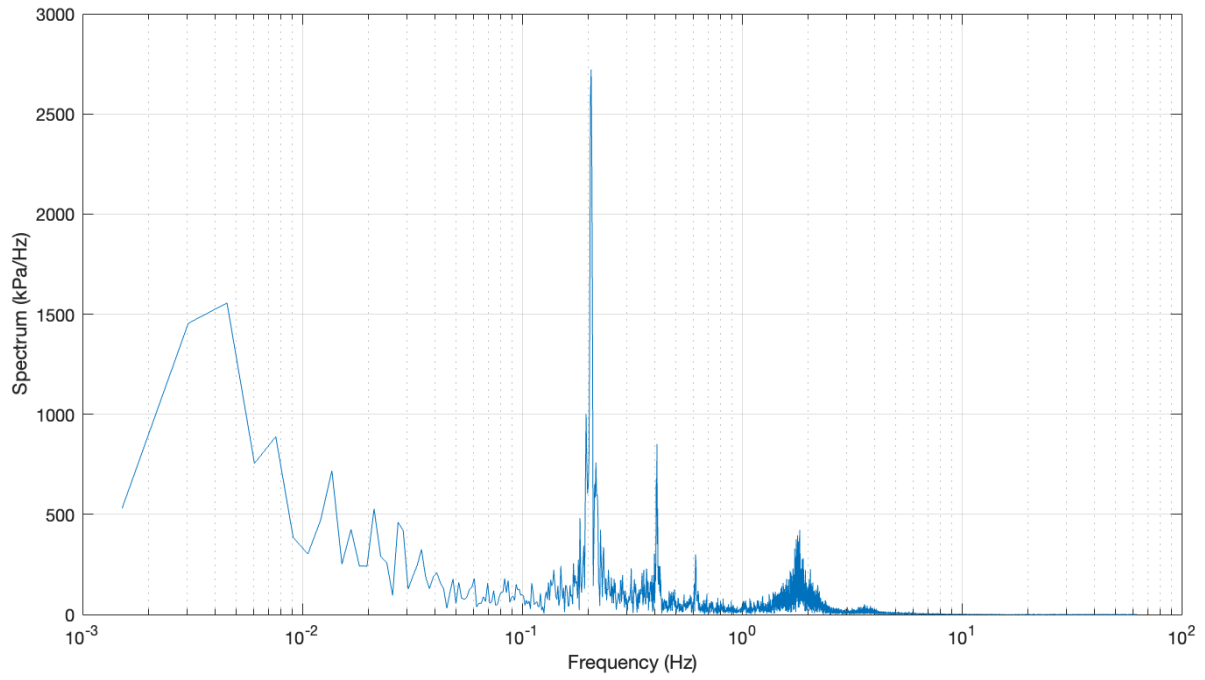
(a) Side-side stresses on the tower for DLC 1.3 in case 2B with maximum RoCoF grid frequency input shown in the frequency domain.
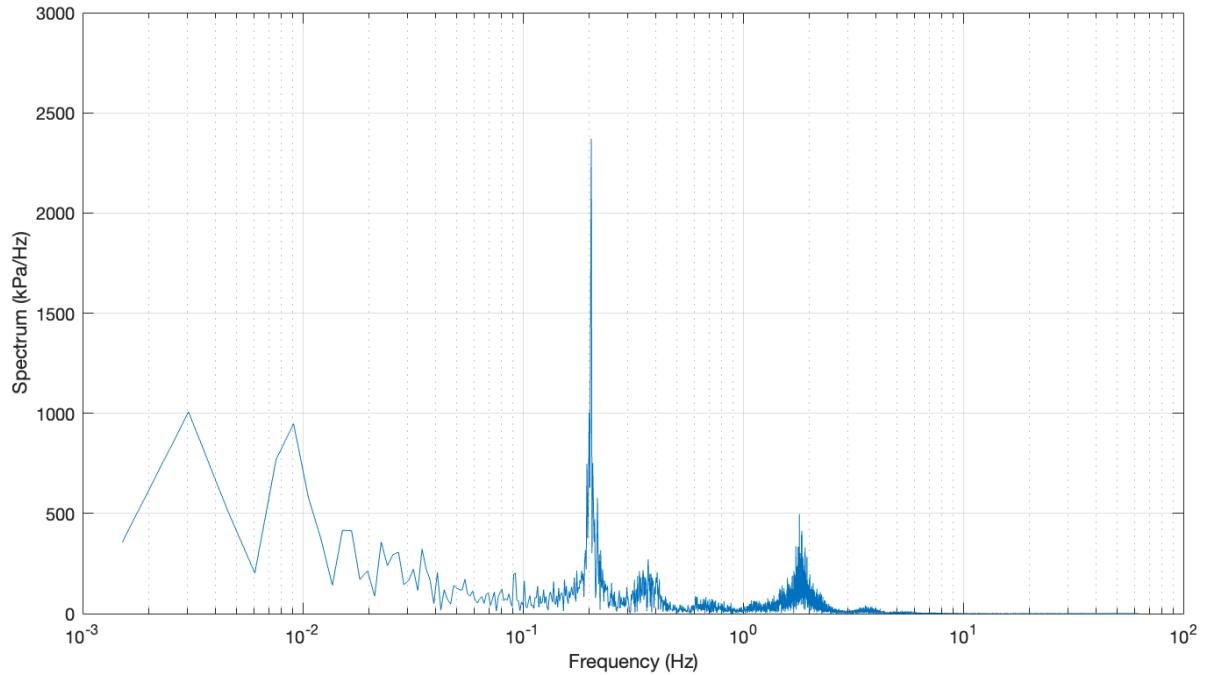
(b) Side-side stresses on the tower for DLC 1.3 in case 1 shown in the frequency domain.

Figure 5.21: Side-side stresses on the tower in DLC 1.3 at a mean wind speed of 10.5 m/s for case 2B and case 1 in the frequency domain.

An increase in amplitude can be seen at low frequencies, as well as around 0.4 and 0.6 Hz. Additionally, the peak corresponding to the first fore-aft natural frequency of the tower at 0.22 Hz is also amplified. The peak at the second fore-aft natural frequency of the tower at 1.94 Hz stays almost the same. The only change seen is a minor decrease in one specific amplitude. This increase is not seen in the amplitudes around this one specific amplitude.

The increase at low frequencies can be traced back to the RoCoF. This can also be seen in figure 5.22, where the RoCoF of the grid frequency input corresponding to the maximum RoCoF is plot in the frequency domain. For the frequencies at 0.22 Hz and higher the amplitudes of the RoCoF are lower compared to those at low frequencies because of the low-pass filter with a cut-off frequency of 0.16 Hz (1 rad/s). However, these amplitudes could still have some impact on the increase of the amplitude of the stresses at 0.22 Hz and slightly higher.
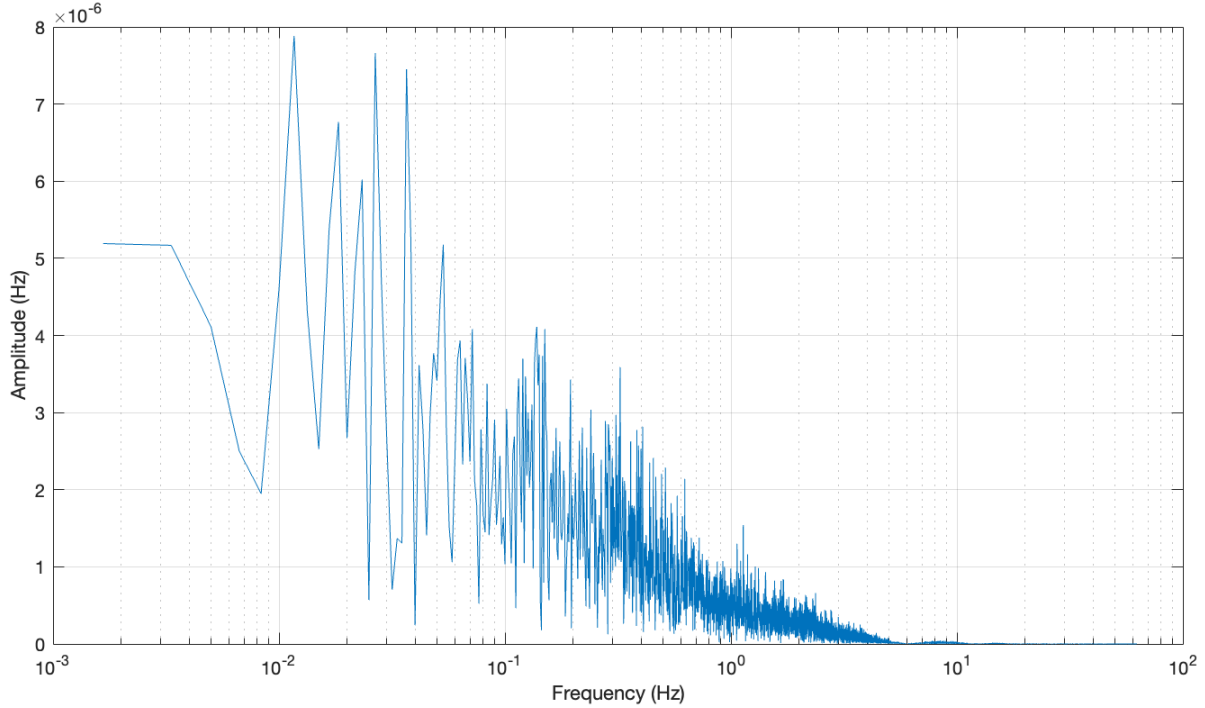
Figure 5.22: RoCoF of the grid frequency input corresponding to the maximum RoCoF after the low-pass filter shown in the frequency domain.

Figure 5.23 shows the percentage change for the loads in case 3 compared to the baseline case. Similarly to case 2, this figure shows an overall increase in stresses for the supply of FFR in case 3B compared to case 3A.

		Case 3A: NF	Case 3B: NF	Case 3A: ED	Case 3B: ED	Case 3A: ER	Case 3B: ER
DLC 1.3	Flap-wise -	-15,0%	-3,6%	-11,5%	3,2%	-13,5%	0,1%
	Edge-wise -	-0,9%	2,2%	-3,0%	3,7%	-1,3%	-0,8%
	Fore-aft -	-22,2%	-7,6%	-15,3%	6,8%	-22,4%	-0,1%
	Side-side -	7,1%	-3,4%	1,5%	-8,4%	-0,8%	0,2%
DLC 2.1	Flap-wise -	-13,0%	-2,8%	-12,9%	1,8%	-15,2%	1,0%
	Edge-wise -	-6,1%	-5,4%	-3,6%	-3,2%	-1,0%	-3,4%
	Fore-aft -	-21,8%	-6,1%	-14,3%	6,2%	-24,6%	2,6%
	Side-side -	-5,1%	16,5%	8,4%	-3,4%	5,4%	12,0%
DLC 3.2	Flap-wise -	-20,2%	-19,0%	-17,2%	3,3%	-19,6%	-8,1%
	Edge-wise -	-8,1%	5,2%	-8,6%	6,7%	-8,1%	-2,4%
	Fore-aft -	-25,3%	-23,5%	-21,8%	-1,5%	-24,4%	-8,4%
	Side-side -	6,0%	-1,1%	7,2%	-16,7%	6,0%	4,0%
DLC 5.1	Flap-wise -	-15,4%	-3,0%	-13,9%	8,3%	-16,1%	1,4%
	Edge-wise -	0,2%	3,2%	-2,6%	3,8%	-0,2%	7,5%
	Fore-aft -	-18,2%	-2,9%	-14,6%	14,6%	-21,2%	1,3%
	Side-side -	-6,6%	2,0%	-1,0%	1,1%	-16,8%	4,2%

Figure 5.23: Percentage change maximum stresses in case 3 compared to baseline case. The grid frequency inputs are denoted as NF for the normal grid frequency, ED for the extreme deviation grid frequency and ER for the extreme RoCoF.

Two big differences can be seen when comparing the results of the loads associated with the supply of synthetic inertia and FFR. Firstly, the loads for supplying FFR with a low proportional gain in case 3A show large decreases from the baseline case ranging from about 10 to 25%. This decrease is mainly seen for the flap-wise and fore-aft stresses. The maximum stresses in the edge-wise and side-side direction in case 3A decrease less or not at all compared to the other two directions in case 3A. This can be explained by diving deeper into the maximum stresses in these directions. This shows that the maximum stresses in the edge-wise and side-side direction do decrease, this only is not the case for the stresses at 25 m/s. As the edge-wise and side-side stresses are dominated by the stresses at 25 m/s, this does not show in figure 5.23. The decrease in maximum loads in case 3A can be explained by the de-loaded operation of the wind turbine. This completely changes when the amount of FFR supplied is increased 100 times. The maximum stresses for this situation show an overall increase compared to the baseline case. This increase is largest for the grid frequency input including the extreme deviation from 50 Hz, which again is logical as for this operation the response from the controller is largest. The increase is smallest for the normal grid frequency input. This can be explained by the fact that the response from the FFR controller is smallest for this grid frequency input.
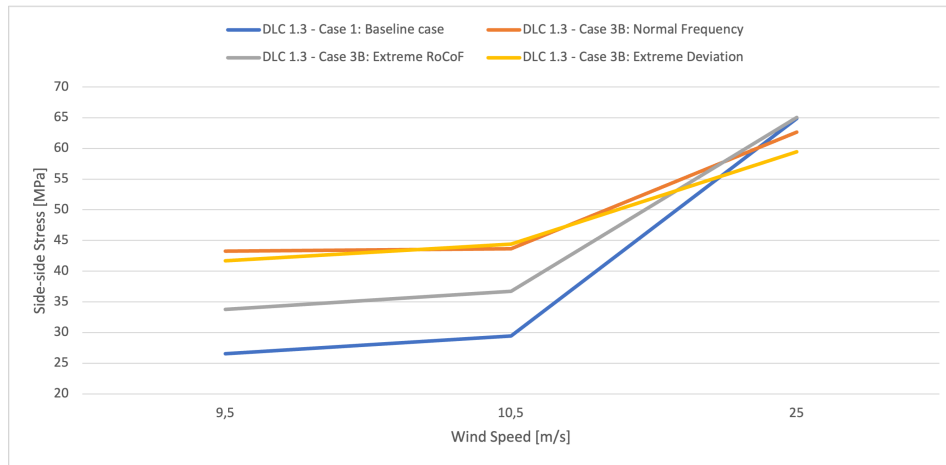
(a) Side-side maximum stress on the tower at different wind speeds for DLC 1.3 in case 3B.
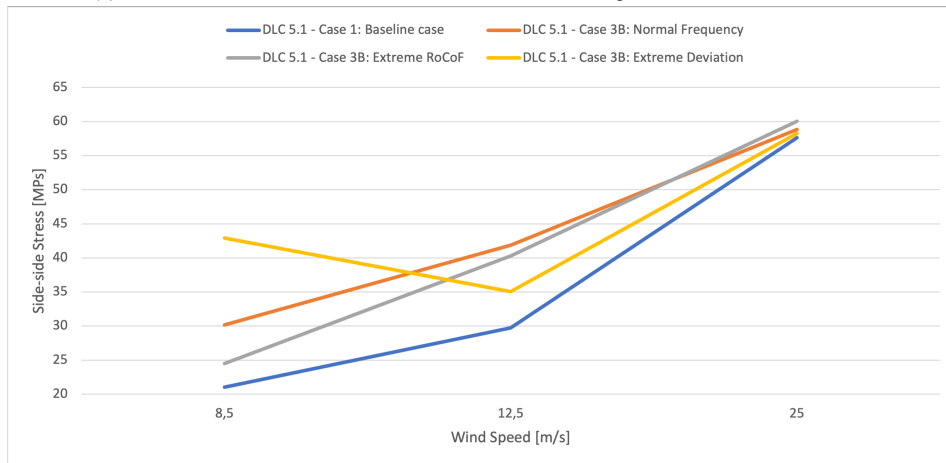
(b) Side-side maximum stress on the tower at different wind speeds for DLC 5.1 in case 2B.

Figure 5.24: Side-side stress trend in DLCs 1.3 and 5.1 for case 3B. The grid frequency inputs are denoted as NF for the normal grid frequency, ED for the extreme deviation grid frequency and ER for the extreme RoCoF.

This side-side stresses in DLC 1.3 and DLC 5.1 for case 3B can be seen in figure 5.24 at different wind speeds. The maximum side-side stresses on the tower base in DLC 1.3 and 5.1 in case 3B show

similar behavior as the side-side stresses in case 2B. The maximum stresses in the side-side direction show a larger increase when studied at individual wind speeds compared to the increase shown in figure 5.23. Considerably larger maximum stresses are seen at 9.5 and 10.5 m/s for the results of case 3B compared to the baseline case.

The last part of the comparison of the ultimate load analysis for the different cases is the comparison of the maximum tip deflection. It was found that the maximum tip deflection for case 2A, 2B and 3B increased slightly with 0.5, 0.1 and 0.6 meters, respectively, from the baseline tip deflection of 26.5 meter. Thus, no problems were seen, as sufficient tower clearance was maintained in all cases compared to the maximum allowable tip deflection of 30 meter. For case 2A, a decrease of 3.8 meter was seen. This decrease is caused by the lower loads on the blades of the wind turbine due to the de-loaded operation.

Fatigue Load Comparison

Figure 5.25 shows the percentage change for the lifetime FDEL calculated corresponding to the supply of synthetic inertia in case 2 compared to the baseline case. The results show a small decrease of maximum 5% compared to case 1. This overall decrease in FDEL is also captured in the slightly lower FDEL per wind speed when comparing the FDELs found for case 2A in section 5.2.2 to the FDELs per wind speed for the baseline case in section 5.2.1. On the other hand, an increase in the side-side lifetime FDEL on the tower base ranging from 15 to 25% was found for case 2B.

	Case 2A: NF	Case 2B: NF	Case 2A: ED	Case 2B: ED	Case 2A: ER	Case 2B: ER
FDEL Flap-wise -	-5%	-2%	-1%	-1%	-1%	-4%
FDEL Edge-wise -	-1%	4%	-1%	3%	1%	4%
FDEL Fore-aft -	0%	1%	1%	4%	-4%	0%
FDEL Side-side -	-1%	16%	1%	16%	2%	25%

Figure 5.25: Percentage change lifetime FDEL case 2 compared to baseline case. The grid frequency inputs are denoted as NF for the normal grid frequency, ED for the extreme deviation grid frequency and ER for the extreme RoCoF.

A similar increase can be found for the percentage change of the lifetime FDEL corresponding to the supply of FFR. Besides the increase in side-side lifetime FDEL, the fore-aft FDEL also shows large increases ranging from 48 to 75%. However, it should be kept in mind that the FDELs for case 3 are influenced significantly by the unwanted behavior of the wind turbine between 10 and 12 m/s as was shown in figure 5.18. An increase in FDEL due to this unwanted behavior was mostly seen in the FDEL in the flap-wise direction on the blade roots and on the fore-aft direction on the tower, as is in the lifetime FDEL.

	Case 3A: NF	Case 3B: NF	Case 3A: ED	Case 3B: ED	Case 3A: ER	Case 3B: ER
FDEL Flap-wise -	-6%	4%	0%	45%	-5%	6%
FDEL Edge-wise -	-3%	0%	-4%	0%	-5%	0%
FDEL Fore-aft -	-4%	48%	-5%	70%	-6%	75%
FDEL Side-side -	-1%	49%	0%	19%	0%	17%

Figure 5.26: Percentage change lifetime FDEL case 3 compared to baseline case. The grid frequency inputs are denoted as NF for the normal grid frequency, ED for the extreme deviation grid frequency and ER for the extreme RoCoF.

Finally, the increase in lifetime damage will be highlighted. The increase in lifetime FDEL is amplified in the lifetime damage because of the Wöhler exponent m. This can for instance be seen in the increase in lifetime damage for case 2A with the extreme deviation grid input. For this case, the lifetime FDEL in the flap-wise and edge-wise direction both decrease for about 1%. The lifetime damage for this case shows a decrease in the flap-wise and edge-wise direction of 11% and 8% respectively. Similar behavior can be seen in the lifetime damage for case 2B, case 3A and case 3B. It should again be noted

that due to the large increases around rated wind speed in the fatigue damage as shown by the FDEL, the large increases in damage in case 3B will likely be lower than calculated. The lifetime damages can again be found in table C.1.

<div align="right">

6

</div>

Discussion of Implications

6.1. Introduction of the Different Perspectives

Since there is great uncertainty about what future grids will look like, this discussion chapter is important for the interpretation of the case study. The results of the case studies can be interpreted in many ways and from different perspectives. To capture these perspectives, this discussion chapter is divided into three parts. It starts with the perspective of the wind turbine owner. For this perspective, this could be the owner of a single turbine, many turbines or even wind farm(s). The second viewpoint is that of the system, where the system is seen as the entire grid in which the wind turbine is placed. Since the grid is operated by the transmission system operator (TSO), it could be argued that this is the TSO's perspective. However, this is not the only perspective of the TSO that will be used. Finally, the results will be interpreted from a market perspective. Since the markets are regulated by the TSO, this is naturally also a TSO's point of view.

6.2. The Wind Turbine Owner

The results of the case study show promising results for the wind turbine owner with regard to the supply of synthetic inertia and FFR at normal proportional gains, referring to the situations in case 2A and 3A, but some concerns are highlighted. The results show only minor differences between the supply of synthetic inertia at normal proportional gain and the baseline simulations. Furthermore, the results show a decrease in maximum stresses and FDEL on the wind turbine when supplying FFR at normal proportional gain compared to the baseline case. However, extra attention is needed when the wind turbine has to supply synthetic inertia or FFR at proportional gains that are much higher. The results for the supply of synthetic inertia show an increase of about 2 to 9% in the maximum stresses in the side-side direction of the tower, as well as an increase of 16 to 25% in the lifetime FDEL in the same direction for the simulations with a proportional gain that is 100 times larger. The results for the supply of FFR show an increase of 2 to 16% in the overall maximum stresses, and an increase ranging from 17 to 75% in the lifetime FDEL.

First, the results for the supply of synthetic inertia will be discussed. The increase in lifetime FDEL at normal proportional gain is consistent with previous research. Researchers in [24] show a small increase in side-side FDEL of about 0.2% for a 3.x MW three-bladed wind turbine, while researchers in [22] show an increase in side-side FDEL on the tower of 2.4% for 600 kW three-bladed wind turbine. This corresponds to the increases found in DLC 1.3 for the extreme grid deviation and extreme RoCoF grid input, which is about 1 and 2% respectively. This increase was not found for the normal grid frequency results. However, this is not unexpected, since the grid behavior in this frequency input does not show an incident as was the case in the study of [22].

The research in [22] was conducted with the same inertial gain as in case 2A, and is therefore valuable information for the interpretation of the FDEL calculated for the supply of synthetic inertia. This shows that the size of the wind turbine itself has a small influence on the change in FDEL compared to the size of the gain in the synthetic inertia controller.

The change in maximum stresses in an ultimate load analysis was not studied in these studies. However, the results show that the maximum stresses at normal proportional gains for the synthetic inertia controller are mostly dominated by external conditions unrelated to the controller response. In contrast, the results of especially DCL 1.3, DLC 2.1 and DLC 3.2 show an increase of about 2 to 9% in the maximum side-side stresses on the tower for the increased proportional gain. The simulations therefore provide a new insight on the effect of the size of the proportional gain of the synthetic inertia controller on the maximum stresses. It is shown that with increasing proportional gain, the effect of the synthetic inertia control on the maximum side-side stresses on the tower increases. Further research is therefore needed for specific wind turbines before they would supply synthetic inertia at these sizes to see if similar increases in stresses are seen and if they would cause any problems in the integrity of the wind turbine.

This research did show that increasing the size of the synthetic inertia response significantly increases the amount of synthetic inertia that a single wind turbine can add to the grid. If the increased FDEL and maximum loads would not result in any failure of the wind turbine, this would enable the wind turbine owner to supply much larger amounts of synthetic inertia to the grid than suggested in current research [22], [45].

Next, the results for the supply of FFR will be discussed. The decrease in maximum stresses and FDEL at a normal proportional gain is consistent with research performed in [21]. In this study, a decrease of 8 to 10% was seen in the FDEL of a 600 kW three-bladed wind turbine. This is slightly higher than the decrease of 1 to 6% found for the 15MW wind turbine in this research. However, it should be noted that the study in [21] only examines the loads associated with de-loading the wind turbine. Therefore, it is logical that the loads found for the de-loading of the wind turbine together with FFR supply are slightly higher at normal proportional gain. Moreover, the FDELs calculated in this research are increased by the undesirable behavior of the wind turbine around rated wind speed. Further development of the de-loading controls of the wind turbine could eliminate these unwanted increases of the FDEL. A possible solution could be to use a PI controller on the torque, instead of the feed-forward controller currently used in FASTTool.

At a high proportional gain, the results show a large increase for the lifetime FDEL. This is partly because of the undesirable behavior between 10 en 12 m/s because of the de-loading strategy. However, inspection of the FDEL per wind speed does also show that the flap-wise, fore-aft and side-side FDEL increase significantly for wind speeds above 12 and below 10 m/s at a higher proportional gain.

The decrease in maximum loads in [21] ranges from 0.6 to 14%. The decrease found in this research is generally slightly larger. This could indicate a larger decrease in ultimate loads for larger wind turbines when providing FFR at normal proportional gains. However, since some simplifications were applied in determining the stresses, more research is needed before such conclusions can be made.

As with the FDEL, an increase is seen in the maximum stresses at a higher proportional gain. The largest increase is seen for the case with the extreme grid frequency deviation as grid frequency input. This is as expected since this frequency input triggers the largest response from the FRR controller.

Furthermore, the validation in section 4.4 showed that the wind turbine can supply a larger amount of FFR which could increase grid stability. At full load this showed a smooth increase in torque and power. At partial load this resulted in a big overshoot in power, due to the large dip in rotor speed. This shows that the size of the response of the FFR controller should be well matched with the changes in

grid frequency. However, this also shows that if the increases in FDEL and maximum loads do not cause any failures, one wind turbine would be able to supply higher quantities of FFR than suggested in current research [22], [45].

No problems were found in the case study concerning the maximum tip deflection. The maximum tip deflection only slightly increased for the synthetic inertia controller and for the FFR controller with a high proportional gain. These small increases do not cause any problems for the wind turbine regarding tower clearance. Furthermore, a decrease in maximum tip deflection was seen when using the FFR controller with a normal proportional gain. This would suggest that no immediate redesign of the blades is needed in order to supply synthetic inertia and FFR with the IEA 15MW reference turbine.

The overall results indicate that the maximum stresses and FDEL mainly increase with controller proportionality and not with wind turbine size. It would therefore be preferable to spread the supply of these ancillary services over many wind turbines. It should be noted that the FDEL and maximum stresses in this research are used to determine a change in ultimate and fatigue load, and not to see if the wind turbine would fail. The stresses were calculated using uniform properties and therefore do not include stress concentrations. Moreover, both the FDEL and the damage calculated with Miner's rule using the Wöhler curve do not take into account the mean stress of the stress cycles. Since these are large simplifications of reality, fatigue and ultimate load analysis should be performed for the specific wind turbine that will be used to provide synthetic inertia and FFR, with special attention on the side-side stresses of the tower base.

The absence of the implementation of hydrodynamic loads is the last big simplification which should be taken into account from the perspective of the wind turbine owner. Due to time constraints, the hydrodynamic loads have not been included in this research. However, these do have an influence on the loads of the offshore wind turbine. The effect of the hydrodynamic loads on the fatigue damage monopile foundations range between 6 to 30% for the fatigue damage [54]. These should be included in the calculations by using a non-linear wave model, as the loads are mainly influenced by the amplitude of the wave and not by the mean [54]. Adding hydrodynamic loads to this study will probably increase the stresses, due to which the ultimate stresses and FDEL will likely increase. The results found in this study are therefore likely to be an underestimation of the ultimate and fatigue loads.

6.3. The System

From a system perspective, the first reason to investigate to which extent a wind turbine can provide synthetic inertia and FFR was to see how a wind turbine can be used to help maintain frequency stability in the grid. In a grid with a high penetration of vRES, a larger initial RoCoF and frequency dip can be expected. The TSO in the Netherlands, Tennet, is already planning to increase the frequency restoration reserve from 2030 onwards [55]. The expected reference incident the frequency restoration reserve should be able to take is planned to increase from 1304MW to 2GW [55]. Thus, the size of the frequency restoration reserve will almost double. The main reason mentioned for increasing the frequency restoration reserve is the arrival of multiple wind farms in the North Sea with a 2GW connection to shore. This is thus done to anticipate the possibilities for major incidents due to the larger penetration of variable wind energy into the grid.

The results of this research show that the frequency containment reserve can be provided by FFR from wind turbines. The de-loading of the wind turbine and the subsequent supply of FFR at normal proportional gains show no problems concerning the integrity of the wind turbine. Additionally, the results show a good response of the FFR controller at larger proportional gains. This allows a wind turbine to supply larger quantities of FFR. If FFR would need to be supplied at larger proportional gains, a ultimate and fatigue load analysis is necessary to ensure that the size of the response does not cause failure of the wind turbine. The failure of a wind turbine designated to supply FFR will of course

result in an even larger frequency decrease.

Moreover, a high penetration of vRES and a subsequent decrease in grid inertia will result in a higher initial RoCoF. As a result, the system will have less time to react to frequency deviations. Very small grid inertia will result in an unstable grid operation. To overcome this, the system can use the natural inertia of the wind turbine as synthetic inertia at normal proportional gain without major impact on the wind turbine. Additionally, the synthetic inertia response can very well be increased from a systems perspective if the side-side FDEL and maximum stresses are checked for the particular wind turbine and do not cause failure.

If the supply of synthetic inertia or FFR from wind turbines becomes a crucial part of the stability of the grid, more research is needed in the safe and efficient operation of wind turbines in these roles. This is needed to gain even more insight in what the exact scales are the wind turbine can supply synthetic inertia and FFR before this would cause failure in the wind turbine. In doing so, technical standards and regulations can be established to ensure a safe provision of these ancillary services. Additionally, insights would be needed on the optimum size of the synthetic inertia and FFR controller response taking into account the limits of the wind turbine.

However, from a system perspective it is not advantageous to provide all inertial or primary frequency control using vRES. If all these alternative sources of inertia and frequency control were provided by vRES, availability issues would arise. In weather conditions with little to no wind combined with little sun, this could lead to little to no availability of ancillary services.

Finally, the grid frequency measurement was left out of the scope of this research. However, the frequency measurements are extremely important because the wind turbine can only give a good frequency response if the frequency measurements are correct. Therefore, it is advised to ensure proper measurement before starting to supply these ancillary services with wind turbines.

6.4. The Market

To ensure the goals from a system perspective can be achieved, this needs to be facilitated by the market. As of now, grid requirements in the Netherlands do not include specific inertia specifications for vRES. This is not yet necessary as the Netherlands is connected to the Central European synchronous system. An example of where measurements were needed can be seen in Ireland, where inertia issues play a bigger role because the grid is synchronously independent. In Ireland, measures have been taken to monitor grid inertia, a minimum inertia limit has been introduced, synchronous generators are asked to reduce the minimum continuous operating level and the use of FFR is being introduced [56]. Since a large increase in vRES across Europe can lead to low system inertia and frequency stability issues, experiences from grids as that in Ireland can provide valuable information.

To anticipate this, the results show that wind turbines would not experience large differences in fatigue and ultimate loads if they were required by the market to provide synthetic inertia at normal proportional gains. Again, it should be noted that for offshore wind turbines, the effect of hydrodynamic loads should be researched in future studies.

It is beyond the scope of this study to investigate the exact impact on the energy that the wind turbine can supply in the day-ahead market at larger proportional gains. This could cause energy losses and hence a lower capacity factor and efficiency for the wind turbine. If future research were to establish this, it is likely that grid operators would have to compensate industry for providing these ancillary services. This could be avoided if the provision of a minimum amount of FFR or synthetic inertia becomes a grid requirement.

The energy market in the Netherlands does include a frequency containment reserve. Using the FFR controller, wind turbines can operate in this market, replacing traditional generation units. However,

allowing wind turbines to participate in the frequency containment reserve may introduce uncertainties due to varying wind conditions. Currently, the frequency containment reserve is organised in auctions of 4-hourly blocks [55]. Due to uncertainty in output power, there may be differences in the actual available power for the frequency containment reserve. Should it prove necessary for wind turbines to operate in the frequency containment reserve, the TSO would need to address this uncertainty to ensure the stability and effectiveness of the frequency containment reserve.

7

Conclusion and Recommendations

7.1. Conclusion

The primary objective of this research was to gain an understanding of the extent to which an offshore wind turbine can provide synthetic inertia and fast frequency response (FFR) and how this affects the ultimate and fatigue loads on the wind turbine. This study has shown that the extent to which an offshore wind turbine can deliver synthetic inertia and FFR depends mainly on the size of the controller response and not on the size of the wind turbine. This was shown in the research by a significant increase in fatigue damage equivalent load (FDEL) and maximum stresses due to an increase in size of the synthetic inertia and FFR response.

It was found that the proportionality of the synthetic inertia or FFR response provided has a major influence on the fatigue and ultimate loads imposed on the wind turbine. The stresses on the blades and tower of the IEA 15 MW wind turbine were studied in both ultimate and fatigue load cases through simulations in FASTTool for the normal operation of the wind turbine, as well as for the wind turbine providing synthetic inertia and FFR as a response to three different grid frequency inputs. The influence of the proportionality of the controllers on the fatigue and ultimate loads was shown in the research by studying the response of both controllers at two different sizes, where the magnitude of the response was determined by the proportional gain in the controller settings. Taking into account the effect of the size of the inertial response or FFR on the fatigue and ultimate loads is thus crucial when designing the controller for the ancillary service.

This study shows that at lower proportional gains, the side-side FDEL on the tower shows a small increase of 1 to 2% when supplying synthetic inertia compared to the normal operation. Moreover, the fatigue and ultimate loads decrease for the 10% de-loaded wind turbine delivering FFR and thus do not cause any problems. On the other hand, by increasing the amount of synthetic inertia and FFR, the loads show a significant increase. This raises the questions of where a possible optimum would lie and how this optimum would behave for different turbines. Comparing the results from the case study with previous research shows similar results for the low proportional gains. This suggests that the most important factor for the size of the fatigue and ultimate loads would be the size of the proportional gain. However, future research is needed to see if the increase in fatigue and ultimate loads behaves similar for wind turbines of different sizes.

7.2. Recommendations

The research yielded some interesting findings. However, some recommendations can be made for future research. As the study was bound by time constraints on the one hand and due to the availability

of different controller options and research approaches on the other, simplifications needed to be made.

Firstly, the torque controller used to de-load the wind turbine uses a feed-forward controller. As a result, the de-loading around rated power shows unwanted behavior. To properly study the loads at these wind speeds, a different de-loading controller design is necessary to avoid this behavior.

Next, it would be of interest to see what the exact relation is between an increase in proportional gain for the synthetic inertia and FFR controller and the increase in fatigue and ultimate loads. This would be interesting as this study only gives conclusions on the fact that the loads increase, but not on the relation between these two parameters.

This study did not research the effect of the supply of synthetic inertia and FFR on the energy supply of the wind turbine in the day-ahead market. Insights are needed on this to see how wind turbine owners need to be compensated for the delivery of these ancillary services.

Additionally, the grid measurements needed to react to the RoCoF and grid deviation are not included in this research. However, the quality of the measurements will impact the ability of a wind turbine to supply synthetic inertia and FFR. It is therefore of interest to see how the grid measurements can best be done to ensure a proper synthetic inertia and FFR response.

Furthermore, the stresses used in determining the ultimate and fatigue loads are determined based on a moment of inertia which is calculated using uniform properties and therefore does not take into account stress concentrations in the material. Moreover, the fatigue analysis uses the Wöhler curve, which does not take into account the mean stress of the stress cycles. To ensure the numerical value calculated for the fatigue and ultimate loads is trustworthy, the stresses should be determined such that it takes into account the non-uniform properties of the wind turbine blade root and tower base. Moreover, the fatigue damage should be calculated using a method which takes into account the mean stress.

Finally, as also mentioned earlier, hydrodynamic loads are not included in the FASTTool simulation and therefore do not affect the loads in the case study. To demonstrate that the supply of synthetic inertia and FFR will not critically damage the structure of the wind turbine, these should be included in future research.

References

[1] CBS, *Lower renewable energy share despite more solar and wind energy*, 2022. [Online]. Available: `https://www.cbs.nl/en-gb/news/2022/26/lower-renewable-energy-share-despite-more-solar-and-wind-energy`.

[2] A. Fernández-Guillamón, E. Gómez-Lázaro, E. Muljadi, and Á. Molina-Garcia, "A Review of Virtual Inertia Techniques for Renewable Energy-Based Generators," *Renewable Energy - Technologies and Applications*, May 2020. DOI: `10.5772/INTECHOPEN.92651`. [Online]. Available: `https://www.intechopen.com/state.item.id`.

[3] P. Denholm, T. Mai, R. W. Kenyon, B. Kroposki, and M. O'malley, "Inertia and the Power Grid: A Guide Without the Spin," 2020. [Online]. Available: `www.nrel.gov/publications.`.

[4] Y. G. Rebours, D. S. Kirschen, M. Trotignon, and S. Rossignol, "A survey of frequency and voltage control ancillary services - Part I: Technical features," *IEEE Transactions on Power Systems*, vol. 22, no. 1, pp. 350–357, Feb. 2007, ISSN: 08858950. DOI: `10.1109/TPWRS.2006.888963`.

[5] J. Aho, A. Buckspan, J. Laks, *et al.*, "A tutorial of wind turbine control for supporting grid frequency through active power control," in *Proceedings of the American Control Conference*, Institute of Electrical and Electronics Engineers Inc., 2012, pp. 3120–3131, ISBN: 9781457710957. DOI: `10.1109/acc.2012.6315180`.

[6] I. Ngamroo, "Review of DFIG wind turbine impact on power system dynamic performances," *IEEJ Transactions on Electrical and Electronic Engineering*, vol. 12, no. 3, pp. 301–311, May 2017, ISSN: 19314981. DOI: `10.1002/TEE.22379`.

[7] R. Eriksson, N. Modig, and K. Elkington, "Synthetic inertia versus fast frequency response: A definition," in *IET Renewable Power Generation*, vol. 12, Institution of Engineering and Technology, Apr. 2018, pp. 507–514. DOI: `10.1049/iet-rpg.2017.0370`.

[8] J. Morren, S. W. de Haan, W. L. Kling, and J. A. Ferreira, "Wind turbines emulating inertia and supporting primary frequency control," *IEEE Transactions on Power Systems*, vol. 21, no. 1, pp. 433–434, Feb. 2006, ISSN: 08858950. DOI: `10.1109/TPWRS.2005.861956`.

[9] J. Ekanayake and N. Jenkins, "Comparison of the response of doubly fed and fixed-speed induction generator wind turbines to changes in network frequency," *IEEE Transactions on Energy Conversion*, vol. 19, no. 4, pp. 800–802, Dec. 2004, ISSN: 08858969. DOI: `10.1109/TEC.2004.827712`.

[10] N. W. Miller and K. Clark, "Advanced controls enable wind plants to provide ancillary services," in *IEEE PES General Meeting, PES 2010*, 2010, ISBN: 9781424483570. DOI: `10.1109/PES.2010.5589787`.

[11] S. Wachtel and A. Beekmann, "Contribution of wind energy converters with inertia emulation to frequency control and frequency stability in power systems," 2009.

[12] I. Erlich and M. Wilch, "Primary frequency control by wind turbines," in *IEEE PES General Meeting, PES 2010*, 2010, ISBN: 9781424483570. DOI: `10.1109/PES.2010.5589911`.

[13] S. Engelken, A. Mendonca, and M. Fischer, "Inertial response with improved variable recovery behaviour provided by type 4 WTs," in *IET Renewable Power Generation*, vol. 11, Institution of Engineering and Technology, 2017, pp. 195–201. DOI: `10.1049/iet-rpg.2016.0333`.

[14] F. M. Gonzalez-Longatt, "Activation schemes of synthetic inertia controller on full converter wind turbine (type 4)," in *IEEE Power and Energy Society General Meeting*, vol. 2015-September, IEEE Computer Society, Sep. 2015, ISBN: 9781467380409. DOI: `10.1109/PESGM.2015.7286430`.

[15] P. Fernández-Bustamante, O. Barambones, I. Calvo, C. Napole, and M. Derbeli, *Provision of frequency response from wind farms: A review*, Oct. 2021. DOI: `10.3390/en14206689`.

[16] F. Gonzalez-Longatt, "Frequency Control and Inertial Response Schemes for the Future Power Networks," in 2014, pp. 193–231. DOI: `10.1007/978-981-4585-30-9{\_}8`.

[17] A. Teninge, C. Jecu, D. Roye, S. Bacha, J. Duval, and R. Belhomme, "Contribution to frequency control through wind turbine inertial energy storage," in *IET Renewable Power Generation*, vol. 3, 2009, pp. 358–370. DOI: `10.1049/iet-rpg.2008.0078`.

[18] P. K. Keung, P. Li, H. Banakar, and B. T. Ooi, "Kinetic energy of wind-turbine generators for system frequency support," *IEEE Transactions on Power Systems*, vol. 24, no. 1, pp. 279–287, 2009, ISSN: 08858950. DOI: `10.1109/TPWRS.2008.2004827`.

[19] F. M. Gonzalez-Longatt, A. Bonfiglio, R. Procopio, and B. Verduci, "Evaluation of inertial response controllers for full-rated power converter wind turbine (Type 4)," in *IEEE Power and Energy Society General Meeting*, vol. 2016-November, IEEE Computer Society, Nov. 2016, ISBN: 9781509041688. DOI: `10.1109/PESGM.2016.7741837`.

[20] IEC, "IEC 61400-3 Wind turbines-Part 3: Design requirements for offshore wind turbines," Tech. Rep., 2009. [Online]. Available: `www.iec.ch/searchpub/cur_fut-f.htm`.

[21] P. A. Fleming, J. Aho, A. Buckspan, *et al.*, "Effects of power reserve control on wind turbine structural loading," *Wind Energy*, vol. 19, no. 3, pp. 453–469, Mar. 2016, ISSN: 10991824. DOI: `10.1002/we.1844`.

[22] X. Wang, W. Gao, A. Scholbrock, *et al.*, "Evaluation of different inertial control methods for variable-speed wind turbines simulated by fatigue, aerodynamic, structures and turbulence (FAST)," *IET Renew. Power Gener*, vol. 11, p. 12, 2017, ISSN: 1752-1416. DOI: `10.1049/iet-rpg.2017.0123`. [Online]. Available: `www.ietdl.org`.

[23] F. Guo and D. Schlipf, "A spectral model of grid frequency for assessing the impact of inertia response on wind turbine dynamics," *Energies*, vol. 14, no. 9, May 2021, ISSN: 19961073. DOI: `10.3390/en14092492`.

[24] A. Gloe, C. Jauch, B. Craciun, A. Zanter, and J. Winkelmann, "Influence of Continuous Provision of Synthetic Inertia on the Mechanical Loads of a Wind Turbine," *Energies 2021, Vol. 14, Page 5185*, vol. 14, no. 16, p. 5185, Aug. 2021, ISSN: 1996-1073. DOI: `10.3390/EN14165185`. [Online]. Available: `https://www.mdpi.com/1996-1073/14/16/5185/htm%20https://www.mdpi.com/1996-1073/14/16/5185`.

[25] E. Gaertner, J. Rinker, L. Sethuraman, *et al.*, "Definition of the IEA Wind 15-Megawatt Offshore Reference Wind Turbine Technical Report," Tech. Rep., Mar. 2020. [Online]. Available: `www.nrel.gov/publications.`.

[26] P. Verschuren and H. Doorewaard, "Designing a Research Project," Tech. Rep., 2010.

[27] S. P. Mulders, M. B. Zaaijer, R. Bos, and J. W. van Wingerden, "Wind turbine control: open-source software for control education, standardization and compilation," *Journal of Physics: Conference Series*, vol. 1452, no. 1, p. 012 010, Jan. 2020, ISSN: 1742-6588. DOI: `10.1088/1742-6596/1452/1/012010`.

[28] J. M. Jonkman and M. L. Buhl, "FAST User's Guide," Tech. Rep., 2005. [Online]. Available: `www.nrel.gov`.

[29] E. Bossanyi, "Developments in closed loop controller design for wind turbines," in *2000 ASME Wind Energy Symposium*, Reston, Virigina: American Institute of Aeronautics and Astronautics, Jan. 2000. DOI: `10.2514/6.2000-27`.

[30] *GitHub - IEAWindTask37/IEA-15-240-RWT: 15MW reference wind turbine repository developed in conjunction with IEA Wind*. [Online]. Available: `https://github.com/IEAWindTask37/IEA-15-240-RWT`.

[31] IEC, "IEC 61400-1 Wind turbines-Part 1: Design requirements," Tech. Rep., 2005. [Online]. Available: `www.iec.ch/searchpub`.

[32]   D. Veldkamp, *Standards and Load Calculations*, 2022.

[33]   Y. Gong, *Simple Rain Flow Counting Algorithm*, 2023. [Online]. Available: `https://nl.ma thworks.com/matlabcentral/fileexchange/38834-simple-rain-flow-counting-algorithm`.

[34]   CBS, PBL, RIVM, and WUR, *Windvermogen in Nederland, 1990-2021*, 2022. [Online]. Available: `https://www.clo.nl/indicatoren/nl0386-windvermogen-in-nederland`.

[35]   T. Kerdphol, F. S. Rahman, M. Watanabe, Y. Mitani, D. Turschner, and H. P. Beck, "Enhanced Virtual Inertia Control Based on Derivative Technique to Emulate Simultaneous Inertia and Damping Properties for Microgrid Frequency Regulation," *IEEE Access*, vol. 7, pp. 14 422–14 433, 2019, ISSN: 21693536. DOI: `10.1109/ACCESS.2019.2892747`.

[36]   H. Thiesen, A. Gloe, and C. Jauch, *Grid Frequency Data - WETI*, Aug. 2023.

[37]   Siemens Gamesa, *Offshore Wind Turbine SG 14-236 DD*. [Online]. Available: `https://www.siemensgamesa.com/en-int/products-and-services/offshore/wind-turbine-sg-14-236-dd`.

[38]   Vestas, *V236-15.0 MW™*. [Online]. Available: `https://www.vestas.com/en/products/offshore/V236-15MW`.

[39]   L. Y. Pao and K. E. Johnson, "Control of Wind Turbines: Approaches, challenges, and recent developments," *IEEE Control Systems*, vol. 31, no. 2, pp. 44–62, 2011, ISSN: 1066033X. DOI: `10.1109/MCS.2010.939962`.

[40]   K. J. Åström and R. M. Murray, "Stability Margins," in *Feedback Systems: An introduction for Scientists and Engineers*, Princeton University Press, 2012, pp. 278–282.

[41]   W. E. Leithead, D. J. Leith, F. Hardan, and H. Markou, "GLOBAL GAIN-SCHEDULING CONTROL FOR VARIABLE SPEED WIND TURBINES," EWEC-CONFERENCE, Tech. Rep., 1999.

[42]   B. T. Kulakowski, J. F. Gardner, and J. L. Shearer, "CLOSED-LOOP SYSTEMS AND SYSTEM STABILITY," in *Dynamic Modeling and Control of Engineering Systems*, Cambridge University Press, Jul. 2007, pp. 329–355. DOI: `10.1017/CBO9780511805417.015`.

[43]   J. Jonkman, S. Butterfield, W. Musial, and G. Scott, "Definition of a 5-MW Reference Wind Turbine for Offshore System Development," Tech. Rep., 2009. [Online]. Available: `http://www.osti.gov/bridge`.

[44]   J. Morren, J. Pierik, and S. W. de Haan, "Inertial response of variable speed wind turbines," *Electric Power Systems Research*, vol. 76, no. 11, pp. 980–987, Jul. 2006, ISSN: 03787796. DOI: `10.1016/j.epsr.2005.12.002`.

[45]   J. Lee, E. Muljadi, P. Sørensen, and Y. C. Kang, "Releasable kinetic energy-based inertial control of a DFIG wind power plant," *IEEE Transactions on Sustainable Energy*, vol. 7, no. 1, pp. 279–288, Jan. 2016, ISSN: 19493029. DOI: `10.1109/TSTE.2015.2493165`.

[46]   G. Ramtharan, J. B. Ekanayake, and N. Jenkins, "Frequency support from doubly fed induction generator wind turbines," *IET Renewable Power Generation*, vol. 1, no. 1, pp. 3–9, 2007, ISSN: 17521416. DOI: `10.1049/iet-rpg:20060019`.

[47]   M. Dreidy, H. Mokhlis, and S. Mekhilef, *Inertia response and frequency control techniques for renewable energy sources: A review*, Mar. 2017. DOI: `10.1016/j.rser.2016.11.170`.

[48]   L. D. Avendaño-Valencia, I. Abdallah, and E. Chatzi, "Virtual fatigue diagnostics of wake-affected wind turbine via Gaussian Process Regression," *Renewable Energy*, vol. 170, pp. 539–561, Jun. 2021, ISSN: 18790682. DOI: `10.1016/j.renene.2021.02.003`.

[49]   H. F. Veldkamp and J. Van Der Tempel, "Influence of wave modelling on the prediction of fatigue for offshore wind turbines," in *Wind Energy*, vol. 8, John Wiley and Sons Ltd, 2005, pp. 49–65. DOI: `10.1002/we.138`.

[50]   L. Colone, A. Natarajan, and N. Dimitrov, "Impact of turbulence induced loads and wave kinematic models on fatigue reliability estimates of offshore wind turbine monopiles," *Ocean En-*

gineering, vol. 155, pp. 295–309, May 2018, ISSN: 00298018. DOI: `10.1016/j.oceaneng.2018.02.045`.

[51] A. Molina, M. R. Piña-Monarrez, and J. M. Barraza-Contreras, "Weibull S-N Fatigue Strength Curve Analysis for A572 Gr. 50 Steel, Based on the True Stress-True Strain Approach," 2020. DOI: `10.3390/app10165725`. [Online]. Available: `www.mdpi.com/journal/applsci`.

[52] Rijksoverheid, *Waar staan en komen de windparken op zee? - Wind op zee*. [Online]. Available: `https://windopzee.nl/onderwerpen/wind-zee/waar/`.

[53] *Global Wind Atlas*. [Online]. Available: `https://globalwindatlas.info/en`.

[54] J. P. A. A. Blasques and A. Natarajan, "Mean load effects on the fatigue life of offshore wind turbine monopile foundations," Tech. Rep., 2013, pp. 818–829.

[55] Tennet, *Dutch Ancillary Services*, 2023. [Online]. Available: `https://www.tennet.eu/markets/dutch-ancillary-services`.

[56] I. Renewable Energy Agency, "Grid codes for renewable powered systems," 2022. [Online]. Available: `www.irena.org/publications`.

A
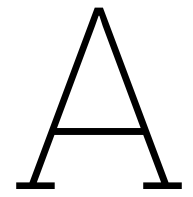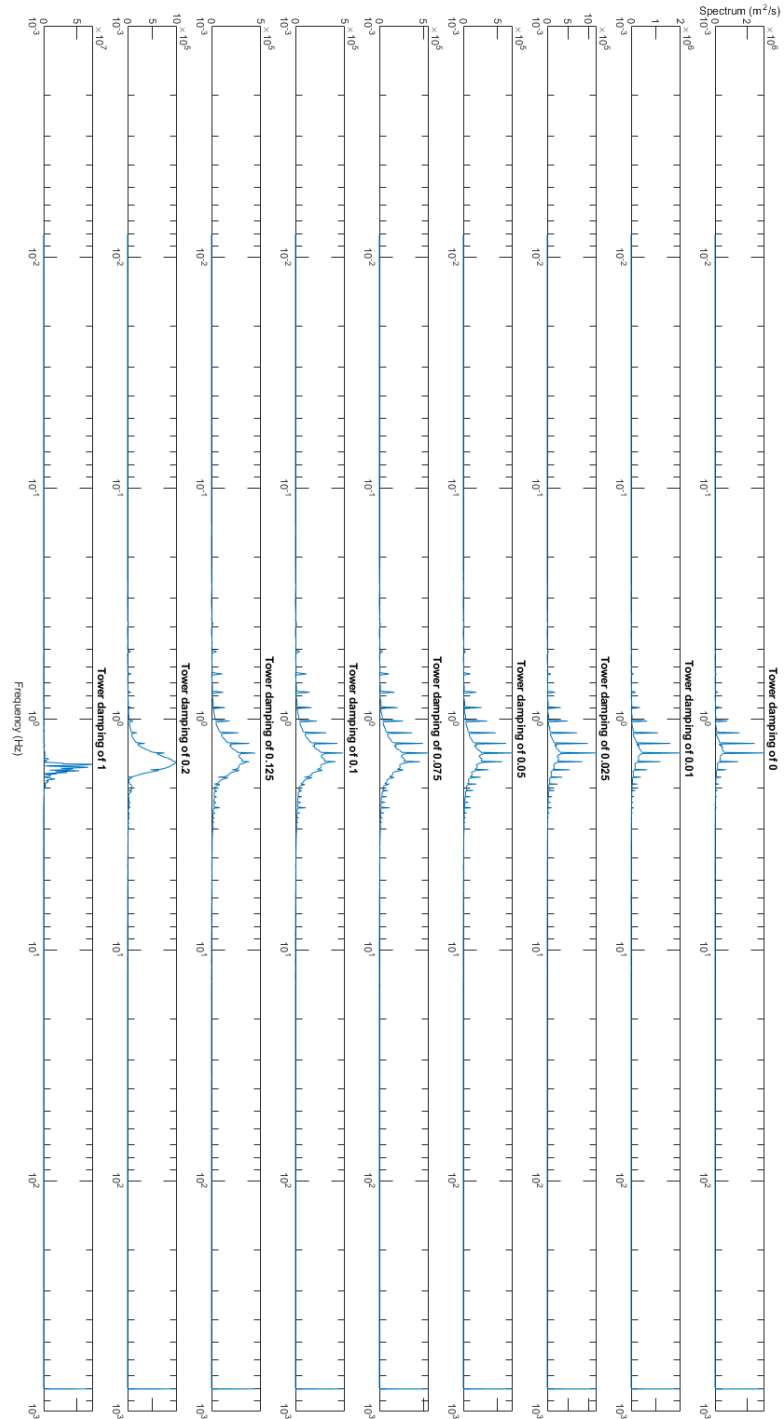
Plots Fore-Aft Controller Design
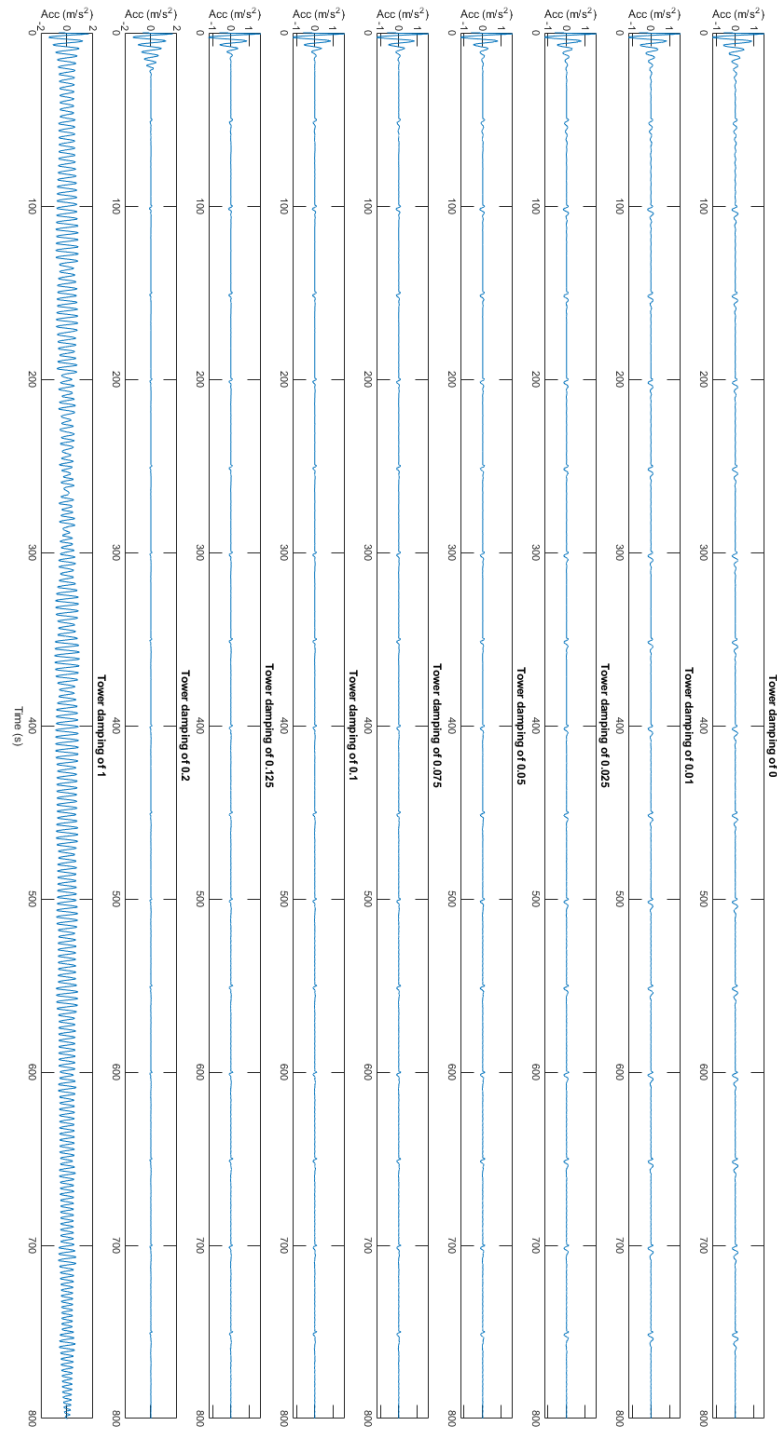
Figure A.1: Fore-aft acceleration of the tower in the time domain for different controller gains.
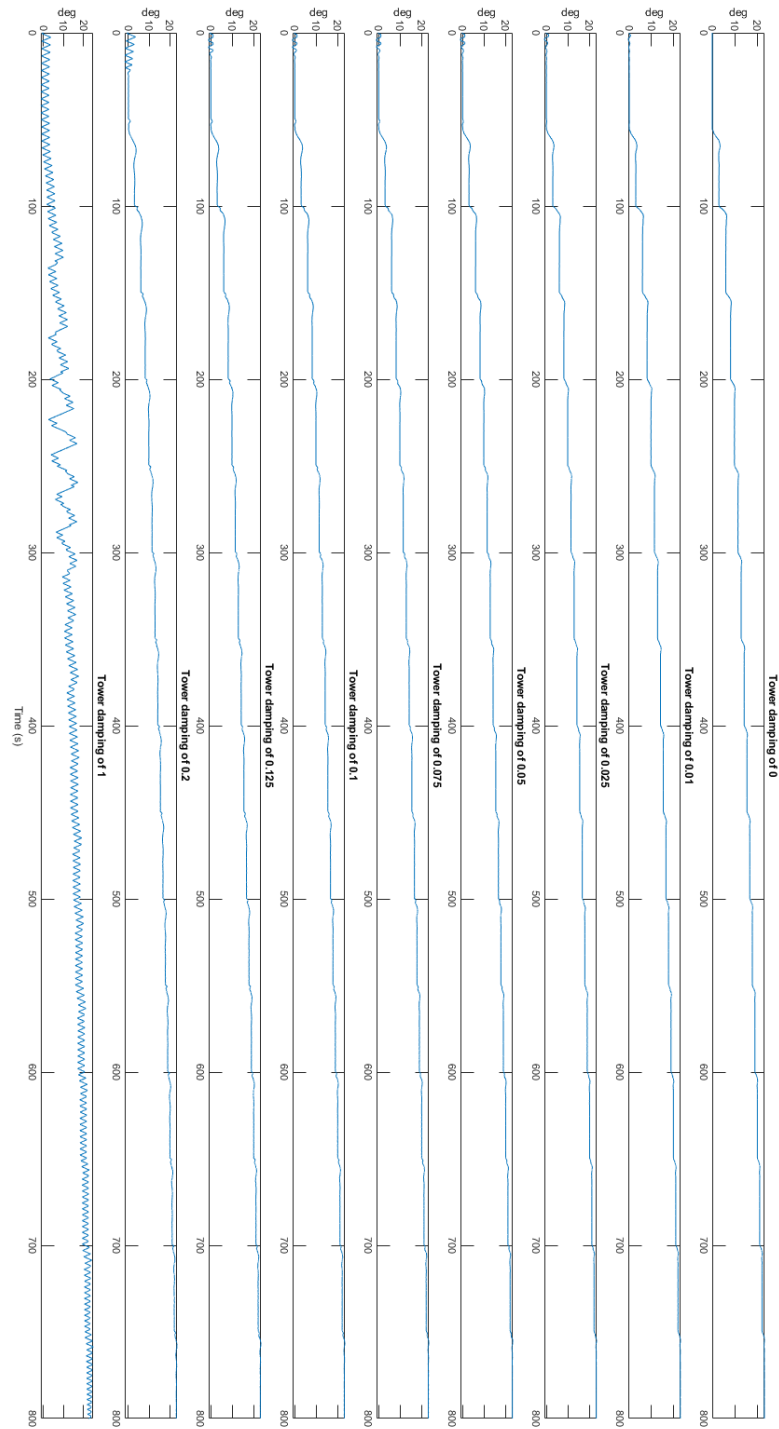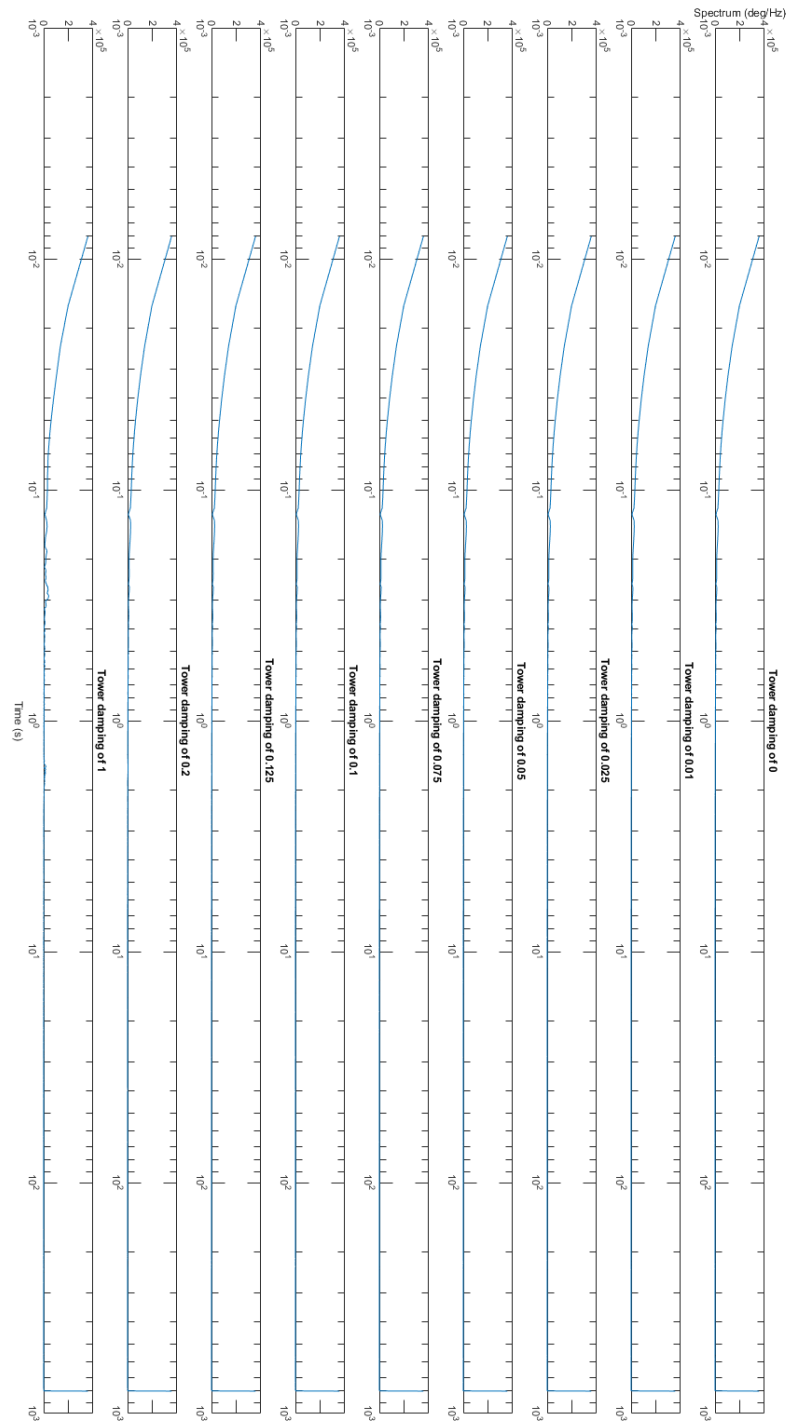
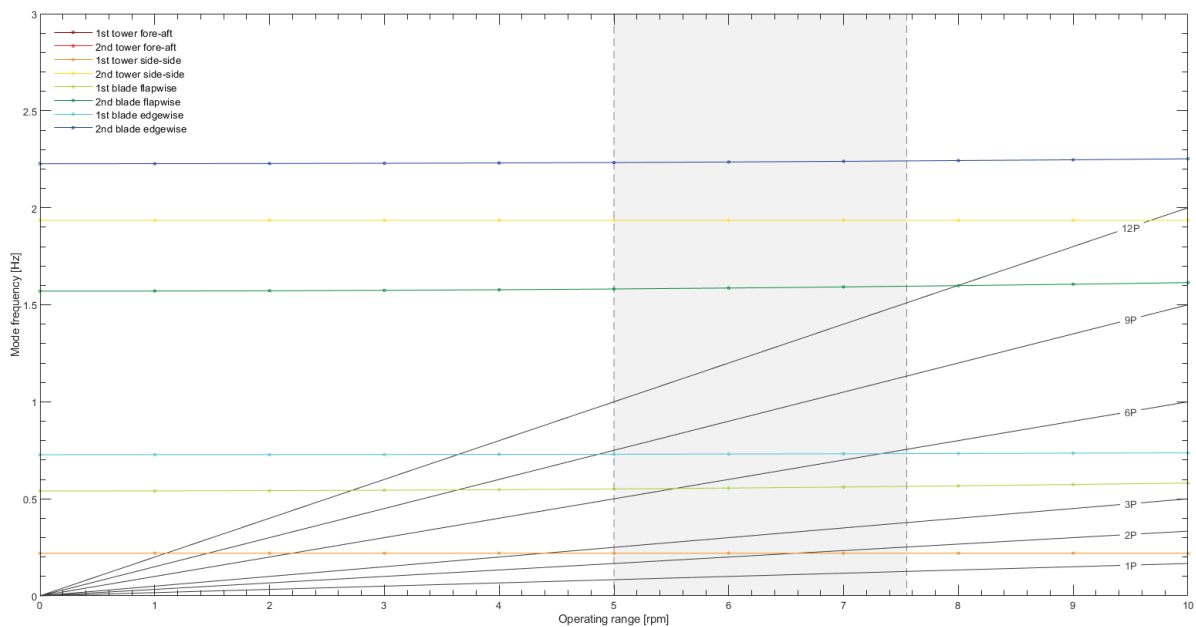**Figure A.2:** Pitch angle in the time domain for different controller gains.

Figure A.3: Fore-aft acceleration of the tower in the frequency domain for different controller gains.

Figure A.4: Pitch angle in the frequency domain for different controller gains.

B

Campbell Diagram IEA 15MW Reference Wind Turbine

Figure B.1: Campbell diagram IEA 15MW reference turbine constructed using FASTTool.

C

Lifetime Damages IEA 15MW Wind Turbine

	Damage flap-wise	**%**	**Damage edge-wise**	**%**	**Damage fore-aft**	**%**	**Damage side-side**	**%**
Baseline	3,92506E-10	0	6,78826E-11	0	0,00130568	0	0,00036541	0
2A NF	2,45233E-10	-38	6,4237E-11	-5	0,00128419	-2	0,00035102	-4
2A ED	3,48165E-10	-11	6,27044E-11	-8	0,00133403	2	0,00038618	6
2A ER	3,46381E-10	-12	7,61068E-11	12	0,00110003	-16	0,00039676	9
2B NF	3,28538E-10	-16	9,54277E-11	41	0,00138086	6	0,00067237	84
2B ED	3,572E-10	-9	8,48534E-11	25	0,00151632	16	0,00066118	81
2B ER	2,69511E-10	-31	9,96619E-11	47	0,00131866	1	0,0008935	145
3A NF	2,06295E-10	-47	5,33707E-11	-21	0,00110625	-15	0,00035459	-3
3A ED	3,70244E-10	-6	4,58524E-11	-32	0,00106402	-19	0,00036031	-1
3A ER	2,29403E-10	-42	4,12987E-11	-39	0,00101414	-22	0,00036284	-1
3B NF	5,66307E-10	44	6,59919E-11	-3	0,00641585	391	0,00179136	390
3B ED	1,71573E-08	4271	6,49402E-11	-4	0,01171667	797	0,00073741	102
3B ER	9,89044E-10	152	6,7827E-11	0	0,01213408	829	0,00067681	85

Table C.1: Lifetime damage on the tower and blades in all cases and the percentage change from the lifetime damage in the same direction for the baseline scenario.